International Journal of
Environmental Research and Public Health

MDPI

Article

Impact of HVAC-Systems on the Dispersion of Infectious Aerosols in a Cardiac Intensive Care Unit

Larisa Anghel [1,2], Cătălin-George Popovici [3], Cristian Stătescu [1,2,*], Radu Sascău [1,2,*], Marina Verdeș [3], Vasilică Ciocan [3], Ionela-Lăcrămioara Șerban [4], Minela Aida Mărănducă [4], Sebastian-Valeriu Hudișteanu [3] and Florin-Emilian Țurcanu [3]

1 Internal Medicine Department, Grigore T. Popa University of Medicine and Pharmacy, 700503 Iași, Romania; larisa.anghel@umfiasi.ro
2 Cardiology Department, Cardiovascular Diseases Institute, Prof. Dr. George I.M. Georgescu, 700503 Iași, Romania
3 Building Services Department, Faculty of Civil Engineering and Building Services, Gheorghe Asachi Technical University, 700050 Iași, Romania; catalin.popovici@tuiasi.ro (C.-G.P.); marina.verdes@tuiasi.ro (M.V.); vasilica.ciocan@tuiasi.ro (V.C.); sebastian.hudisteanu@tuiasi.ro (S.-V.H.); emilian-florin.turcanu@tuiasi.ro (F.-E.Ț.)
4 Physiology Department, Grigore T. Popa University of Medicine and Pharmacy, 700503 Iași, Romania; ionela.serban@umfiasi.ro (I.-L.Ș.); minela.maranduca@umfiasi.ro (M.A.M.)
* Correspondence: cstatescu@gmail.com (C.S.); radu.sascau@gmail.com (R.S.); Tel.: +40-0232-211834 (C.S. & R.S.)

Received: 19 July 2020; Accepted: 7 September 2020; Published: 10 September 2020



Abstract: At the end of 2019, a variation of a coronavirus, named SARS-CoV-2, has been identified as being responsible for a respiratory illness disease (COVID-19). Since ventilation is an important factor that influences airborne transmission, we proposed to study the impact of heating, ventilation and air-conditioning (HVAC) with a variable air volume (VAV) primary air system, on the dispersion of infectious aerosols, in a cardiac intensive care unit, using a transient simulation with computational fluid dynamics (CFD), based on the finite element method (FEM). We analyzed three scenarios that followed the dispersion of pathogen carrying expiratory droplets particles from coughing, from patients possibly infected with COVID-19, depending on the location of the patients in the intensive care unit. Our study provides the mechanism for spread of infectious aerosols, and possibly of COVID-19 infection, by air conditioning systems and also highlights important recommendations for disease control and optimization of ventilation in intensive care units, by increasing the use of outdoor air and the rate of air change, decreasing the recirculation of air and using high-efficiency particulate air (HEPA) filters. The CFD-FEM simulation approach that was applied in our study could also be extended to other targets, such as public transport, theaters, philharmonics and amphitheaters from educational units.

Keywords: COVID-19; airborne transmission; intensive care unit; air conditioning systems; hospital-acquired infections; risk factors

1. Introduction

Hospital-acquired respiratory tract infections, also known as nosocomial respiratory tract infections, have proven to be a challenge and sometimes a tragic problem for the practitioner. They can be caused by a variety of viruses that spread through three different routes: contact (direct and indirect), droplet and aerosol transmission [1,2]. Transmission by direct contact means that, from an infected patient to a susceptible person, the virus spreads through contaminated hands, for example. When the virus is transmitted through intermediate objects, such as fomites, we are talking about indirect virus transfer. The virus can also be transmitted via the air, droplets or aerosols [3–5]. Pulmonary activities

such as coughing [6,7], breathing [8], sneezing [8] or talking [9], are sources of bio-aerosols that can have respiratory tract infections pathogens [7–9]. Large droplets (>10 microns), formed especially from coughing and sneezing, fall on surfaces and objects not further than 1–2 m from the infected patient [3,10]. People can catch the infection directly by standing within 1–2 meters of an infected person and breathing in these droplets. When people are standing within 1–2 meters of an infected patient or when they touch their mouth, nose or eyes after they touched the contaminated surfaces or objects, they can catch the infection [10]. Droplets that evaporate (10 microns droplets evaporate in 0.2 s) and desiccate, form small particles (droplet nuclei or residue). Aerosols are small particles (<5 microns), with a slow velocity and may remain suspended in the air for hours and can be transported long distances [1,4,11].

Respiratory viruses spread via these three routes depends on environmental factors, such as humidity or temperature and crowding of people, and also on host factors such as receptor distribution all over the respiratory tract [5,11].

Airborne transmission is responsible for more than one third of hospital-acquired infections [12,13]. This dangerous threat of airborne infection to human health has been reiterated by the severe acute respiratory syndrome (SARS) in 2002–2003 [14,15], pandemic influenza A virus subtype H1N1 (A/H1N1) in 2009 [16], Middle East Respiratory Syndrome (MERS) in 2012 [17] and the ongoing pandemic of coronavirus disease 2019 (COVID-19), caused by severe acute respiratory syndrome coronavirus 2 (SARS-CoV-2) [18].

Since 31 December 2019, when the Wuhan Municipal Health Commission reported 27 cases of viral pneumonia, there was a rapid spread around the country and the entire world. This disease was named Coronavirus Disease 2019 (COVID-19) by the World Health Organization. On 19 July 2020, the number of confirmed cases reached 14,007,791, with 597,105 deaths worldwide, according to the World Health Organization [19–21]. Coronaviruses have a small size of 70–120 nanometers [20–22] and SARS-CoV-2 remains active up to three hours in indoor air and up to three days on room surfaces, unless there is specific cleaning [20–26]. Because SARS-CoV-2 has such a small size, it can be carried by airflows, either in the room or in the extract air ducts of ventilation systems, and it can travel long distances [25]. It is known that SARS-CoV-2 is mainly transmitted via respiratory droplets released from infected persons [19]. Current studies suggest that COVID-19 may be transmitted through droplets from patients with mild symptoms and even from asymptomatic ones [22], but not through long-range inhalation of aerosols, as in the case of tuberculosis or measles. However, considering that many respiratory infectious agents have a short-range aerosol transmission, this cannot be excluded in the case of SARS-CoV-2 infection, especially in poorly ventilated spaces or in crowded medical departments [19]. According to the World Health Organization, during "medical aerosol generating procedures," an airborne transmission of SARS-CoV-2 infection, through droplet nuclei (aerosols), can be encountered [26]. Until now, airborne transmission of SARS-CoV-2 has been demonstrated only in a few experimental studies, and not for humans. In the absence of aerosol-generating procedures, further studies are needed in order to determine the role of aerosols in SARS-CoV-2 transmission. Considering the small number of studies that evaluated the SARS-CoV-2 transmission in medical departments, we aimed to evaluate the impact of heating, ventilation and air-conditioning (HVAC) systems on the dispersion of infectious aerosols, and possibly of COVID-19 transmission, in a cardiac intensive care unit. We chose this coronary intensive care unit due to the increased addressability of patients with serious health problems, who may require orotracheal intubation and mechanical ventilation.

Airborne transmission occurs more frequently in indoor environments where people spend over 90% of their time [27], and it involves generation, transformation, transport and finally inhalation of aerosols. Ventilation is one of the most important factors that influence airborne transmission [10]. Thus far, few studies have demonstrated an association between ventilation of buildings and the transmission of airborne infections [28–30]. Furthermore, there are no sufficient studies regarding the minimum ventilation requirements in hospitals, and especially in intensive care units, regarding the

airborne transmission infections. Air purifiers with high-efficiency particulate air (HEPA) filters may be a complementary way for removal of SARS-CoV-2 aerosols in healthcare settings. It is known that the disease spreads through droplet transmission, but studies are ongoing on what can stop or aid the transmission, despite social distancing and a proper disinfection [31]. Maintaining distance from an infected person might be insufficient and increasing the ventilation might be useful, considering that this will remove more particles [20].

Because ventilation is one of the most important factors that influence airborne transmission, it is necessary to study the dispersion, heat and mass transfer of pathogen carrying expiratory droplets for better infection control strategies. Patients hospitalized in the cardiac intensive care units are at high risk of developing major infections [32], which sometimes are associated with lethal clinical consequences and higher costs, due to prolonged hospitalizations and more frequent readmissions [33]. Reducing the risk of hospital-acquired respiratory tract infections associated with air conditioning systems is a key priority for improving intensive cardiac therapy. Considering that patients from cardiac intensive care units are older and have other comorbidities that further increases their infection risk, COVID-19 infection represents a management challenge in these cases [34].

Considering the worldwide spread of the SARS-CoV-2 infection, the large number of infected people and also deaths, we consider that it is critical to understand the modes of transmission of SARS-CoV-2, in order to develop effective prevention and control strategies. In this clinical and epidemiological context, we proposed to study the impact of heating, ventilation and air-conditioning with a variable air volume (VAV) primary air system on the dispersion of infectious aerosols, and possibly on COVID-19 transmission, in a cardiac intensive care unit.

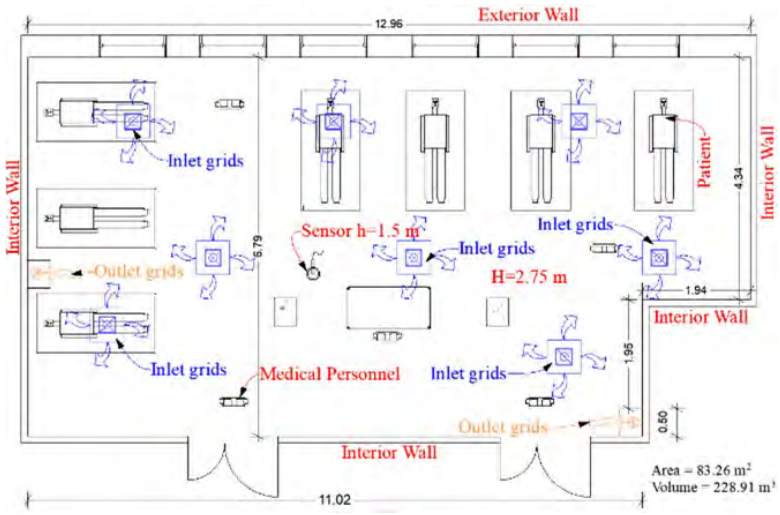
2. Materials and Methods

2.1. Room Model

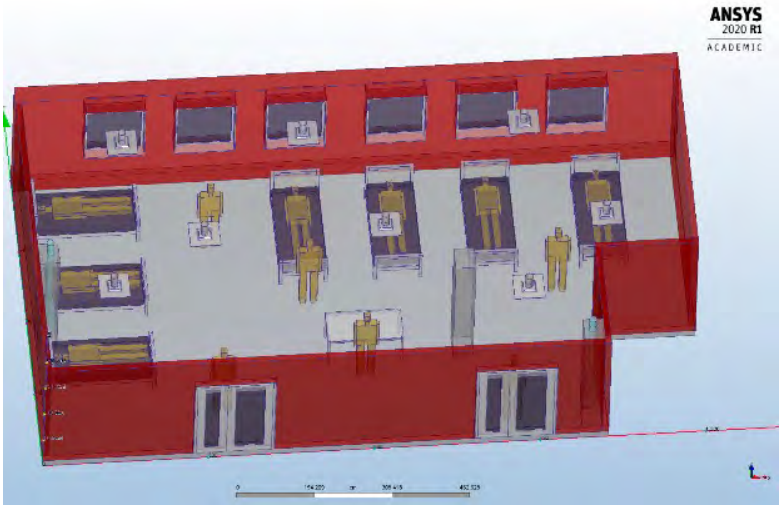
The study was performed in a Cardiac Intensive Care Unit with an increased addressability of patients with serious health problems. The cardiac intensive care unit room contains seven beds with the following geometry: Length × Width × Height = 13.00 m × 6.80 m × 2.75 m. The area of the room is around 83 m^2 and the volume is 229 m^3. The intensive care unit is placed in the third wind zone and the third climatic zone of Romania, with an outdoor temperature during winter of −18 °C (the design temperature). In order to study the dispersion of particles from coughing, influenced by air conditioning systems, we used the Computational Fluid Dynamics (CFD) approach, based on the finite element method (FEM). The CFD models are the most used in order to improve the indoor air quality, but there still are two major challenges: turbulence modeling and experimental validation. Data acquisition was performed using a TESTO 480 equipment with an indoor air quality (IAQ) sensor for airflow and particle concentration. Additionally, we used a TESTO DiSCmini particle counter to study the particle dispersion characteristics for PM_{10} and $PM_{2.5}$. We evaluated these two parameters to see the indoor air quality from the intensive care unit, with the existing heating system. Following the measurements, we observed values above the upper limit in case of $PM_{2.5}$ (the mean value was 29 μg/m^3) and at the upper limit of normal for PM_{10} (the mean value was 48 μg/m^3). We used these results to define the particle concentration when we made the CFD simulation for the existing heating system. The software used for CFD analysis was ANSYS FLUENT 2020 R1, with Elastic Licensing Number 1078891, and we performed a three-dimensional (3D) numerical study of the indoor air.

The heating system from the cardiac intensive care unit used static heaters, but, unfortunately, two years ago it was severely damaged by a fire. Considering the recommendation of the Federation of European Heating, Ventilation and Air Conditioning Associations (REHVA) [10] and the needs for thermal comfort and indoor air quality, it was changed with a heating, ventilation and air conditioning system (HVAC) (Figure 1). The HVAC system has seven inlet grids with the dimension of 600 × 600 mm and two outlet grids of 700 × 300 mm, placed in the lower third of the room height. The total airflow rate is 8400 m^3/h and the system work with 100% fresh air supply. The airflow rate for each inlet grid

is 1200 m^3/h and for the outlet grids is 85% of the total flow, in order to maintain an overpressure of 12.5 Pa, compared to the connecting rooms. The HVAC system has the following operating parameters: temperatures 24–26 °C and humidity between 30 and 60%.



(**a**)



(**b**)

Figure 1. (**a**) Floor plan of the cardiac intensive care unit with the proposed heating, ventilation and air conditioning system (HVAC); (**b**) the proposed three-dimensional (3D) model of the cardiac intensive care unit from Ansys 2020 R1 software.

We measured the indoor and outdoor temperatures during winter and also taking into account the envelope parameters and the thermal resistance of the walls and windows, we had the boundary conditions to develop the model for computational fluid dynamics.

2.2. Modeling Turbulence

Based on literature studies, we selected three different turbulence models for CFD analysis and for the validation of the model: the standard k-ε model, SST-k-ω and RNG-k-ε.

The most used models for indoor climate modeling are k-ε and k-ω. These two models fall into the Reynolds-Averaged Navier-Stokes (RANS) model category. The standard k-ε model is the most

used today. The basic idea was to develop an equation for ε, including reasonable approximations for coefficients and to solve the equation of k with a similar equation.

The equations are expressed as follows:

$$\frac{\partial(\rho\, u_i)}{\partial t} + \frac{\partial(\rho\, u_i u_j)}{\partial x_j} = \frac{\partial}{\partial x_j}\left[(\mu + \mu_t)\left(\frac{\partial \overline{u}_i}{\partial x_j} + \frac{\partial \overline{u}_j}{\partial x_i}\right)\right] - \frac{\partial p}{\partial x_j} \quad (1)$$

where:

$$\mu_t = C_\mu k^2/\varepsilon \quad (2)$$

The kinetic energy equation is of the form:

$$\rho\,\frac{\partial k}{\partial t} + \rho\, u_j \frac{\partial k}{\partial x_j} = \frac{\partial}{\partial x_j}\left[(\mu + \mu_t/\sigma_k)\frac{\partial k}{\partial x_j}\right] + P_k - \varepsilon \quad (3)$$

Dissipation rate:

$$\rho\,\frac{\partial \varepsilon}{\partial t} + \rho\, u_j \frac{\partial \varepsilon}{\partial x_j} = \frac{\partial}{\partial x_j}\left[(\mu + \mu_t/\sigma_\varepsilon)\frac{\partial \varepsilon}{\partial x_j}\right] + C_{\varepsilon 1}\frac{\varepsilon}{k}P_k - C_{\varepsilon 2}\frac{\varepsilon^2}{k} \quad (4)$$

where the closing coefficients are defined as follows: $C_{\varepsilon 1} = 1.44$; $C_{\varepsilon 2} = 1.92$; $C_\mu = 0.09$; $\sigma_k = 1.0$; $\sigma_\varepsilon = 1.3$.

In a more recent version of the k-ε model a group renormalization theory (RNG) is used [35]. The RNG model proposes a modification of the transport equation where the source term is solved as follows:

$$S_\varepsilon = \frac{\varepsilon}{k}(C_{\varepsilon 1}P - C_{\varepsilon 2}D) - R \quad (5)$$

In the standard model k-ε, the term R is missing; the term R is defined as follows:

$$R = \frac{C_\mu \eta^3(1 - \eta/\eta_0)}{1 + \beta\eta^3}\frac{\varepsilon^2}{k} \quad (6)$$

where β and η_0 are constant and have the values 0.015 and 4.38, respectively.

The effect that the correction has on the standard model k-ε, the introduction of this term R is the ability to react to the rapid change of voltage and the simplification of the curvature of current lines.

The constants in the turbulent transport equation have the following values: $C_\mu = 0.0845$, $\sigma_k = 0.718$; $\sigma_\varepsilon = 0.718$, $C_{\varepsilon 1} = 1.42$; $C_{\varepsilon 2} = 1.68$.

The RNG k-ε model is better to model high and low Reynolds numbers in the same flow. This is the reason why this turbulence model is preferred for ventilation, air quality problems and airborne infection in healthcare units. Additionally, in our study, we observed the validation of the model for the RNG k-ε turbulence model.

The k-ω model was developed by Kolmogorov [36]. It has several advantages over the k-ε model, being able to calculate the unfavorable effects of pressure gradients. The Shear Stress Transport model (SST-k-ω) was first stated by Menter [37]. The equations describing the SST-k-ω model is based on both components of the k-ε and k-ω turbulence model.

Kinetic energy equation:

$$\frac{\partial \rho\, k}{\partial t} = \tau_{ij}\frac{\partial u_i}{\partial x_j} - \beta * \rho\, k\omega + \frac{\partial}{\partial x_j}\left[(\mu + \sigma_k \mu_t)\frac{\partial k}{\partial x_j}\right] \quad (7)$$

Dissipation rate:

$$\frac{\partial \rho\, \omega}{\partial t} = \frac{\gamma}{\nu_t}\tau_{ij}\frac{\partial u_i}{\partial x_j} - \beta * \rho\, \omega^2 + \frac{\partial}{\partial x_j}\left[(\mu + \sigma_k \mu_t)\frac{\partial \omega}{\partial x_j}\right] - 2\rho\,(1 - F_1)\sigma_{\omega 2}\frac{1}{\omega}\frac{\partial k}{\partial x_j}\frac{\partial \omega}{\partial x_j} \quad (8)$$

where:

$$2\rho\,(1-F_1)\sigma_{\omega 2}\frac{1}{\omega}\frac{\partial k}{\partial x_j}\frac{\partial \omega}{\partial x_j} \quad (9)$$

represents the cross-diffusion rate

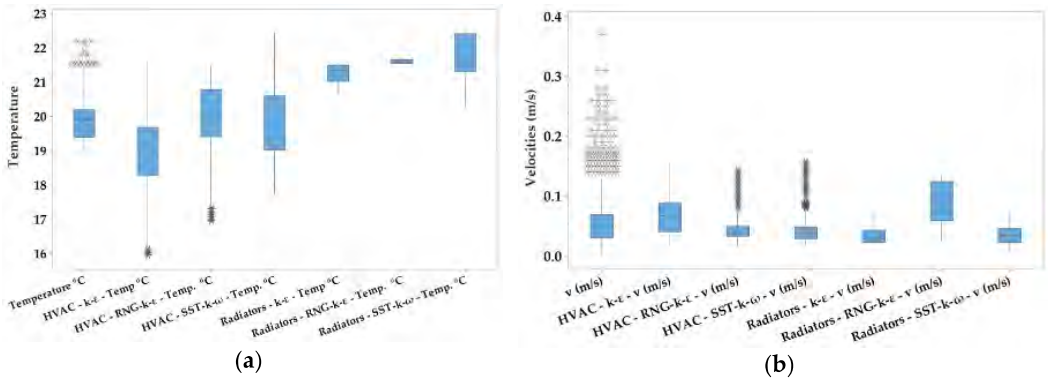
$$P_\omega = \gamma\frac{\omega}{k}\tau_{ij}\frac{\partial u_i}{\partial x_j} \quad (10)$$

represents the production term

$$\nu_t = \frac{k}{\omega}. \quad (11)$$

The model constants have the following values: $\sigma_{k,1} = 1.176$, $\sigma_{k,2} = 1$, $\sigma_{\omega,1} = 2$, $\sigma_{\omega,2} = 1.168$, $\alpha_1 = 0.31$, $\beta_{i,1} = 0.075$, $\beta_{i,2} = 0.0828$.

Subsequently, we compared the values for temperature and air velocities measured with the indoor air quality sensor with those from numerical simulations, and we observed the validation of our model only for the RNG-k-ε turbulence model, the differences between these values being below 10% (Figure 2). Considering the validation of our model for the RNG-k-ε turbulence model, the results presented in our study are only for this turbulence model.



(**a**) (**b**)

Figure 2. Boxplot of temperature (**a**) and air velocities (**b**) variation from indoor air quality sensors, static heaters and heating, ventilation and air conditioning (HVAC) system, for the three turbulence models (standard k-ε, SST-k-ω and RNG-k-ε).

2.3. Time Discretization

In addition to the steady-state analysis, we used a transient analysis to see the time dispersion of particles from coughing, influenced by air conditioning systems. The proper selection of cough simulation and particle advancement time steps are very important and also challenging. It depends on the nature and turbulent characteristics of the flow and also on the space grid refinement [30]. For an accurate dispersion of the droplets in time, we considered three criteria: the droplets did not cross more than one grid cell for each time step; the time step was smaller than that of the eddy lifetime and crossing time. To investigate the behavior of the cough droplets induced from the patients and influenced by HVAC, the discrete phase model was used in ANSYS FLUENT 2020 R1, in order to predict the trajectory of the droplets. Lagrangian simulations can predict the trajectory of a particle through the airflow and also permits the simulation of airflow with particles, being appropriate for solid and liquid particles from airflow [38]. In order to analyze the particle motion within the room, we used the discrete phase model, based on the Lagrangian discrete random walk model. This can be made by integrating and equating the particle inertia with the force that acts on the droplet in the Lagrangian reference [39]. In our case, the equation for the z-direction is:

$$\frac{du_d}{dt} = F_D(U-U_d) + g_z\frac{(\rho_d-\rho)}{\mu} + F_z \quad (12)$$

where:

$F_D(U - U_d)$ is the drag force per unit droplet mass;

U_d is the velocity of the droplet;

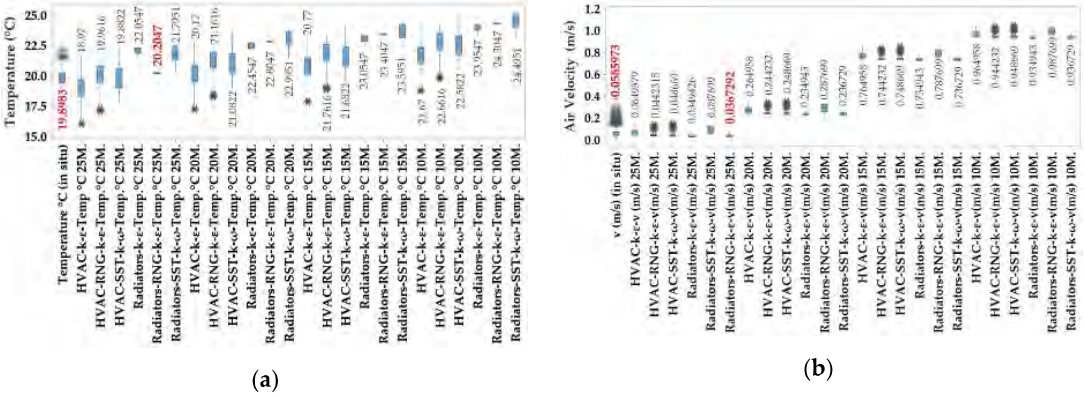
ρ_d is the density of the droplet;

g_z is the force of gravity of the droplet in z direction;

μ is the molecular viscosity

F_z is an additional force.

Using an HP Platform Z840, with two Xeon Processor E5-2690 v4, we performed the simulation on this model, which lasted over 672 h (4 weeks). We made an initial discretization of 10 million elements. Afterwards, we increased the number of meshing elements to 15, 20 and 25 million, until the difference between the models was under 1% variation (Figure 3).



(**a**) (**b**)

Figure 3. Results for mesh dependents (**a**) temperature and (**b**) air velocities from indoor air quality sensors, static heaters and heating, ventilation and air conditioning (HVAC) system, for the three turbulence models (standard k-ε, SST-k-ω and RNG-k-ε) and four cases of discretization (10, 15, 20, 25 M).

2.4. Boundary Conditions

In order to validate our study, ANSYS FLUENT 2020 R1 was used. The validation process consists in observing the reliability and accuracy of the ANSYS Fluent CFD program used to simulate a numerical case by comparing it with experimental data. Additionally, we used the same boundary conditions that were used during the experiment.

For the HVAC system, we analyzed three scenarios that followed the dispersion of pathogen carrying expiratory droplets particles from patients admitted to the intensive care unit and possibly infected with COVID-19. Coughing and sneezing are the most important processes of virus transmission because of the highest droplet concentration [40]. Considering that coughing is the common symptom for most respiratory tract infections, in our study we used boundary conditions for the coughing process. The characteristics of coughed droplets for the CFD simulation were selected by taking into account the existing data from the literature [40–44]. We used seven manikins as patients and four manikins as medical personnel. The dimensions of the manikins were similar to those of a real human body, and the mouth opening area of the manikin was 3.5 cm^2 [41]. We observed the dispersion in time and space of the particles from coughing, influenced by the HVAC system, depending on the location of the patients in the intensive care unit: in the right side, left side and in the middle part of the intensive care unit (Figure 4).

The advantage of CFD simulations is that they are inexpensive compared to experiments, but they need accurate flow-thermal boundary conditions, which are very important for the prediction of disease transmission. The most important boundary conditions for expiration are coughing flow rate and jet direction, mouth opening areas, temperature and size distribution of the virus droplets [41–44]. In all three proposed scenarios, the manikin coughed three times, and the duration of one act of coughing was 0.3 s. The CFD simulations for prediction of disease transmission used the same velocity,

cough flow rate and mouth opening area. The particle size was between 2.5 μm and 200 μm. In Table 1 we presented the boundary conditions used in our CFD simulations.

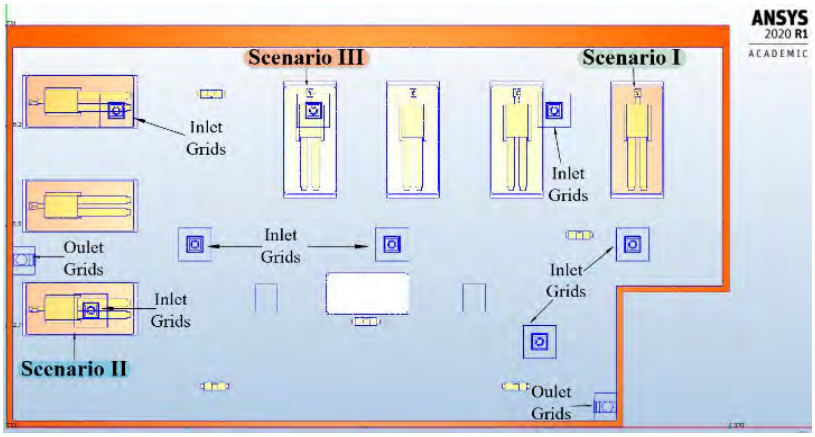


Figure 4. The three scenarios for the HVAC system, according to the location of the patients in the intensive care unit.

Table 1. The boundary conditions used for computational fluid dynamics (CFD)-finite element method (FEM) simulations.

No.	Envelope Element	Heating System	
		Static Heaters	HVAC Heating System
CFD software—ANSYS FLUENT 2020 R1			
Turbulence model The RNG K-ε model			
Pressure (Pa)—Relative pressure			
Temperature (°C)	Exterior Walls	−16	−16
	Ceiling	+20	+20
	Input grids for hot air		+30
	Floor plate	+20	+20
	Windows and Doors	+18	+18
Heat transfer coefficient (film coefficient) U (W/m^2 K)	Exterior walls	12	12
	Windows and doors	3	3
	Ceiling	3.5	3.5
	Floor plate	3	3
Air velocity(m/s)	Inlet grids for hot air	-	1.2
	Extraction grids	-	1
Heat flux (W/m^2)	Static heater	200	-
Heat flow of mannequins		80 (W)	
Coughing velocity		12 m/s	
The total cough volume		1.1 dm^3	
Mouth opening area		3.5 cm^2	
Cough flow rate		5 dm^3/s (L/s)	
Duration of one act of coughing		0.3 s	
The cough jet direction (supine) position		80°	
Temperature of the droplets		35 °C	
Max droplet diameter		200 μm	
Min droplet diameter		2.5 μm	
Particle cough density		2.5 $μg/dm^3$	
Interaction between particles and walls-discrete phase conditions	Floor—trap; around—escape; inlet—mouth—escape; mannequin body—reflect; ceiling and walls—reflect.		

After establishing the geometric model and the competition of the boundary conditions, we made the following simulations (Figure 5).

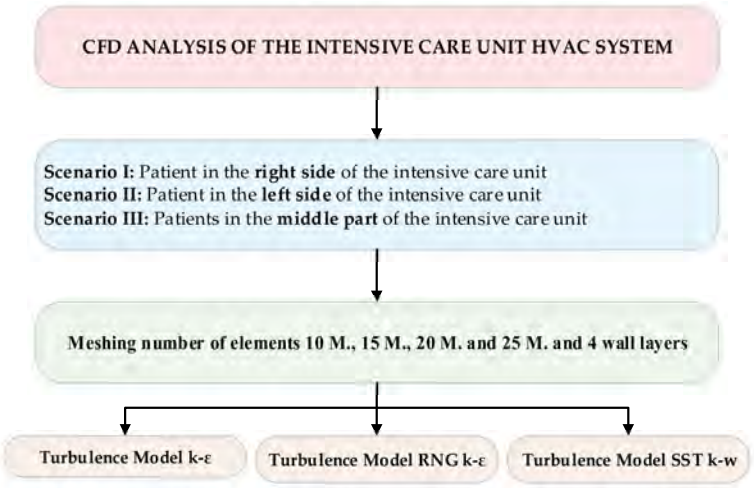


Figure 5. CFD analysis scheme for the cardiac intensive care unit simulations.

3. Results

3.1. Particle Dispersion for Static Heaters and HVAC

Initially, we analyzed the particle dispersion generated by the heating system that was present before the fire: static heaters. Subsequently, we performed the same analysis for the heating system that will be put into use after rehabilitation, namely HVAC. We wanted to highlight the difference between these two heating systems, in terms of dispersion of infectious aerosols (Figure 6).

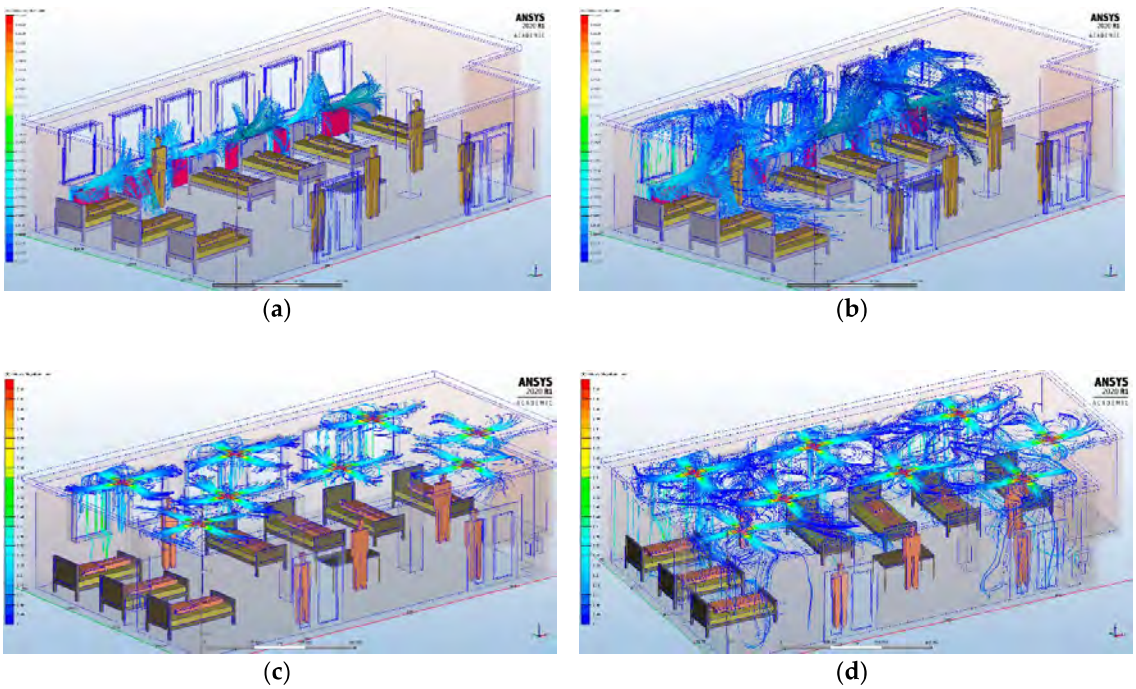


Figure 6. Transient analysis of particles dispersion with no coughing and breathing events of the patients for static heaters at (**a**) 2 s and (**b**) 5 s, and the air inflow dispersion for heating, ventilation and air conditioning systems at (**c**) 2 s and (**d**) 5 s.

For the simulation performed with static heaters, we defined a number of 6000 particles with dimensions between 2.5–200 micrometers, located in the maximum area of influence of the air currents generated by the static heaters. In the case of heating, ventilation and air conditioning systems, we also

used a number of 6000 particles with the same dimensions, which were split equally to the seven inlet grids. In a transient analysis of particle dispersion at 3 s after the air currents are generated by each heating system, we observed the distribution of particles near the static heaters, without them spreading throughout the intensive care unit. With the HVAC system, the particles are distributed on all four directions at the ceiling, foreshadowing a uniform distribution throughout the room. Although the HVAC system may initially appear to achieve a faster and more uniform distribution of infecting particles, this is counterbalanced by the possibility of using HEPA filters, which are an adjunctive means for the decontamination of SARS-CoV-2 aerosols in healthcare settings [45–47].

3.2. Scenario 1

When the infected patient is on the right side of the intensive care unit and coughs, the droplets transmission is prompted by the HVAC system in the middle part of the room. We observe a fast transmission of the infecting particles, and after a period of only 5 s, they are spread almost in the entire intensive care unit (Figure 7).

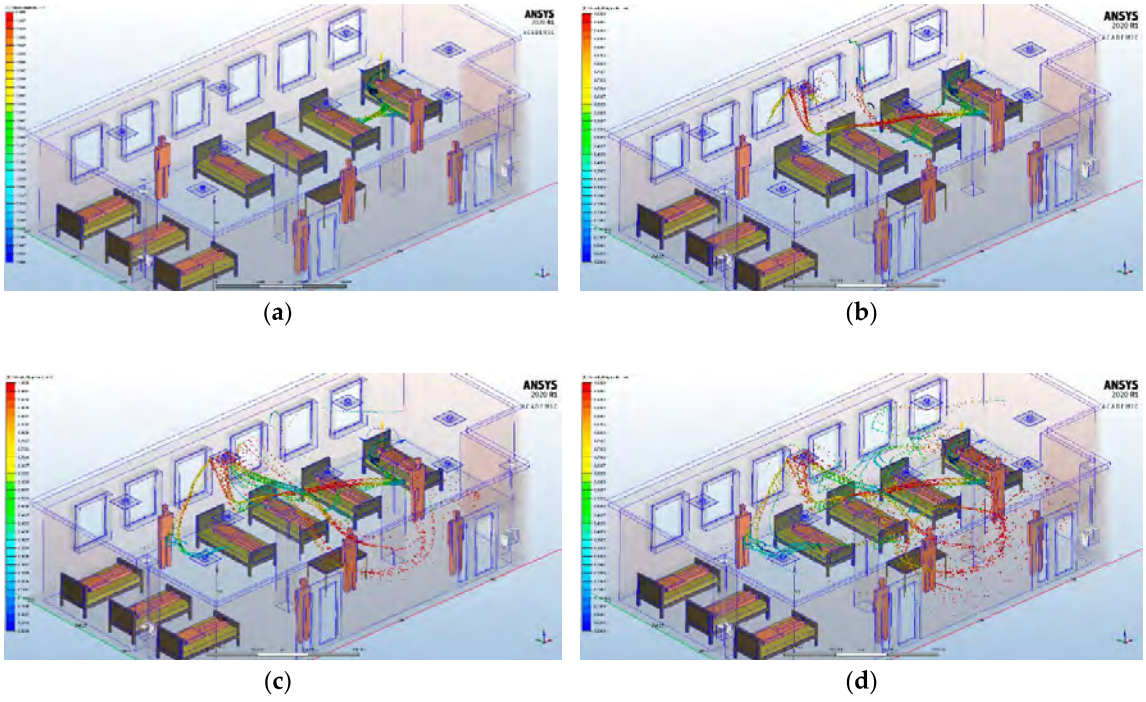


Figure 7. Transient analysis of the lighter particles dispersion carried into the air by buoyancy for HVAC systems, at different time intervals, if the infected patient is in the right part of the intensive care unit: (**a**) 2 s; (**b**) 3 s; (**c**) 4 s; (**d**) 5 s.

3.3. Scenario 2

If the infected patient is on the left side of the intensive care unit and coughs, the droplets are also transmitted by the HVAC system in the central part of the room (Figure 8). Therefore, we observe that the HVAC system acts in the sense of a uniform distribution of the air currents, and consequently, of the infecting particles emitted by the patients' cough. The fact that we did not notice a difference between the way the infecting particles are spread in these two scenarios shows that the HVAC system causes a rapid transmission, from the walls to the center, of the infecting particles. This is mainly influenced by the distribution of the outlets grids of the HVAC system, which in our case are located at the center of the intensive care unit.

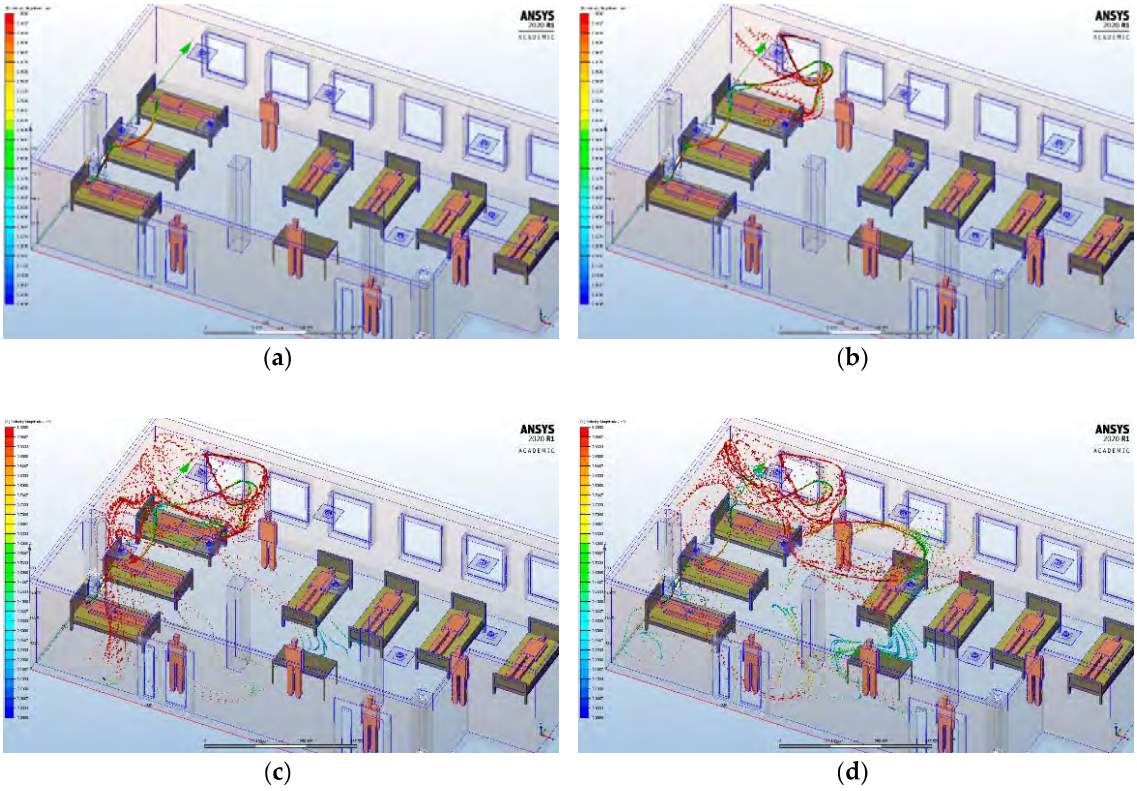


Figure 8. Transient analysis of the lighter particles dispersion carried into the air by buoyancy for HVAC systems, at different time intervals, if the infected patient is in the left part of the intensive care unit: (**a**) 2 s; (**b**) 3 s; (**c**) 4 s; (**d**) 5 s.

3.4. Scenario 3

In the third scenario, we aimed to evaluate the infecting particle transmission if the patient is sitting in the bed from the middle of the intensive care unit (Figure 9). In case of this patient, considering that the inlet grid is located above the patient's bed and also the fact that we simulated the patient's cough almost in a vertical direction, determined a different transmission of the particles inside the intensive care unit. Thus, they were initially carried on the wall and the window behind the bed, then down under the bed, and after that to the office from the center of the intensive care unit. We can conclude that the presence of an HVAC system causes a distribution of infectious particles not only on directly exposed surfaces, but also on less exposed or hidden areas.

Comparing the results of the three proposed scenarios, it appears that, for our proposed HVAC system, the flow field and velocity distribution induced by the high turbulence of inlet grids, combined with the air outlet grids, determines wide recirculation zones, from the walls to the center of the room. These results could be due to the high rate level of ventilation. In the first two scenarios, we did not observe a difference between the way the infecting particles are spread, from the walls to the center of the intensive care unit. In the third scenario, it can be found that the location of the patient in the intensive care unit, the position of the inlet grid above the patient's bed and also the fact that we simulated the patient's cough almost in a vertical direction determined a different transmission of the infecting particles. However, the final path of the infecting particles was also to the center of the room.

For the HVAC system used in our simulation, the variable directions of the airflow due to the high turbulence air inlet grids provide a widespread and a homogeneous distribution of the infecting particles ("coanda effect") on the ceiling, followed by a progressive drop down.

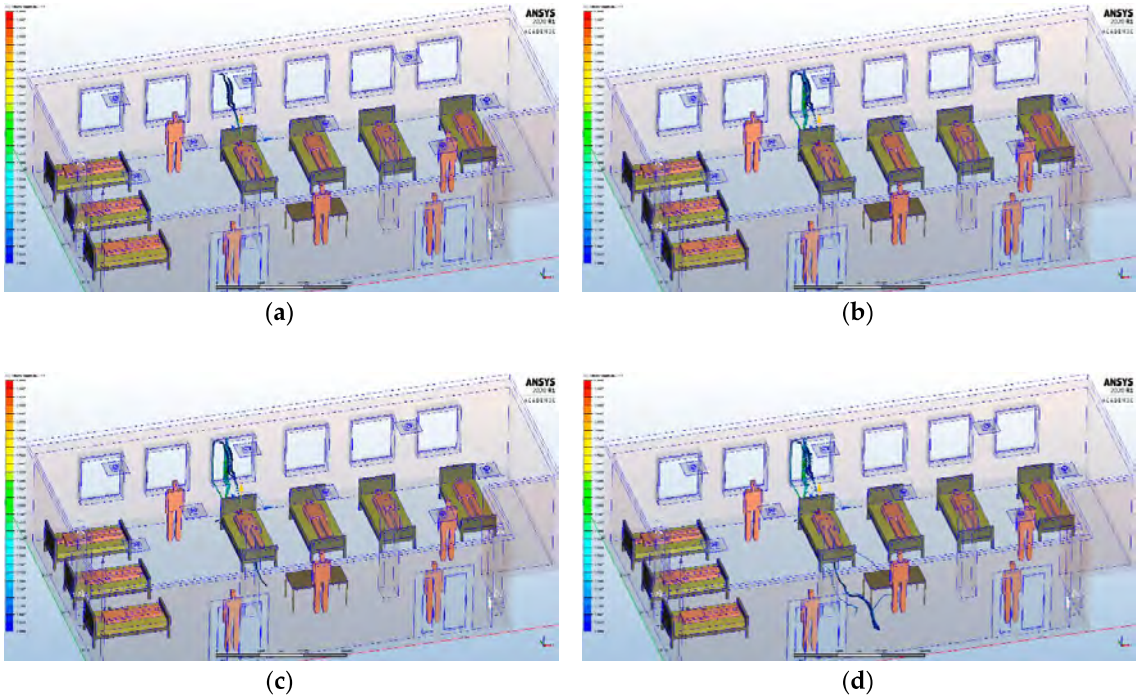


Figure 9. Transient analysis of the lighter particles dispersion carried into the air by buoyancy for HVAC systems, at different time intervals, if the infected patient is in the bed from the middle of the intensive care unit: (**a**) 2 s; (**b**) 3 s; (**c**) 4 s; (**d**) 5 s.

4. Discussion

In an intensive care unit, it is necessary to control the patient risk from airborne diseases, and the HVAC system can have a beneficial impact on patients' healing processes and minimizing COVID-19 transmission. The present study highlights that CFD-FEM approach is useful for understanding the dispersion of infectious aerosols, and possibly of COVID-19-carrying droplets in a cardiac intensive care unit equipped with an HVAC system that has a variable air volume. The transient analysis of simulation results regarding particle tracing, paths and distance highlights the rapidity of the appearance of contaminated areas. Although it is known that a poor ventilation in confined indoor spaces increases the risk of respiratory infections transmission [48,49], we consider that the results from our CFD particle simulations have a great importance on the dispersion of infectious aerosols, and possibly of SARS-CoV-2 infection. The novelty of our study is that it provides useful indications for controlling dispersion and concentration zones for infectious aerosols and possibly of COVID-19-carrying droplets. Additionally, our results can provide important recommendations on the selection of the best position of the inlet and outlet grids. From our CFD simulations, we observed that it is very important to select a proper position for inlet and outlet grids, considering the fact that in scenario 2 the particles were dispersed more than those from the other two scenarios, which we did not expect. An explanation may be the onset of local turbulences that can cause an unpredictable particle dispersion.

Only a few isolated cases of COVID-19 transmission events have been associated with closed spaces, also in asymptomatic patients [50,51], aided by air conditioning systems. A recent Chinese study pointed out the possibility of COVID-19 transmission, aided by air-conditioning systems in a restaurant. There were 10 cases from three families that have eaten lunch at the same restaurant. Those who were sitting along the line of airflow generated by the air-conditioning were infected, while those from other parts of the restaurant were not infected. They concluded that droplet transmission was facilitated by air-conditioned ventilation and the most important factor for infection was the direction of the airflow [52]. Additionally, two outbreaks in China have been described, where the authors suspected the air conditioning systems using a recirculating mode as a probable aid to COVID-19

transmission [53]. Thus, while the virus can be airborne, air-conditioning systems could aid virus transmission, under certain conditions such as airflow, improper filters or lack of ventilation.

High Efficiency Particulate Air filters have demonstrated good performance with particles of the SARS Cov-2 virus size (approximately 70−120 nm) and are used in airplanes and in healthcare settings. Their important role in reducing the infection risk and in maintaining thermal comfort was demonstrated in a modeling study of the infection risk from SARS Cov-1 [54]. There are also some speculations regarding the use of air filtration technology (HEPA filters) in damping the rate of viral spread. Studies show that droplets typically expelled by infected patients, range from droplets that we are all able to see, to those too small for our eyes (0.5 to 15 microns). Additionally, studies of other viruses suggest that droplets of 1 micron are capable of carrying enough virus particles to cause infections [44]. HEPA filters capture particles of this size and also capture 99.97% of particles that are more than or equal to 0.3 microns in diameter. In theory, some experts say that considering the possibility of HEPA filters to capture particles of such small size, all SARS Cov-2 virions could be filtered and captured, in this way reducing the contamination of the space [31]. Thus, they propose installing HVAC systems with HEPA filters not only in the intensive care units, but also in high-traffic spaces, in order to decrease the number of viral particles present.

On 3 April 2020, the Federation of European Heating, Ventilation and Air Conditioning Associations (REHVA), published the latest version of a guidance document where they summarize the advice on the operation and use of building services in order to prevent the spread of the COVID-19 [10].

1. Increase air supply in order to bring as much outside air as reasonably possible. Thus, their recommendation is to start ventilation at least two hours before the building usage time and switch to lower speed two hours after the building usage time, and keep the ventilation on 24/7, with lowered, but not switched off, ventilation rates when people are absent [10].
2. Humidification and air-conditioning have no effect in limiting the transmission of the virus, thus, they do not need to be adjusted. Coronaviruses are susceptible only to a humidity above 80% and a high temperature, above 30 °C [10]. Unfortunately, these parameters are not acceptable in buildings, because they will increase the microbial growth and will affect the indoor thermal comfort [10].
3. Another recommendation is to inspect the heat recovery devices considering the fact that maintenance personnel should follow the standard safety procedures of dusty work [10]. They also mention that when the HVAC system is equipped with a twin coil unit or another heat recovery device that completely separates the exhaust air side to the supply airside, virus particle transmission via heat recovery devices is no longer a problem. Regarding the use of recirculation, it is recommended to avoid central recirculation during SARS-CoV-2 episodes, in order to avoid resuspension of virus particles at room level [10].
4. Regarding the normal duct cleaning and maintenance procedures, no changes are needed and the most important two things are to increase fresh air supply and avoid recirculation of air [10].
5. Change of outdoor air filters or their replacement with other types of filters is not recommended sooner than normal [10].
6. Room air cleaners have a similar effect compared to ventilation and they remove particles from air. Devices that use electrostatic filtration principles for the supply or room air treatment may be useful [10].

Our study has some limitations and can be further improved. Firstly, this is only a numerical simulation study that evaluated the dispersion of infectious aerosols, and possibly of COVID-19 airborne transmission, based on the characteristics of SARS-CoV-2 and on the methods used in previous studies to evaluate airborne transmission for other infectious diseases. Further studies are needed in order to determine the impact of HVAC-systems on SARS-CoV-2 transmission in real cases. Secondly, the results of numerical simulations are only qualitative, by images, and we only considered exhaled droplets by coughing. Other investigations may consider quantitative results for other respiratory activities, such as breathing, sneezing or speaking. Thirdly, the composition of the

infectious aerosols is of great significance in order to evaluate the infectious risk, and this deserves further study. Another limitation of our study is that we removed from our simulations the heavier particles, which usually fall to the ground, and we only focused on the lighter ones, which are carried into the air. This may be the reason why it seems that droplets air-dispersion is linear, rather than "clouds of droplets." Additionally, the CFD characterization of the proposed HVAC system is more "case specific" for our cardiac intensive care unit. We are working now to find a more general CFD characterization that can be useful for the analysis of other targets, such as public transport, theaters, philharmonics and amphitheaters from educational units.

In an intensive care unit, it is necessary to have a negative pressure in order to reduce aerosol escape and also a high air-change rate to remove the infectious particles. Unfortunately, with the static heaters, these parameters cannot be achieved. By using an HVAC system, it is possible to create not only a negative pressure; in addition, we can prevent the transmission of the infectious particles outside the room when the medical staff use the door. Transmission of the infecting particles due to the air inlet grids is widespread and homogeneously distributed. This is counterbalanced by the possibility of using HEPA filters that are able to remove at least 90% of small particles, from inside and outside air.

5. Conclusions

In conclusion, our study provides the mechanism for the dispersion of infectious aerosols, and the possibly of COVID-19 infection, by air conditioning systems. It also highlights important recommendations regarding the selection of the best position of the inlet and outlet grids in an HVAC system. Additionally, it can provide important recommendations for disease control and optimization of ventilation in intensive care units, by increasing the rate of air change, decreasing recirculation of air and increasing the use of outdoor air and HEPA filters.

Author Contributions: Conceptualization, L.A., F.-E.Ț., R.S. and C.S.; methodology, C.-G.P., S.-V.H.; software, F.-E.Ț., S.-V.H.; validation, M.V., V.C. and C.S.; formal analysis, R.S.; investigation, L.A. and F.-E.Ț.; resources, C.-G.P.; data curation, S.-V.H.; writing—original draft preparation, L.A.; writing—review and editing, L.A., R.S., M.A.M. and C.S.; visualization, I.-L.Ș. and M.A.M.; supervision, M.V., V.C. and I.-L.Ș. All authors contributed equally to this manuscript. All authors have read and agreed to the published version of the manuscript.

Funding: This research received no external funding.

Conflicts of Interest: The authors declare no conflict of interest.

References

1. Kutter, J.S.; Spronken, M.I.; Fraaij, P.L.; Fouchier, R.A.; Herfst, S. Transmission routes of respiratory viruses among humans. *Curr. Opin. Virol.* **2018**, *28*, 142–151. [CrossRef] [PubMed]
2. Siegel, J.D.; Rhinehart, E.; Jackson, M.; Chiarello, L.; Health Care Infection Control Practices Advisory Committee. 2007 guideline for isolation precautions: Preventing transmission of infectious agents in health care settings. *Am. J. Infect. Control* **2007**, *35*, S65–S164. [CrossRef] [PubMed]
3. Gralton, J.; Tovey, E.; McLaws, M.L.; Rawlinson, W.D. The role of particle size in aerosolised pathogen transmission: A review. *J. Infect.* **2011**, *62*, 1–13. [CrossRef] [PubMed]
4. Fernstrom, A.; Goldblatt, M. Aerobiology and its role in the transmission of infectious diseases. *J. Pathog.* **2013**, *2013*, 493960. [CrossRef] [PubMed]
5. Herfst, S.; Böhringer, M.; Karo, B.; Lawrence, P.; Lewis, N.S.; Mina, M.J.; Russell, C.J.; Steel, J.; de Swart, R.L.; Menge, C. Drivers of airborne human-to-human pathogen transmission. *Curr. Opin. Virol.* **2017**, *22*, 22–29. [CrossRef]
6. Villafruela, J.M.; Olmedo, I.; Berlanga, F.A.; Ruiz de Adana, M. Assessment of displacement ventilation systems in airborne infection risk in hospital rooms. *PLoS ONE* **2019**, *14*, e0211390. [CrossRef]
7. Tang, J.W.; Nicolle, A.; Pantelic, J.; Koh, G.C.; De Wang, L.; Amin, M.; Klettner, C.A.; Cheong, D.K.; Sekhar, C.; Tham, K.W. Airflow dynamics of coughing in healthy human volunteers by shadowgraph imaging: An aid to aerosol infection control. *PLoS ONE* **2012**, *7*, e34818. [CrossRef]

8. Tang, J.W.; Nicolle, A.D.; Klettner, C.A.; Pantelic, J.; Wang, L.; Suhaimi, A.B.; Tan, A.Y.; Ong, G.W.; Su, R.; Sekhar, C.; et al. Airflow dynamics of human jets: Sneezing and breathing-potential sources of infectious aerosols. *PLoS ONE* **2013**, *8*, e59970. [CrossRef]
9. Gupta, J.K.; Lin, C.H.; Chen, Q. Characterizing exhaled airflow from breathing and talking. *Indoor Air* **2010**, *20*, 31–39. [CrossRef]
10. Federation of European Heating VaACA. COVID-19 Guidance: REHVA. 2020. Available online: https://www.rehva.eu/fileadmin/user_upload/REHVA_COVID-9_guidance_document_ver2_20200403_1.pdf (accessed on 3 April 2020).
11. Pica, N.; Bouvier, N.M. Environmental factors affecting the transmission of respiratory viruses. *Curr. Opin. Virol.* **2012**, *2*, 90–95. [CrossRef]
12. Dancer, S.J. Controlling hospital-acquired infection: Focus on the role of the environment and new technologies for decontamination. *Clin. Microbiol. Rev.* **2014**, *27*, 665–690. [CrossRef] [PubMed]
13. Beggs, C.; Knibbs, L.D.; Johnson, G.R.; Morawska, L. Environmental contamination and hospital-acquired infection: Factors that are easily overlooked. *Indoor Air* **2015**, *25*, 462–474. [CrossRef] [PubMed]
14. Qian, H.; Zheng, X. Ventilation control for airborne transmission of human exhaled bio-aerosols in buildings. *J. Thorac. Dis.* **2018**, *10*, S2295–S2304. [CrossRef] [PubMed]
15. Zhong, N.S.; Zheng, B.J.; Li, Y.M.; Poon, L.L.M.; Xie, Z.H.; Chan, K.H.; Li, P.H.; Tan, S.Y.; Chang, Q.; Xie, J.P.; et al. Epidemiology and cause of severe acute respiratory syndrome (SARS) in Guangdong, People's Republic of China, in February, 2003. *Lancet* **2003**, *362*, 1353–1358. [CrossRef]
16. Van Kerkhove, M.D.; Vandemaele, K.A.; Shinde, V.; Jaramillo-Gutierrez, G.; Koukounari, A.; Donnelly, C.A.; Carlino, L.O.; Owen, R.; Paterson, B.; Pelletier, L.; et al. Risk factors for severe outcomes following 2009 influenza A (H1N1) infection: A global pooled analysis. *PLoS Med.* **2011**, *8*, e1001053. [CrossRef]
17. Kim, C.J.; Choi, W.S.; Jung, Y.; Kiem, S.; Seol, H.Y.; Woo, H.J.; Choi, Y.H.; Son, J.S.; Kim, K.H.; Kim, Y.S.; et al. Surveillance of the Middle East respiratory syndrome (MERS) coronavirus (CoV) infection in healthcare workers after contact with confirmed MERS patients: Incidence and risk factors of MERS-CoV seropositivity. *Clin. Microbiol. Infect.* **2016**, *22*, 880–886. [CrossRef]
18. Sanche, S.; Lin, Y.T.; Xu, C.; Romero-Severson, E.; Hengartner, N.; Ke, R. High contagiousness and rapid spread of severe acute respiratory syndrome coronavirus 2. *Emerg. Infect. Dis.* **2020**, *26*, 1470–1477. [CrossRef]
19. WHO. Coronavirus Disease 2019 (COVID-19) Situation Report-73. Available online: https://apps.who.int/iris/handle/10665/331686 (accessed on 7 September 2020).
20. Ali, S.A.; Baloch, M.; Ahmed, N.; Ali, A.A.; Iqbal, A. The outbreak of Coronavirus Disease 2019 (COVID-19)—An emerging global health threat. *J. Infect. Public Health* **2020**, *13*, 644–646.
21. Sohrabi, C.; Alsafi, Z.; O'Neill, N.; Khan, M.; Kerwan, A.; Al-Jabir, A.; Iosifidis, C.; Agha, R. World Health Organization declares global emergency: A review of the 2019 novel coronavirus (COVID-19). *Intern. J. Surg.* **2020**, *76*, 71–76. [CrossRef]
22. Kelvin, K.-W.T.; Owen, T.-Y.T.; Cyril, C.-Y.Y.; Kwok-Hung, C.; Tak-Chiu, W.; Jacky, M.-C.C.; Wai-Shing, L.; Thomas, S.-H.C.; Chris, Y.-C.C.; Darshana, H.K.; et al. Consistent detection of 2019 novel coronavirus in saliva. *Clin. Infect. Dis.* **2020**, *71*, 841–843.
23. Eslami, H.; Jalili, M. The role of environmental factors to transmission of SARS-CoV-2 (COVID-19). *AMB Express* **2020**, *10*, 92. [CrossRef] [PubMed]
24. Van Doremalen, N.; Bushmaker, T.; Morris, D.H.; Holbrook, M.G.; Gamble, A.; Williamson, B.N.; Tamin, A.; Harcourt, J.L.; Thornburg, N.J.; Gerber, S.I.; et al. Aerosol and surface stability of SARS-CoV-2 as compared with SARS-CoV-1. *N. Engl. J. Med.* **2020**, *382*, 1564–1567. [CrossRef] [PubMed]
25. Guan, W.J.; Ni, Z.Y.; Hu, Y.; Liang, W.H.; Ou, C.Q.; He, J.X.; Liu, L.; Shan, H.; Lei, C.L.; Hui, D.S.; et al. Clinical characteristics of 2019 novel coronavirus infection in China. *N. Engl. J. Med.* **2020**, *382*, 1708–1720. [CrossRef] [PubMed]
26. WHO. Transmission of SARS-CoV-2: Implications for Infection Prevention Precautions. Available online: https://www.who.int/publications/i/item/modes-of-transmission-of-virus-causing-covid-19-implications-for-ipc-precaution-recommendations (accessed on 7 September 2020).
27. Zayas, G.; Chiang, M.C.; Wong, E.; MacDonald, F.; Lange, C.F.; Senthilselvan, A.; King, M. Cough aerosol in healthy participants: Fundamental knowledge to optimize droplet-spread infectious respiratory disease management. *BMC Pulm. Med.* **2012**, *12*, 1–12. [CrossRef] [PubMed]

28. Li, Y.; Leung, G.M.; Tang, J.W.; Yang, X.; Chao, C.Y.; Lin, J.Z.; Lu, J.W.; Nielsen, P.V.; Niu, J.; Qian, H.; et al. Role of ventilation in airborne transmission of infectious agents in the built environment–A multidisciplinary systematic review. *Indoor Air* **2007**, *17*, 2–18. [CrossRef] [PubMed]
29. Gao, X.; Wei, J.; Lei, H.; Xu, P.; Cowling, B.J.; Li, Y. Building ventilation as an effective disease intervention strategy in a dense indoor contact network in an ideal city. *PLoS ONE* **2016**, *11*, e0162481. [CrossRef] [PubMed]
30. Gao, X.; Wei, J.; Cowling, B.J.; Li, Y. Potential impact of a ventilation intervention for influenza in the context of a dense indoor contact network in Hong Kong. *Sci. Total Environ.* **2016**, *569*, 373–381. [CrossRef]
31. Morawska, L.; Tang, J.W.; Bahnfleth, W.; Bluyssen, P.M.; Boerstra, A.; Buonanno, G.; Cao, J.; Dancer, S.; Floto, A.; Querol, X.; et al. How can airborne transmission of COVID-19 indoors be minimised? *Environ. Int.* **2020**, *142*, 105832. [CrossRef]
32. Setti, L.; Passarini, F.; De Gennaro, G.; Barbieri, P.; Perrone, M.G.; Borelli, M.; Palmisani, J.; Di Gilio, A.; Piscitelli, P.; Miani, A. Airborne transmission route of COVID-19: Why 2 meters/6 feet of inter-personal distance could not be enough. *Int. J. Environ. Res. Public Health* **2020**, *17*, 2932. [CrossRef]
33. Alfonso-Sanchez, J.L.; Martinez, I.M.; Martín-Moreno, J.M.; González, R.S.; Botía, F. Analyzing the risk factors influencing surgical site infections: The site of environmental factors. *Can. J. Surg.* **2017**, *60*, 155–161. [CrossRef]
34. Shajahan, A.; Culp, C.H.; Williamson, B. Effects of indoor environmental parameters related to building heating, ventilation, and air conditioning systems on patients' medical outcomes: A review of scientific research on hospital buildings. *Indoor Air* **2019**, *29*, 161–176. [CrossRef] [PubMed]
35. Cortés, M.; Fazio, P.; Rao, J.; Bustamante, W.; Vera, S. CFD modelling of basic convection cases in enclosed environments: Needs of CFD beginners to acquire skills and confidence on CFD modelling. *Rev. Ing. Constr.* **2014**, *29*, 22–45. [CrossRef]
36. Kolmogorov, A.N. Equations of turbulent motion in an incompressible fluid. *Doklady Akademii Nauk* **1941**, *30*, 299–303.
37. Menter, F.R. Two-equation eddy-viscosity turbulence models for engineering applications. *AIAA J.* **1994**, *32*, 1598–1605. [CrossRef]
38. Qian, H.; Li, Y.; Nielsen, P.V.; Huang, X. Spatial distribution of infection risk of SRAS transmission in a hospital ward. *Build. Environ.* **2009**, *44*, 1651–1658. [CrossRef]
39. Ansys, I. *ANSYS Fluent Theory Guide*; Ansys, Inc.: Canonsburg, PA, USA, 2020.
40. Zhao, B.; Zhang, Z.; Li, X. Numerical study of the transport of droplets or particles generated by respiratory system indoors. *Build. Environ.* **2005**, *40*, 1032–1039. [CrossRef]
41. Gupta, J.K.; Lin, C.H.; Chen, Q. Flow dynamics and characterization of a cough. *Indoor Air* **2009**, *19*, 517–525. [CrossRef]
42. Zhu, S.; Kato, S.; Yang, J.H. Study on transport characteristics of saliva droplets produced by coughing in a calm indoor environment. *Build. Environ.* **2006**, *41*, 1691–1702. [CrossRef]
43. Mahajan, R.P.; Singh, P.; Murty, G.E.; Aitkenhead, A.R. Relationship between expired lung volume, peak flow rate and peak velocity time during a voluntary cough manoeuvre. *Br. J. Anaesth.* **1994**, *72*, 298–301. [CrossRef]
44. Jayaweera, M.; Perera, H.; Gunawardana, B.; Manatunge, J. Transmission of COVID-19 virus by droplets and aerosols: A critical review on the unresolved dichotomy. *Environ. Res.* **2020**, *188*, 109819. [CrossRef]
45. Tay, J.K.; Khoo, M.L.C.; Loh, W.S. Surgical considerations for tracheostomy during the COVID-19 pandemic: Lessons learned from the severe acute respiratory syndrome outbreak. *JAMA Otolaryngol. Head Neck Surg.* **2020**, *146*, 517–518. [CrossRef] [PubMed]
46. Omolo, C.A.; Soni, N.; Fasiku, V.O.; Mackraj, I.; Govender, T. Update on therapeutic approaches and emerging therapies for SARS-CoV-2 virus. *Eur. J. Pharmacol.* **2020**, *883*, 173348. [CrossRef] [PubMed]
47. Chigurupati, R.; Panchal, N.; Henry, A.M.; Batal, H.; Sethi, A.; D'innocenzo, R.; Mehra, P.; Krishnan, D.G.; Roser, S.M. Considerations for oral and maxillofacial surgeons in COVID-19 era: Can we sustain the solutions to keep our patients and healthcare personnel safe? *J. Oral Maxillofac. Surg.* **2020**, *78*, 1241–1256. [CrossRef] [PubMed]
48. Correia, G.; Rodrigues, L.; Silva, M.G.; Gonçalves, T. Airborne route and bad use of ventilation systems as non-negligible factors in SARS-CoV-2 transmission. *Med. Hypotheses* **2020**, *141*, 109781. [CrossRef] [PubMed]
49. Luongo, J.C.; Fennelly, K.P.; Keen, J.A.; Zhai, Z.J.; Jones, B.W.; Miller, S.L. Role of mechanical ventilation in the airborne transmission of infectious agents in buildings. *Indoor Air* **2016**, *26*, 666–678. [CrossRef] [PubMed]

50. Lu, J.; Gu, J.; Li, K.; Xu, C.; Su, W.; Lai, Z.; Zhou, D.; Yu, C.; Xu, B.; Yang, Z. COVID-19 outbreak associated with air conditioning in restaurant, Guangzhou, China, 2020. *Emerg. Infect. Dis.* **2020**, *26*, 1628–1631. [CrossRef]
51. Rothe, C.; Schunk, M.; Sothmann, P.; Bretzel, G.; Froeschl, G.; Wallrauch, C.; Zimmer, T.; Thiel, V.; Janke, C.; Guggemos, W.; et al. Transmission of 2019-nCoV infection from an asymptomatic contact in Germany. *N. Engl. J. Med.* **2020**, *382*, 970–971. [CrossRef]
52. Liu, Y.; Ning, Z.; Chen, Y.; Guo, M.; Liu, Y.; Gali, N.K.; Sun, L.; Duan, Y.; Cai, J.; Westerdahl, D.; et al. Aerodynamic analysis of SARS-CoV-2 in two Wuhan hospitals. *Nature* **2020**, *582*, 557–560. [CrossRef]
53. Morawska, L.; Cao, J. Airborne transmission of SARS-CoV-2: The world should face the reality. *Environ. Int.* **2020**, *139*, 105730. [CrossRef]
54. You, R.; Lin, C.H.; Wei, D.; Chen, Q. Evaluating the commercial airliner cabin environment with different air distribution systems. *Indoor Air* **2019**, *29*, 840–853. [CrossRef]



© 2020 by the authors. Licensee MDPI, Basel, Switzerland. This article is an open access article distributed under the terms and conditions of the Creative Commons Attribution (CC BY) license (http://creativecommons.org/licenses/by/4.0/).

energies

MDPI

Article

Indoor Climate Modelling and Economic Analysis Regarding the Energetic Rehabilitation of a Church

Florin-Emilian Țurcanu *, Cătălin-George Popovici, Marina Verdeș, Vasilică Ciocan and Sebastian-Valeriu Hudișteanu

Department of Building Services, Faculty of Civil Engineering and Building Services, Gheorghe Asachi Technical University of Iasi, 700050 Jassy, Romania; catalin.popovici@tuiasi.ro (C.-G.P.); marina.verdes@tuiasi.ro (M.V.); vasilica.ciocan@tuiasi.ro (V.C.); sebastian.hudisteanu@tuiasi.ro (S.-V.H.)

* Correspondence: emilian-florin.turcanu@tuiasi.ro; Tel.: +40-0748-034-588

Received: 11 April 2020; Accepted: 1 June 2020; Published: 2 June 2020



Abstract: Background: The aim of our study was to identify an optimal heating system for the analyzed church. We also evaluated the energy consumption of the existing system and of those proposed in order to choose the best heating system. Methods: We analyzed the current existing heating system, a mixed system (static heaters and hot air heating) in a Romanian heritage church, build in the 16th century, and we compared it with an underfloor heating system that has been mentioned in the literature as an alternative for church heating. We used a computational fluid dynamics (CFD) analysis of the indoor climate with two turbulence models (k-ε and k-ω). Results: Comparing the two heating systems through boxplot graphs, we could highlight pertinent conclusions regarding the temperatures and velocities of the measured air currents. Thus, of all the heating systems, the underfloor heating had the lowest temperatures, but the highest air velocities, in the churchgoers area, especially under the towers zone. Conclusions: We observed that the underfloor heating system was more efficient than the existing heating system (static heaters and hot air heating), ensuring heritage conservation and high thermal comfort to the churchgoers.

Keywords: indoor climate; energetic rehabilitation; church heating; CFD modelling

1. Introduction

Buildings are key elements for European Union (EU) actions on energy efficiency. In Romania, 45% of the total energy consumption of a building is used for heating it. This is the reason why improvements to the energy efficiencies of buildings are required [1].

Buildings that function as a place of worship, whether or not they are located within monastic settlements that also have heritage value, are usually painted churches, and their fresco gives value to the heritage [2,3]. The preservation of interior paintings should be a major concern at the state level, as both national and world heritage are involved. This is the minimum requirement that is associated with heritage buildings in the spirit of European Directive 31/2020/EU [4].

Churches are part of the heritage of Romania, and this must be preserved and cherished. Their construction meant the fulfilment of a Christian ritual that created sacred buildings in which man would bring glory and honor to divinity. Throughout time, man has integrated various techniques and technologies into these constructions to increase their comfort. These have resulted in new methods of construction, better and more durable materials, impressive paintings and frescoes, uplifting, and increased thermal comfort during religious services through the adoption of heating systems [5,6].

The quality of heritage buildings automatically implies the inclusion of places of worship/monastic settlements in the tourist circuit. The main difference concerning the initial function of the buildings is

the presence of tourists and the development of activities related to tourism in the space of the monastic settlement. The attraction represented by heritage-painted churches included in intensely publicized tourist routes leads to significant increases in the number of people temporarily attending the religious service. These people come from the internal microclimate and represent a major disturbance with the reference situation. On the other hand, the modernization of buildings to achieve conditions of thermal comfort in the cold season amplifies the presence of tourists and the disturbance of the indoor climate [7,8]. This can reveal appearance of condensation in the areas with high thermal bridges, at the intersections of the walls, at the base, and at the roof (Figure 1) [5,6].



(**a**) (**b**)

Figure 1. (**a**) Degradation due to the appearance of condensation at the base; (**b**) Degradation captured in images with thermal vision cameras show the areas with thermal bridges that favor the appearance of condensation.

Historical monument buildings that have a large number of operating hours per year, and so they must be energy efficient. Museums, schools, offices, hospitals, hotels, etc., belong to this category. They exist in almost all localities and have an important shares in energy consumption. Some of them also involve the provision of special indoor humidity conditions in order not to affect the exhibited heritage objects. In Jassy, for example, there are numerous such buildings, like the St. Three Hierarchs Monastery Assembly, the Metropolitan Cathedral, the Palace of Culture, the University of Al. I. Cuza, a military hospital (former high school), a railway station, a city hall, the National Theatre. Churches are a special category due to the intermittent nature of their use and the fact that, in churches, the faithful keep their street clothes, so the demands for thermal comfort are more modest [5,6].

Even if the current normatives do not require the existence of an energy efficiency certificate for historical monuments, the architects recommend it in order to see the thermal insulation and the energy consumption of the building [7].

The actions of the rehabilitation and thermal modernization of buildings aims to reduce energy consumption for heating, the preparation of hot water for consumption, and lighting. In 2013, Beck Water and his coworker reported some results from studies on non-warming cult buildings in Austria exposed to an alpine climate. They found that cult buildings with a high thermal mass did not show rapid variations in the interior microclimate, the temperatures of the inside walls were between 2 and 5 °C in winter and between 13 and 15 °C in the warm period, indoor air temperatures during winter had an average value of 0 °C and had of around 20 °C during summer, the relative humidity of the indoor microclimate was between 60% and 65%, except for some days with lower temperatures [8]. A study of this type establishes the starting point for assessing the indoor climate and the strategy of heating or heritage conservation where appropriate, considering that the temperate continental climate is specific to Austria and Romania. It is also very important to establish the parameters that may influence the indoor climate, for each type of system heating. For example, Camuffo et al. observed that setting the floor temperature is often a compromise between three factors: the outdoor climate, the comfort of the churchgoers, and the conservation of heritage

three factors: the outdoor climate, the comfort of the churchgoers, and the conservation of heritage [6]. Additionally, in some studies, it was observed that condensation and mold formation occur in over 30% of churches due to the fact that they are not provided with adequate thermal insulation, and these phenomena are much more pronounced around thermal bridges [9,10].

Increasing energy efficiency has beneficial effects on the environment. Solutions that are adopted for the modernization of heating, hot water, and lighting systems—correlated with those of thermal rehabilitation—must meet the aesthetic criteria that sometimes affect the historical value of buildings [11].

Thus, the existing literature on this topic has only evaluated indoor climates for existing heating systems or indoor comfort in churchgoers' areas without a complete and comparative evaluation of existing and proposed heating systems [12,13].

The aim of our study was to evaluate the energy consumption of an existing system and of a proposed one in a Romanian church in order to identify the optimal heating system for it.

2. Materials and Methods

In order to achieve our goal, we analyzed the current existing heating system of the chosen church, a mixed system (static heaters and hot air heating). Furthermore, we compared this system with an underfloor heating system, considering that it is also a good alternative for heating in the church. We studied an orthodox church built to the dedication of the Three Holy Hierarchs, located in the city of Jassy, in the third wind zone and the third climatic zone of Romania, with an outdoor temperature during winter of −18 °C (the design temperature). The building was constructed in the 16th century. Due to earthquakes and fires, the church has been restored several times. The church has the plan view of a Greek cross, with the following parts: a narthex (at the entrance), a middle section for the nave, and the altar in the front. (Figure 2). The architecture of the church is that of the Moldavian churches, with the influence of Transylvanian gothic style (Figure 3).

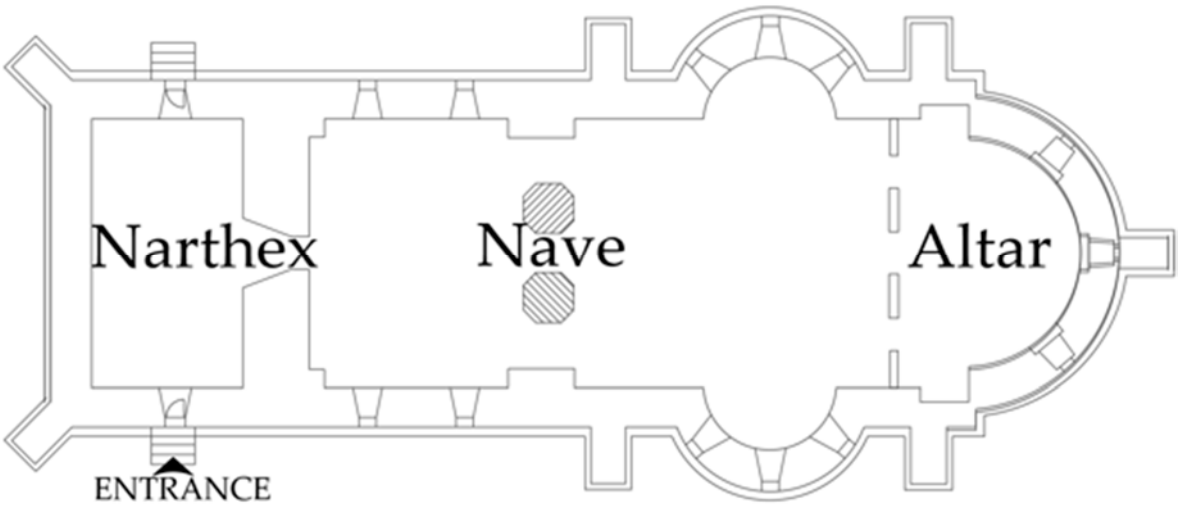
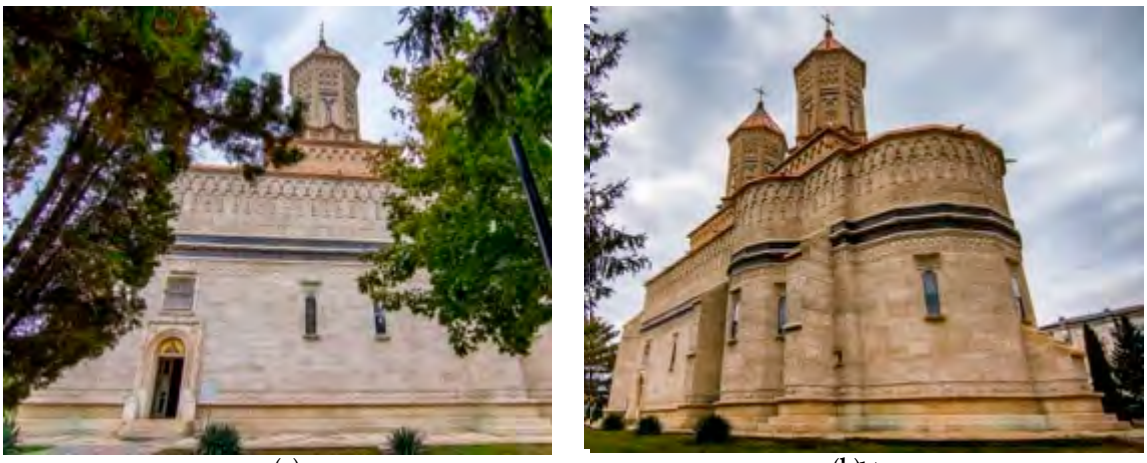


Figure 2. The current form in the church plan of Three Holy Hierarchs in Jassy.



(**a**) (**b**)

Figure 3. View of the Three Holy Hierarchs church in Iassy: (**a**) main entrance and (**b**) side view.

Figure 3. View of the Three Holy Hierarchs church in Iassy: (**a**) main entrance and (**b**) side view.

The interior microclimate from the church, as well as of the physical parameters, could not be determined without investigative tools. For the microclimate in the church we used sensors from Testo that were mounted in the church during the winter for 2 months. The sensors were placed in the area of the second tower of the church, in a vertical plane. (Figure 4).

The interior microclimate from the church, as well as of the physical parameters, could not be determined without investigative tools. For the microclimate in the church we used sensors from Testo that were mounted in the church during the winter for 2 months. The sensors were placed in the area of the second tower of the church, in a vertical plane. (Figure 4).

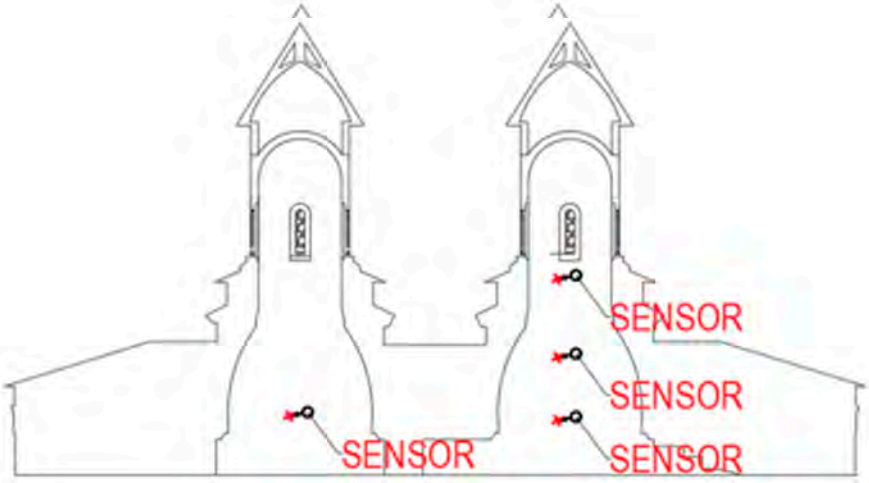


Figure 4. Sensors placed in the church.

Thermal imaging is widespread in the field of construction, in particular in the fields of heat loss assessment and thermal bridge identification. We used the thermal imaging to determine the insulation defects, air infiltration, heat loss through the closing elements of the building, and the discovery of areas with potential to develop dampness and mold. We decided to study other defects of construction materials and to monitor the heating systems in order to detect temperature variations.

Thermal imaging is widespread in the field of construction, in particular in the fields of heat loss assessment and thermal bridge identification. We used the thermal imaging to determine the insulation defects, air infiltration, heat loss through the closing elements of the building, and the discovery of areas with potential to develop dampness and mold. We decided to study other defects of construction materials and to monitor the heating systems in order to detect temperature variations.

With the measuring and recording equipment, the main parameters were captured: temperature, humidity, and air velocities. Sensors were placed at a height of 1.8 meters, in areas that were not affected by drafts or cold radiation of the outer ture elements (exterior walls, windows and exterior doors). Also, the sensors were not under the direct influence of heating equipment.

With the measuring and recording equipment, the main parameters were captured: temperature, humidity, and air velocities. Sensors were placed at a height of 1.8 meters, in areas that were not affected by drafts or cold radiation of the outer ture elements (exterior walls, windows and exterior doors). Also, the sensors were not under the direct influence of heating equipment.

We studied the existing heating system in the church in the year 2017—a mixed heating system (static heaters with hot air system). The indoor and outdoor temperature were measured in the winter. Knowing the envelope parameters and the thermal resistance of the walls and windows, we made the geometrical model for computational fluid dynamics (CFD) of indoor climate (Table 1). The CFD model analysis was used to see the other effects of the heating system, like the deterioration of the paints and walls, that could not be seen with the naked eye.

We studied the existing heating system in the church in the year 2017—a mixed heating system (static heaters with hot air system). The indoor and outdoor temperature were measured in the winter. Knowing the envelope parameters and the thermal resistance of the walls and windows, we made the geometrical model for computational fluid dynamics (CFD) of indoor climate (Table 1). The CFD model analysis was used to see the other effects of the heating system, like the deterioration of the paints and walls, that could not be seen with the naked eye.

Table 1. The boundary conditions imposed for the computation fluid dynamics (CFD) analysis in the Three Hierarchs church.

No.	Envelope Element	Type of the Heating System	
1	2	3	4
		Static heaters with hot air system	Underfloor Heating System
Temperature (°C)	Exterior Walls	−16	−16
	Ceiling	−15	−15
	Input grids for hot air	35	-
	Ground plate	10	10
	Windows and Doors	−16	−16
Pressure (Pa)	Relative pressure		
Heat transfer coefficient U (W/m^2K)	Exterior walls	0.652	0.652
	Windows and doors	2.379	2.379
	Ceiling	1.518	1.518
	Ground plate	0.818	0.818
	Tower walls	1.276	1.276
Air velocity(m/s)	Inlet grids for hot air	0.25	-
	Extraction grids	0.15	-
Heat flux (W/m^2)	Static heater	200	-
	Underfloor heating	-	100
Heat flow generated by people is imposed at 80 (W)			

The limit conditions imposed for the inlet air temperature and air velocity were taken from the operating regime of the heating installation, and the heat flux imposed on the radiators was determined from a guide for determining the thermally equivalent surface of a heating body.

The resultant heat was calculated with the relation:

$$Q = \dot{m} \times C_p \times \Delta T \quad (1)$$

where:

$\dot{m}$—fluid flow rate;

C_p—specific heat of the fluid;

ΔT—the temperature difference between supply pipes lines and return pipes lines from boilers.

Based on literature studies, the turbulence models selected for CFD analysis of the church were k-ε and k-ω [14–16]. We made an initial discretization of 2 million elements with an unstructured meshing type. Subsequently, we increased the number of meshing elements to a maximum of 8 million elements for the existing heating system and 10 million elements for the proposed heating system. This limit was selected by considering the fact that we did not have any variations in the studied parameters at this meshing. After establishing the geometric model, the competition of the boundary condition, and the selection of the underfloor heating system based on the literature studies of the Friendly-Heating Project [5] and Climate for Culture [6], we made the following simulations (Figure 5).

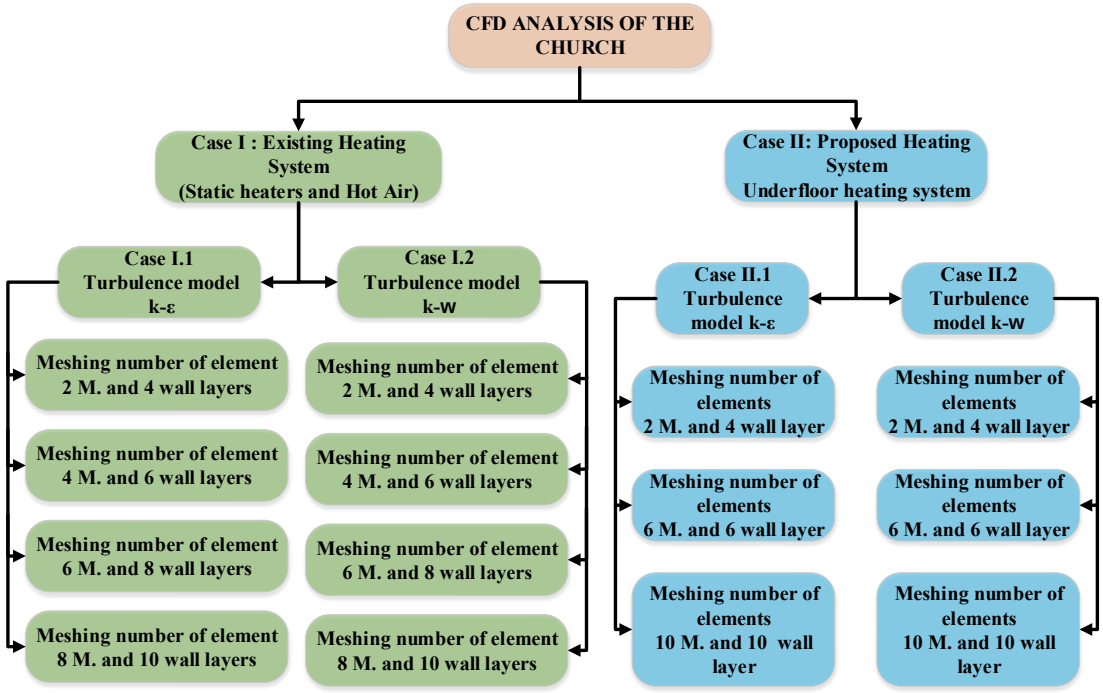


Figure 5. CFD analysis scheme of the church. We evaluated the existing heating system and the proposed one; for each of these, we used two different turbulence models (k-ε and k-ω). We used different levels of meshing and wall layers that were gradually increased until we did not have any variations in the studied parameters.

Figure 5. CFD analysis scheme of the church. We evaluated the existing heating system and the proposed one; for each of these, we used two different turbulence models (k-ε and k-ω). We used different levels of meshing and wall layers that were gradually increased until we did not have any variations in the studied parameters.

3. Results

3. Results

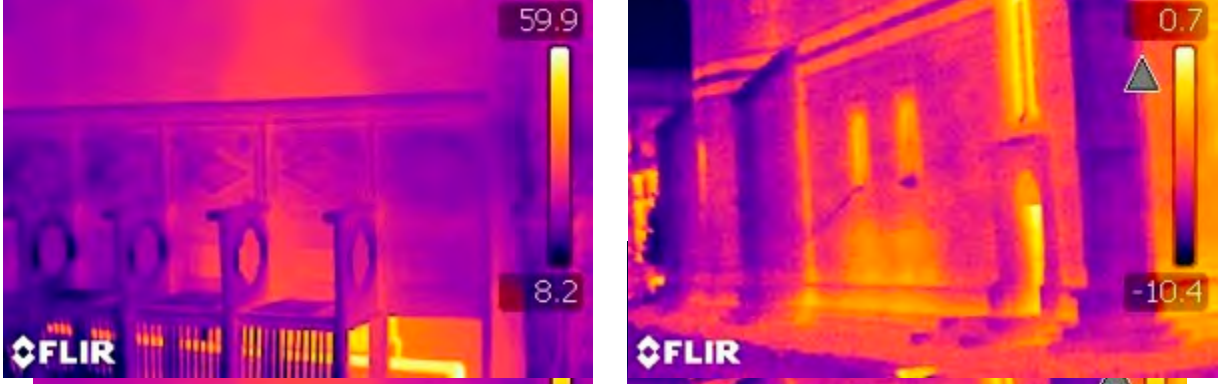
3.1. Thermovision Images

3.1. Thermovision Images

The chosen monument has historical value and is the part of the Romanian cultural heritage because it is representative of this area of the country through its architectural style. Its strong structure is made of solid brick masonry. The edifice being over 350 years old, the materials used in its construction, and the weather conditions it has experienced have led to multiple degradations in the structure of the building. When heat losses are high, several problems arise, such as condensation favored in areas that fall below the dew point temperature in front of the interior elements. This phenomenon primarily affects the finishing details and creates unsightly appearance, but it also leads to deeper degradations such as the detachment of the support layers for paintings and plasters. In Figure 6a, the influence of the convective air current caused by the static heating system that rises and washes the paints from the walls can be observed; this leads, in time, to drying and detachment from the support walls. In Figure 6b we presented the differences in the wall thickness, in the area of crypts created in the side walls that lead to massive heat losses. Due to this and the contribution of the interior humidity, degradations have appeared in this area in the form of condensation and mold that have destroyed the paintings.

The chosen monument has historical value and is the part of the Romanian cultural heritage because it is representative of this area of the country through its architectural style. Its strong structure is made of solid brick masonry. The edifice being over 350 years old, the materials used in its construction, and the weather conditions it has experienced have led to multiple degradations in the structure of the building. When heat losses are high, several problems arise, such as condensation favored in areas that fall below the dew point temperature in front of the interior elements. This phenomenon primarily affects the finishing details and creates unsightly appearance, but it also leads to deeper degradations such as the detachment of the support layers for paintings and plasters. In Figure 6a, the influence of the convective air current caused by the static heating system that rises and washes the paints from the walls can be observed; this leads, in time, to drying and detachment from the support walls. In Figure 6b we presented the differences in the wall thickness, in the area of crypts created in the side walls that lead to massive heat losses. Due to this and the contribution of the interior humidity, degradations have appeared in this area in the form of condensation and mold that have destroyed the paintings.

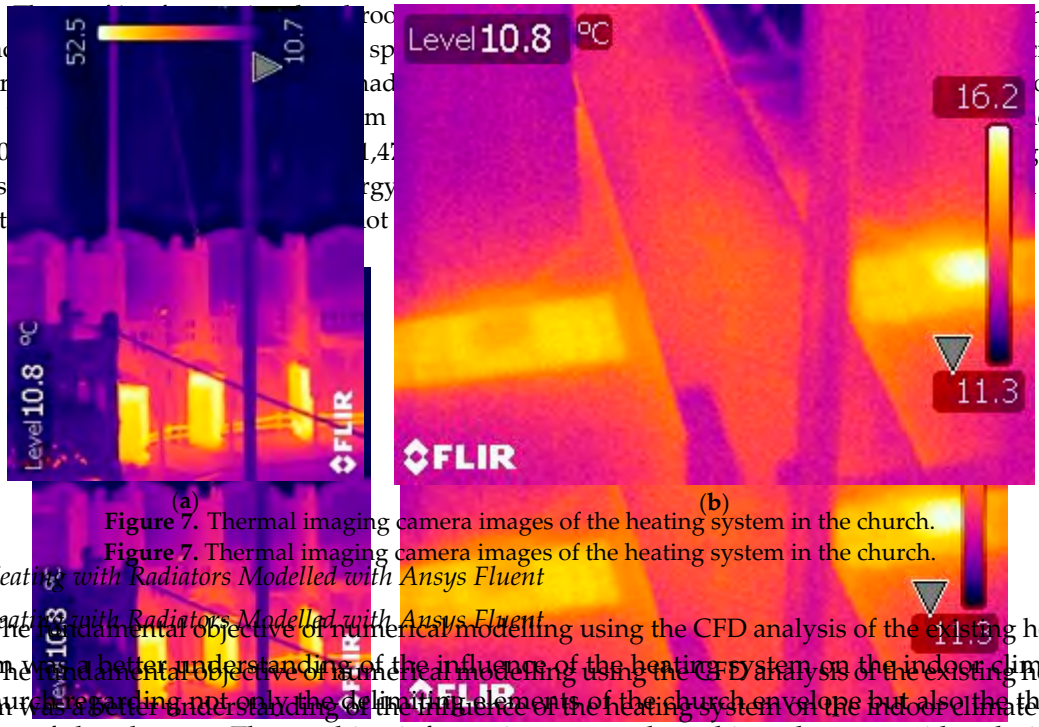
The roof is of a non-insulated roof type with sheet covers. The joinery is metallic with simple windows. The floor above the useful space is made of brick, and there is a layer of reinforced concrete over. The floor is of the cold type made of marble. The thickness of the walls varies from 180 to 80 cm. With widths of 40.61 and 15.04 m and an average height of 9.81 m, the church has a volume of 2710 m^3 with an entire surface of 351.47 m^2. The building service systems that serve the building are those of electricity and thermal energy [3,4]. The lighting is done with incandescent bulbs, and the heating is done with radiators and hot air inlet grids placed in the base floor (Figure 7).



(**a**) (**b**)

Figure 6. Thermal vision images that capture (**a**) the effects of the static heater over the walls and (**b**) thermal bridges in the outer walls.

The roof is of a non-insulated roof type with sheet covers. The joinery is metallic with simple windows. The floor above the useful space is made of brick, and there is a layer of reinforced concrete over. The floor is of the cold type made of marble. The thickness of the walls varies from 180 to 80 cm. With widths of 40.61 and 15.04 m and an average height of 9.81 m, the church has a volume of 2710 m^3 with an entire surface of 351,47 m^2. The building service systems that serve the building are those of heating, ventilation, and air conditioning. The heating system is a hot air inlet grids placed in the base floor (Figure 7).



(**a**) (**b**)

Figure 7. Thermal imaging camera images of the heating system in the church.

Figure 7. Thermal imaging camera images of the heating system in the church.

3.2. Heating with Radiators Modelled with Ansys Fluent

3.2. Heating with Radiators Modelled with Ansys Fluent

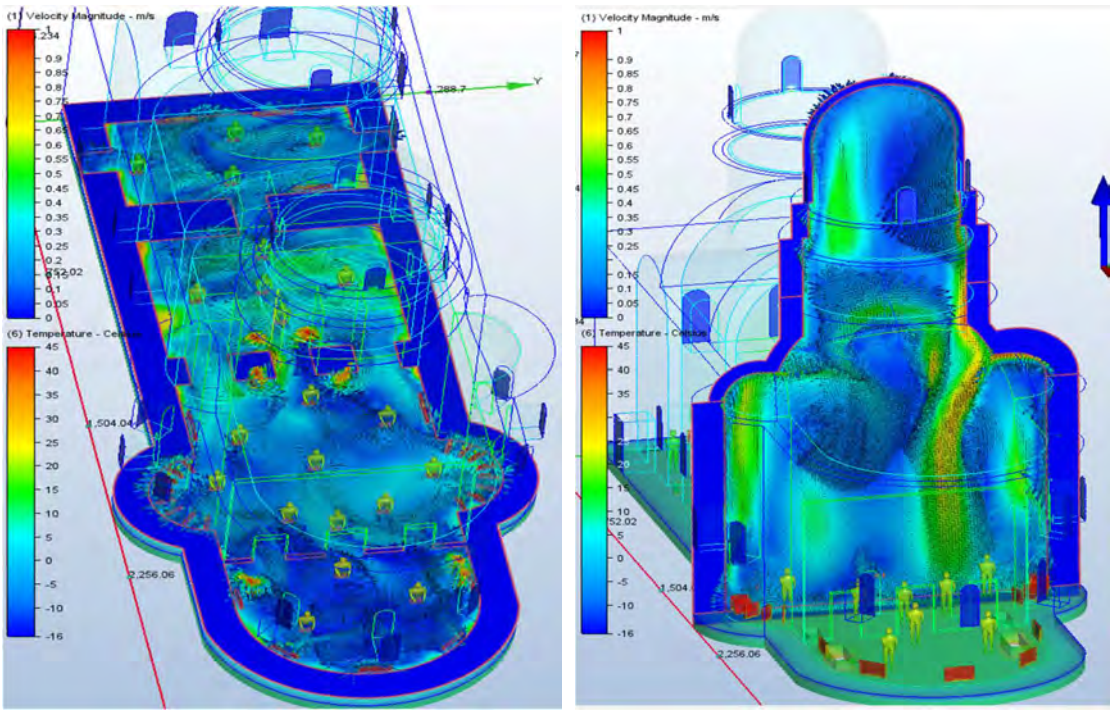
The fundamental objective of numerical modelling using the CFD analysis of the existing heating system was a better understanding of the influence of the heating system on the indoor climate of the church regarding not only the delimiting elements of the church envelope but also the thermal comfort of churchgoers. The resulting information was evaluated in order to provide solutions in response to a series of degradations observed in the church—both with the naked eye and with the help of the thermal imaging cameras. These solutions aimed to improve the indoor climate in order to preserve the heritage of the church, as well as the comfort of the churchgoers.

The fundamental objective of numerical modelling using the CFD analysis of the existing heating system was a better understanding of the influence of the heating system on the indoor climate of the church regarding not only the delimiting elements of the church envelope but also the thermal comfort of churchgoers. The resulting information was evaluated in order to provide solutions in response to a series of degradations observed in the church—both with the naked eye and with the help of the thermal imaging cameras. These solutions aimed to improve the indoor climate in order to preserve the heritage of the church, as well as the comfort of the churchgoers.

The CFD modelling was done with a section plan that was taken on the church in the longitudinal, transversal section of the church and in the plane of the human occupants at the height of 1.8 m.

The software used for CFD analysis was ANSYS FLUENT, and we performed a 3D numerical study of the indoor climate. A fine meshing was generated with a minimum step of 5 cm and a maximum of 8 cm. A Cartesian coordinate system was used to construct the model. In the CFD model, the flow, continuity, and energy equations were solved. The mode of the implementation of these equations was standard, simple, derived from the first order for the momentum, kinetic energy, flow, and energy equations. The standard k-ε model with standard wall functions was used because the heat was not introduced by forced ventilation but by the natural circulation generated by the radiators, while Boussinesq's approximation was used for air density.

Figure 8 shows the result of the analysis performed for the existing heating system for cases I.1 and I.2. It is easy to observe the profiles of the air velocities with different temperatures, their arrangement and the way the church geometry influences them. Also, in this figure are presented the temperatures that exist inside the church. The warm air rises to the ceiling, forming a layer at the top. Colder, denser air accumulates on the floor. After air circulation with different temperatures, they tend to stabilize, forming a strong stratification of the air.



(**a**) (**b**)

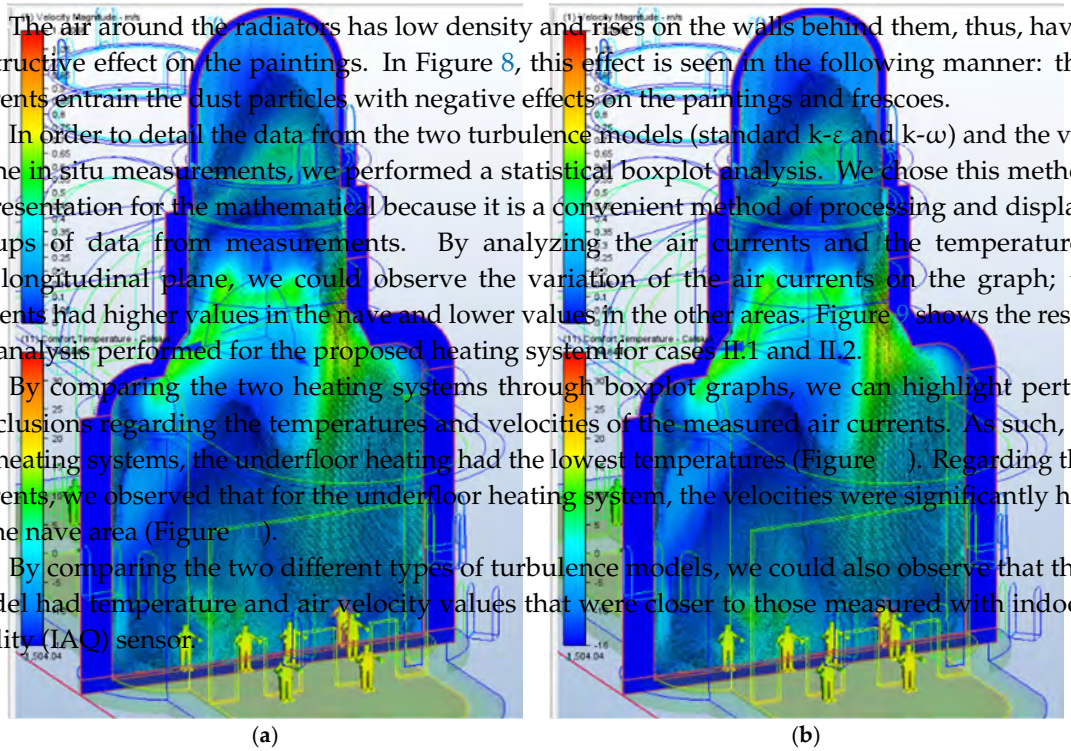
Figure 8. Profiles of temperature and air velocity contour in the church after CFD modelling: (**a**) horizontal velocity field in the occupied area and (**b**) vertical velocity field of air currents in the area of the nave.

The air around the radiators has low density and rises on the walls behind them, thus, having a destructive effect on the paintings. In Figure 8, this effect is seen in the following manner: the air currents entrain the dust particles with negative effects on the paintings and frescoes.

In order to detail the data from the two turbulence models (standard k-ε and k-ω) and the values of the in situ measurements, we performed a statistical boxplot analysis. We chose this method of representation for the mathematical because it is a convenient method of processing and displaying groups of data from measurements. By analyzing the air currents and the temperatures in the longitudinal plane, we could observe the variation of the air currents on the graph; these currents had higher values in the nave and lower values in the other areas. Figure 9 shows the result of the analysis performed for the proposed heating system for cases II.1 and II.2.

By comparing the two heating systems through boxplot graphs, we can highlight pertinent conclusions regarding the temperatures and velocities of the measured air currents. As such, of all the heating systems, the underfloor heating had the lowest temperatures (Figure). Regarding the air currents, we observed that for the underfloor heating system, the velocities were significantly higher in the nave area (Figure).

By comparing the two different types of turbulence models, we could also observe that the k-ε model had temperature and air velocity values that were closer to those measured with indoor air quality (IAQ) sensor.



(**a**) (**b**)

Figure 9. Profiles of temperature and air velocity contour in the church after CFD modelling: (**a**) vertical velocity field of air currents in the area of the nave and (**b**) horizontal velocity field in the longitudinal section.

Figure ity lling: (**a**) horizon l (**b** the area of the n

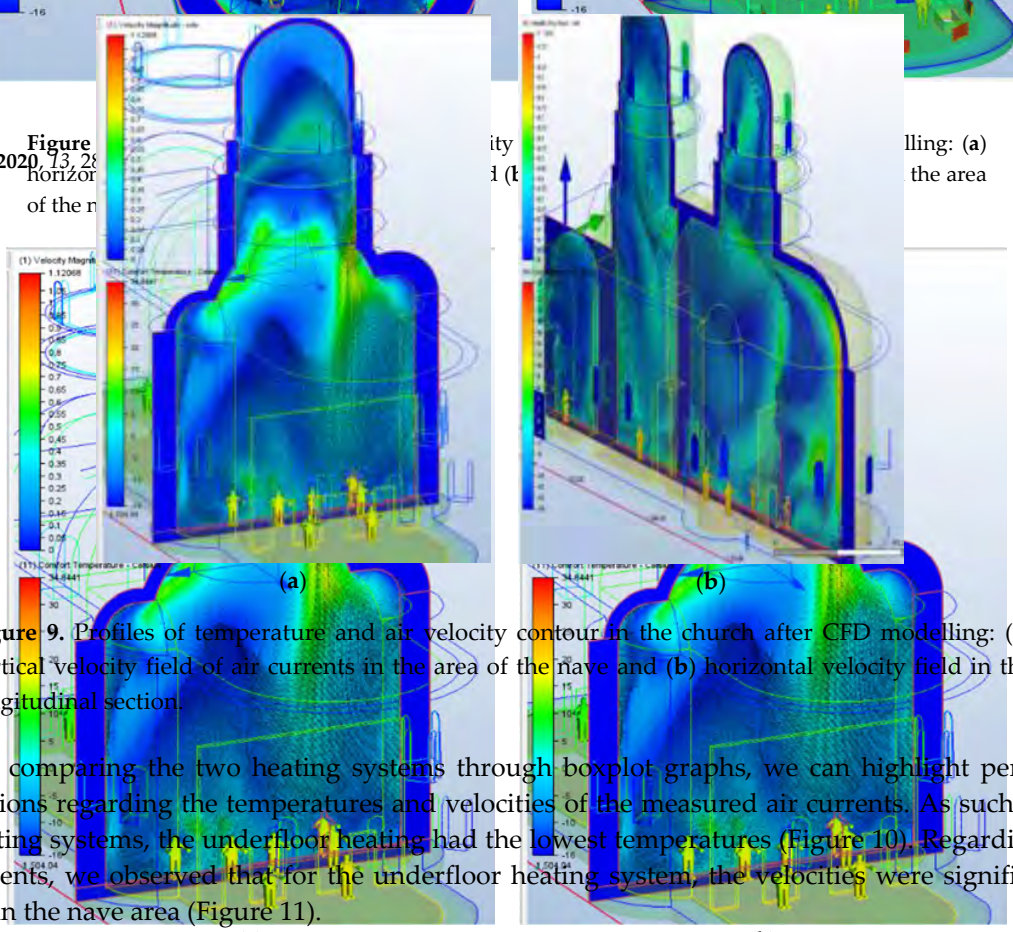


Figure 9. Profiles of temperature and air velocity contour in the church after CFD modelling: (**a**) vertical velocity field of air currents in the area of the nave and (**b**) horizontal velocity field in the longitudinal section.

By comparing the two heating systems through boxplot graphs, we can highlight pertinent conclusions regarding the temperatures and velocities of the measured air currents. As such, of all the heating systems, the underfloor heating had the lowest temperatures (Figure 10). Regarding the air currents, we observed that for the underfloor heating system, the velocities were significantly higher in the nave area (Figure 11).

By comparing the two different types of turbulence models, we could also observe that the k-ε model had temperature and air velocity values that were closer to those measured with indoor air quality (IAQ) sensors.

Figure 9. Profiles of temperature and air velocity contour in the church after CFD modelling: (**a**) vertical velocity field of air currents in the area of the nave and (**b**) horizontal velocity field in the longitudinal section.

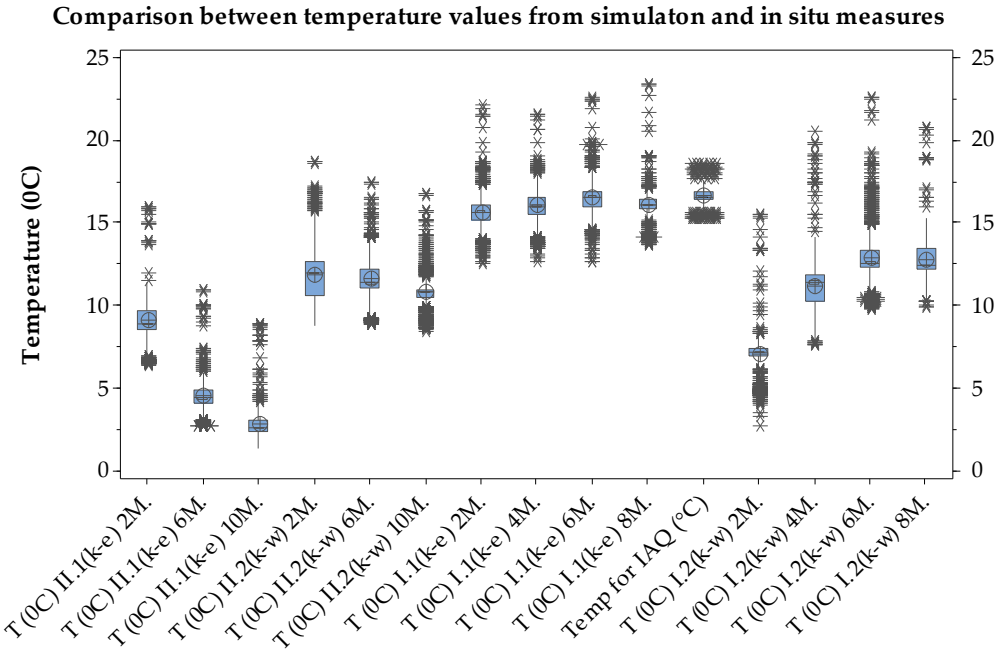


Figure 10. Comparison between temperature values for both turbulence models (standard k-ε and k-ω): the existing heating system, the proposed heating system, and the indoor air quality (IAQ) probe.

Figure 10. Comparison between temperature values for both turbulence models (standard k-ε and k-ω): the existing heating system, the proposed heating system, and the indoor air quality (IAQ) probe.

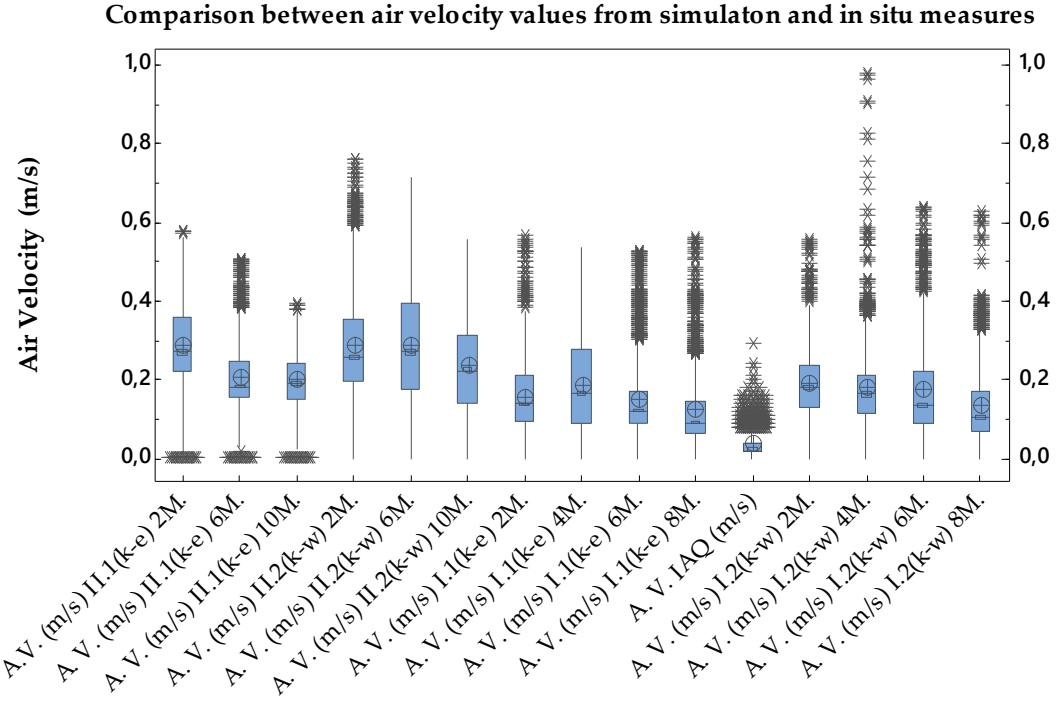


Figure 11. Comparison between air velocity values for both turbulence models (standard k-ε and k-ω): the existing heating system, the proposed heating system, and the indoor IAQ probe.

Figure 11. Comparing between the air velocity values for both turbulence models (standard k-ε and k-ω): the existing heating system, the proposed heating system, and the indoor IAQ probe.

3.3. Analysis of the Studied Building Energy Performance

3.3. Analysis of the Studied Building Energy Performance

We also performed a thermo-technical calculation of the envelope elements according to the normative C107-2005. We determined the corrected thermal resistances of the closing elements R′ (m^2K/W) compared to the standard thermal resistances R′min (m^2K/W). The criterion for satisfying the requirement of thermal insulation was R′ ≥ R′$_{min}$. The comparative values are presented in Table 2.

We also performed a thermo-technical calculation of the envelope elements according to the normative C107-2005. We determined the corrected thermal resistances of the closing elements R′ (m^2K/W) compared to the standard thermal resistances R′min (m^2K/W). The criterion for satisfying the requirement of thermal insulation was R′ ≥ R′$_{min}$. The comparative values are presented in Table 2.

Table 2. The thermomechanical characteristics of the existing envelope.

Elements	A m^2	R′ m^2K/W	R′$_{min}$ m^2K/W
North wall	147.16	0.652	1.800
West wall	51.68	0.652	1.800
East wall	61.41	0.652	1.800
South wall	147.16	0.652	1.800
Roof	305.91	1.518	5.000
Decking	266.01	0.818	4.500
Windows	35.36	0.330	0.770

Table 2. The thermomechanical characteristics of the existing envelope.

Elements	A m^2	R′ m^2K/W	R′$_{min}$ m^2K/W
North wall	147.16	0.652	1.800
West wall	51.68	0.652	1.800
East wall	61.41	0.652	1.800
South wall	147.16	0.652	1.800
Roof	305.91	1.518	5.000
Decking	266.01	0.818	4.500
Windows	35.36	0.330	0.770

The analysis showed that most of the building envelope elements did not meet the minimum thermal insulation requirements. The annual consumptions were calculated according to the normative NP 048–2000. This norm takes the heat transfer in a non-stationary regime through a building envelope into account. The heat contributions due to the human activities and the solar radiation were also considered. The estimation of annual consumptions was used for the energy certificate [7].

The analysis showed that most of the building envelope elements did not meet the minimum thermal insulation requirements. The annual consumptions were calculated according to the normative NP 048–2000. This norm takes the heat transfer in a non-stationary regime through a building envelope into account. The heat contributions due to the human activities and the solar

In this way, the annual consumption was as follows:

Yearly consumption for heating: Q^{year}_{Heat} = 257.35 kWh/m^2year,

Yearly consumption for hot-water preparation: $q^{year}_{hot\ water}$ = 30.15 kWh/m^2year.

radiation were also considered. The estimation of annual consumptions was used for the energy certificate [7].

In this way, the annual consumption was as follows:

Yearly consumption for heating: Q_{Heat}^{year} =257,35kWh/m^{2}year ,

Yearly consumption for hot water preparation: $q_{hotwater}^{year}$ =30,15kWh/m^{2}year ,

Yearly consumption for lighting preparation: $W_{lighting}^{year}$ =28.76kWh/m^{2}year ,

Total annual consumption: Q_{Heat}^{year} =316.26kWh/m^{2}year .

3.4. Completion of the Energy Certificate

3.4. Completion of the Energy Certificate

Churches have intrinsic value via their heritage, and they also have energy consumption, especially in a climatic zone where the duration of the heating season lasts for several months. In Romania, the duration of the heating season is, on average, 3600 degrees-days (K·h). This is the reason why we considered it necessary to carry out an energetic classification of the church that we analyzed. The energy certificate of the building was decided based on its consumptions, and it was attributed the energy classification "D" and a value of Q (Heating/Year) = 3162 kWh/m^2 for the annual consumption of heat for heating, hot water, and lighting (Figure 12).

Churches have intrinsic value via their heritage, and they also have energy consumption, especially in a climatic zone where the duration of the heating season lasts for several months. In Romania, the duration of the heating season is, on average, 3600 degrees-days (K·h). This is the reason why we considered it necessary to carry out an energetic classification of the church that we analyzed. The energy certificate of the building was decided based on its consumptions, and it was attributed the energy classification "D" and a value of Q (Heating/Year) = 3162 kWh/m^2 for the annual consumption of heat for heating, hot water, and lighting (Figure 12).

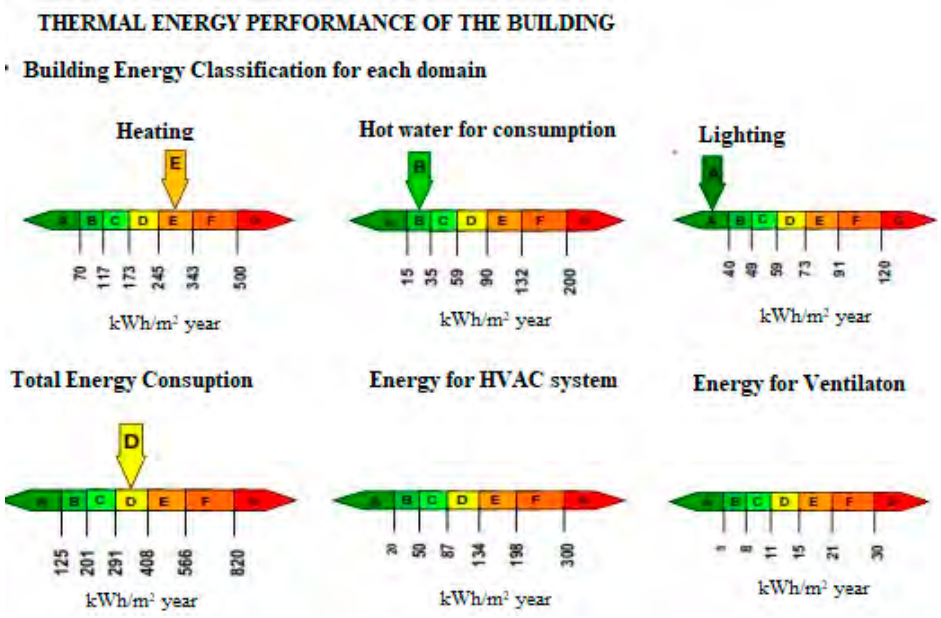


Figure 12. Grids regarding the energy classification of the audited building kWh/m^2 year.

Figure 12. Grids regarding the energy classification of the audited building kWh/m² year.

3.5. Proposals on Energy Modernization Solutions

3.5. Proposals on Energy Modernization Solutions

Based on its historical character, the façade of this church cannot have an increase in thermal resistance to reduce heat transfer. The only place where the thermal resistance can increase is at the levels of the floor and the roof.

Two economic and technical rehabilitation models were analyzed:

Two economic and technical rehabilitation models were analyzed:

The first was solution that only involved the thermal rehabilitation of the building, specifically interventions to the construction site to improve the thermal protection of the floor under the bridge. It was proposed to install a thermal insulation layer made of mineral wool with a thickness of 15 cm. The new, corrected thermal resistance created was R' = 3367 (m^{2}K/W). To improve the thermal protection of the ground floor, it was proposed to install a layer of thermal insulation of extruded polystyrene plates with a thickness of 10 cm. The new, corrected thermal resistance was R' = 3138 (m^{2}K/W).

The first was solution that only involved the thermal rehabilitation of the building, specifically interventions to the construction site to improve the thermal protection of the floor under the bridge. It was proposed to install a thermal insulation layer made of mineral wool with a thickness of 15 cm. The new, corrected thermal resistance created was R' = 3367 (m^{2}K/W). To improve the thermal protection of the ground floor, it was proposed to install a layer of thermal insulation of extruded polystyrene plates with a thickness of 10 cm. The new, corrected thermal resistance was R' = 3138 (m^{2}K/W).

The second solution proposed making the operation of the installations more efficient, together with the first envelope rehabilitation package, as follows: (1): heating installations would use efficient static heaters (with a high index of thermal loads of the metal for life) and a correlation of their size with the solutions of thermal rehabilitation of the envelope of the building, (2): the static heaters would be equipped with thermostatically regulated valves; (3): the thermo–energetic equipment in the thermal point would be automated; (4): sanitary fittings with reduced water consumption would be used for

The second solution proposed making the operation of the installations more efficient, together with the first envelope rehabilitation package, as follows: (1): heating installations would use efficient

the preparation of domestic hot water; (5): modern equipment for domestic hot water preparation (studying the possibility of mounting equipment that uses renewable energy) would be mounted.

In order to reduce the energy consumption of the lighting system, we proposed the following solutions: (1): the complete restoration of the lighting installations and (2) the correct establishment of the number of luminaries according to the destination of the room and the level of illumination required according to the specific activity that is carried out in them, as well as the use of luminaires with fluorescent lamps or LEDs (equipped with capacitors to improve the power and electronic ballasts) because they have a high luminous efficiency (luminous flux related to electrical power).

By applying the thermal rehabilitation solutions of the building envelope, we obtained improvements of the thermal insulation performance of the building, as well as a classification in a higher class regarding the rating in the energy certificate. This the thermal rehabilitation, together with one of the indoor building services system, enabled the improved building to get the energy classification "B" and a value of 151.19 kWh/m^{2}year for the annual consumption of heat for heating, domestic hot water, and lighting. Separately on thermal utilities, the energy classifications of the reference building were:

- For heating: a "C" classification with a specific consumption of 122.97 kWh/m^{2}year.
- For domestic hot water: an "A" classification with a specific consumption of 7.26 kWh/m^{2}year.
- For lighting: an "A" classification with a specific consumption of 20.95 kWh/m^{2}year [7].

3.6. Economic Aspects Regarding the Two Modernization Packages

The economic analysis was a simplified form of assessing the amortization of investments. (Tables 3 and 4). This analysis was based on the following assumptions and values:

- at the date when the energy audit was performed, the average cost of the thermal energy was 55.16 Euro/Gcal, equivalent to 0.12 Euro/kWh [7], in which:

Gcal—gigacalories.

The (simple) duration of the investment recovery, N_R (years) [7]:

$$N_R = \frac{C_{INV}}{\Delta E \times c_{et/ee}} \quad (2)$$

in which:

C_{INV}—the cost of energy modernization works (Euro).

ΔE—energy savings achieved by applying energy modernization solutions (kWh/year).

$c_{et/ee}$—the specific cost of heat/electricity, (Euro/kWh);

The average cost of thermal energy when the energy audit was performed, was:

c_{et} = 0.12 Euro/kWh.

Table 3. Individual consumption per consumption grid and total annual consumption in (kWh/year) for each type of proposed solution.

Modernization Package	Heating Consumption	Domestic Hot Water Consumption	Consumption of Electrical Installation	Total Consumption of the Source
	kWh/Year	kWh/Year	kWh/Year	kWh/Year
Construction	70,516	10,598	10,109	91,223
Constructions and plumbing	43,221	2552	7365	53,138

The average cost of electricity when the energy audit was performed, was: c_{ee} = 0.1 Euro/kWh.

e—the cost of the energy unit saved during the life of the solution (Euro/kWh) [7]:

$$e = \frac{C_{INV}}{\Delta T \times N_S} \quad (3)$$

in which:

N_S—the estimated lifetime of the energy upgrade solution = 15 years [7].

Table 4. Comparison of the proposed solutions.

Modernization Package	Energy-Saving ΔE	Lifespan Ns	Investment Cost	Duration of Recovery NR	The Cost of Energy Saved E
	kWh/Year	Years	Euro	Years	Euro/kWh
Construction	19,933	30	40,256	13.46	0.0673
Constructions and plumbing	58,018	20	43,623	9.40	0.0376

4. Discussion

The main result of our study was that, of all the heating systems, the underfloor heating one had the lowest temperatures but the highest velocities, especially in the nave area. By comparing the two different types of turbulence models, we also observed that the k-ε model had temperature and air velocity values that were closer to those measured with IAQ sensors. To our knowledge, this is the first study that has evaluated two different types of turbulence models for the heating systems in churches and that has validated the k-ε turbulence model for temperature and air velocity values with those measured with IAQ sensors.

The energy rehabilitation and change of the church heating system modified the energy classification of the church from the energy class D to energy class B.

We also observed that:

- The air circulation had negative effects because it generated a premature and rapid drying of all the objects—paintings, frescoes, and different wooden objects of worship—with which it came in contact.
- The volume of air that moved caused dust to rise and to be carried by air and deposited in areas with colder thermal bridges where hot air condenses and dust could be deposited.
- Another negative aspect of heating with radiators was that the discontinuous operating mode of the system caused the heating–cooling cycles of the indoor air to affect the interior finishes and heritage objects whenever religious service took place.
- The high volume of air displaced by the church made the heating of the place of worship difficult, requiring a prolonged period that imposed a continuous operating regime during the cold season.
- Heating with radiators, combined with humidity released from people, favored the phenomenon of condensation on surfaces with reduced temperatures.

In the past, the most common point of view in the design of heating systems was to achieve an economical operation with minimal maintenance effort [17–19]. The inner climate created was ignored in this equation [5].

Given that high humidity and low temperatures present in most churches diminish, the desire for the comfort of occupants in the twentieth century has led to investigations for solutions to heat the indoor climate [6].

"Climate for Culture" was a European project that took place in 2009–2014 in the field of heritage conservation [6]. This research focused on the implementation of regional climate models—new methods for simulating indoor and outdoor climate around heritage buildings. The study integrated a number of 128 heritage buildings, including many religious buildings, to assess their indoor and outdoor microclimates. Various scenarios have also been created to predict the evolution of the parameters pursued by 2100.

The results of high-resolution climate change were achieved with the regional climate model (REMO) for the whole of Europe, including the Mediterranean basin. Within the project, building simulation tools and a simplified building model for worship buildings were developed, and these were subjected to the simulation of regional climatic environmental conditions. The resulting parameters

allowed for the creation of maps with future risks induced by climate change on religious buildings and other heritage buildings, as well as on indoor microclimates [6].

Another study that aimed to evaluate the heating and comfort of people in heritage buildings, as well as the conservation of existing objects in them, was the European Friendly-Heating Project, carried out between 2009 and 2014 [5].

The analysis method using the CFD-Fluent software demonstrated the need for simulations in thermal comfort studies. For a more accurate and detailed analyses, are necessary in-situ investigations that place temperature and humidity sensors for a longer period of time [13,20].

Numerical validation of our results was possible only for the k-ε turbulence model, which had the closest temperature and air velocity values to those measured with IAQ sensors. Additionally, the differences between these values were below 10%.

Our results highlight the need for the evaluation of the heating systems in order to choose the optimal one. If the situation requires even their change to new, more efficient ones with less harmful effects on cult objects (because, in general, people seek their comfort and do not keep the optimal parameters for the preservation of objects and buildings of worship), it is necessary to prioritize and reconsider the comfort needs of such buildings.

To our knowledge, this is the first study that numerically evaluated the entire indoor climate of a church. The analysis of the indoor climate was performed with several models of turbulence, both for the existing heating system and for the proposed one. We observed that the underfloor heating system ensured a high thermal comfort for the churchgoers, and, at the same time, ensured a better conservation of the architectural heritage.

5. Conclusions

In conclusion, our study highlighted that there is a continuous interaction between the parameters of the indoor climate and heritage conservation. Thus, we noticed that the temperature, humidity, and velocity of the air currents influenced the state of conservation of the existing heritage inside the churches, and the k-ε turbulence model had temperature and air velocity values closer to those measured with IAQ sensors. In our study, the underfloor heating system was more efficient than the existing heating system (static heaters and hot air heating), ensuring heritage conservation and high thermal comfort to churchgoers.

Author Contributions: All authors had an equal contribution to this manuscript. All authors have read and agreed to the published version of the manuscript.

Funding: This research received no external funding.

Conflicts of Interest: The authors declare no conflict of interest.

References

1. Rokas, V.; Andrius, J.; Viktoras, D. Method for cost-benefit analysis of improved indoor climate conditions and reduced energy consumption in office buildings. *Energies* **2013**, *6*, 4591–4606.
2. Shui, Y.; Yumeng, C.; Yifei, S.; Fuhong, H. Simulation research on the effect of coupled heat and moisture transfer on the energy consumption and indoor environment of public buildings. *Energies* **2019**, *12*, 141.
3. Lundström, L.; Akander, J.; Zambrano, J. Development of a space heating model suitable for the automated model generation of existing multifamily buildings—A case study in Nordic Climate. *Energies* **2019**, *12*, 485. [CrossRef]
4. Bruelisauer, M.; Chen, K.W.; Iyengar, R.; Leibundgut, H.; Li, C.; Li, M.; Mast, M.; Meggers, F.; Miller, C.; Rossi, D. Bubble ZERO-design, construction and operation of a transportable research laboratory for low exergy building system evaluation in the tropics. *Energies* **2013**, *6*, 4551–4571. [CrossRef]
5. Camuffo, D. The friendly heating project and the conservation of the cultural heritage preserved in churches. In *Developments in Climate Control of Historic Buildings*; Fraunhofer IRB Verlag: Stuttgart, Germany, 2010; pp. 7–12.

6. Camuffo, D.; Pagan, E.; Schellen, H.; Limpens-Neilen, D. A practical guide to the pros and cons of the various heating systems with a view to the conservation of the Cultural Heritage in Churches. In *Results of the European Project Friendly Heating EVK4-CT-2001-00067*; Fraunhofer IRB Verlag: Linderhof, Germay, 2014.
7. MLPTL. *NP 048—Normativ Pentru Expertizarea Termică și Energetică a Clădirilor Existente și al Instalațiilor de Încălzire și Preparare a Apei de Consum Aferente Acestora*; MLPTL: Hamburg, Germany, 2000.
8. Beck, W.; Koller, M. Problems of heating within historic buildings of Austria. *Stud. Conserv.* **2013**, *25*, 22–29. [CrossRef]
9. Zhang, Z.; Zhai, Z.J.; Chen, Q.Y. Evaluation of various turbulence models in predicting airflow and turbulence in enclosed environments by CFD. *HvacR Res.* **2007**, *13*, 871–886. [CrossRef]
10. Cortés, M. CFD modeling of basic convection cases in enclosed environments: Needs of CFD beginners to acquire skills and confidence on CFD modeling. *RIC* **2014**, *29*, 22–45.
11. Wang, H.; Zhiqiang, J.Z. Advances in building simulation and computational techniques: A review between 1987 and 2014. *Energ. Build.* **2016**, *128*, 319–335. [CrossRef]
12. Tian, W.; Sevilla, T.A.; Zuo, W. A systematic evaluation of accelerating indoor airflow simulations using cross-platform parallel computing. *J. Build. Perform. Simul.* **2017**, *10*, 243–255. [CrossRef]
13. Tian, W.; Xu, H.; Wangda, Z.; Sohn, M.D. Building energy simulation coupled with cfd for indoor environment: A critical review and recent applications. *Energ. Build.* **2018**, *165*, 184–199. [CrossRef]
14. Lim, J.; Yoon, M.S.; Al-Qahtani, T.; Nam, Y. Feasibility study on variable-velocity air conditioner under hot climate based on real-scale experiment and energy simulation. *Energies* **2019**, *12*, 1489. [CrossRef]
15. Frontczak, M.; Wargocki, P. Literature survey on how different factors influence human comfort in indoor environments. *Build. Environ.* **2011**, *46*, 922–937. [CrossRef]
16. Bassam, M.; Cantin, R.; Guarracino, G. Comparison of thermal comfort algorithms in naturally ventilated office buildings. *Energy Build.* **2008**, *40*, 2215–2223.
17. Andrea, V.; Luca, M.; Chiara, C. How the urban environment affects the microclimate and the building energy demand for the city of Rome. *Therm. Sci.* **2019**, *23*, S1035–S1042.
18. Yunyang, Y.; Kathryn, H.; Jian, Z.; Wangda, Z.; Gang, W. A methodology to create prototypical building energy models for existing buildings: A case study on U.S. religious worship buildings. *Energy Build.* **2019**, *194*, 351–365.
19. Schellen, H.; Lambertus, H. *Heating Monumental Churches-Indoor Climate and Preservation of Cultural Heritage*; Technische Universiteit Eindhoven: Eindhoven, The Netherlands, 2002.
20. Marco, P.; Kristian, F. Indirect investigation: Building simulation. In *Historic Indoor Microclimate of the Heritage Buildings*; Springer: Berlin, Germany, 2018; pp. 100–102.



© 2020 by the authors. Licensee MDPI, Basel, Switzerland. This article is an open access article distributed under the terms and conditions of the Creative Commons Attribution (CC BY) license (http://creativecommons.org/licenses/by/4.0/).

Available online at www.sciencedirect.com

ScienceDirect

Energy Procedia 85 (2016) 425 – 432

Energy Procedia

Sustainable Solutions for Energy and Environment, EENVIRO - YRC 2015, 18-20 November 2015, Bucharest, Romania

Efficiency improvement of photovoltaic panels by using air cooled heat sinks

Cătălin George Popovici[a], Sebastian Valeriu Hudișteanu[a]*, Theodor Dorin Mateescu[a], Nelu-Cristian Cherecheș[a]

[a]*Faculty of Civil Engineering and Building Services, "Gheorghe Asachi" Technical University of Iasi, 13 Dimitrie Mangeron, Iasi, 700050, Romania*

Abstract

The operating temperature of photovoltaic panels represents an important parameter that influences their conversion efficiency. High operating temperatures determine a decrease of maximum output power in the same conditions of solar radiation. The study presents a numerical approach of the reduction of temperature of the photovoltaic panels by using the air cooled heat sinks. The heat sink is conceived as a ribbed wall, realized of a high thermal conductivity material. The cooling efficiency is studied for different configurations of the heat sink, obtained by modifying the angle between the ribs and the base plate. The numerical model was realized using ANSYS-Fluent software for turbulent flow and the results are presented for the average temperature of the photovoltaic panel.

© 2016 The Authors. Published by Elsevier Ltd. This is an open access article under the CC BY-NC-ND license (http://creativecommons.org/licenses/by-nc-nd/4.0/).

Peer-review under responsibility of the organizing committee EENVIRO 2015

Keywords: photovoltaic panel; heat transfer; numerical model; operating temperature; efficiency; turbulent flow.

1. Introduction

A photovoltaic (PV) panel represents an ensemble made of several photovoltaic cells designed to convert solar radiation into electric energy by photovoltaic effect. The most important characteristic of a photovoltaic panel is the conversion efficiency, which expresses the amount of solar radiation that is transformed into electric power, in certain conditions. The typical maximum values of the efficiency are reached between 14% and 17%, in case of

* Corresponding author. Tel.: 004-0746-328-149.
E-mail address: seby_hudisteanu@yahoo.com

1876-6102 © 2016 The Authors. Published by Elsevier Ltd. This is an open access article under the CC BY-NC-ND license (http://creativecommons.org/licenses/by-nc-nd/4.0/).
Peer-review under responsibility of the organizing committee EENVIRO 2015
doi:10.1016/j.egypro.2015.12.223

mono-crystalline silicon solar cells [1]. The solar radiation that is not converted into electricity is almost entirely transformed into heat.

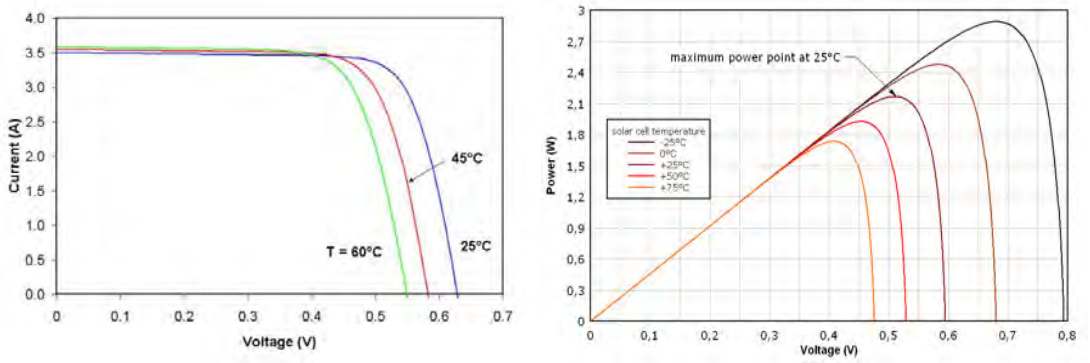


Fig. 1. The influence of PV panel temperature over output parameters [2, 3]

The dependence between the conversion efficiency and the temperature of photovoltaic cell represents an important study domain for researchers. Scientific literature papers [4], results [5, 6] and manufacturers [7-10] confirmed the decrease of efficiency while the temperature of PV cell rises. Most studies [4-10] claim that the maximum power produced varies almost linear with the operating temperature. In Fig. 1 it is noticed that the value of the current produced by PV cell has an insignificant rise when the temperature of the cell is greater, but the voltage has in important reduction, causing a drop of the maximum power generated.

The average reduction of efficiency is about 0.45%, for each degree over the 25 °C [11].

For defining the performance of a PV cell, the concept of Standard Test Conditions (STC) is needed [12]. The reference electrical power produced by a photovoltaic panel is defined for an average temperature of the cell of 25 °C and intensity of solar radiation of 1000 W/m². In these conditions, the PV cell generates the maximum power, which is measured in Watt-peak (W_p). This value is relevant for manufacturers, but in real operating conditions, the power of a PV cell is dependent on temperature changes and solar radiation level.

Different solutions for reducing the operating temperature of PV panels are sustained by specialized literature. Skoplaki et al. [13] present methods and relations for determining the dependence between conversion efficiency and temperature of PV cells. A method for improving the temperature of photovoltaic panels by using the air and passive cooling is studied by Cuce et al. [14].

Investigations regarding air cooling for photovoltaic panels are also proposed by Tonui et al. [15]. This solution consists in cooling the photovoltaic panel by realizing a ventilated channel of 0.1 m width behind it. Therefore, a photovoltaic/thermal (PV/T) system is created, which represents an optimized solution of using photovoltaic panels, with the additional role of producing thermal energy. This aspect is very important because there are generated two of the most used types of energy: electricity and heat. Moreover, the optimum functioning of each one brings benefits to the other [16].

The variation of the temperature of photovoltaic panels is also studied numerically in various works throughout literature. Hamrouni et al. [17] presents a study using MATLAB/Simulink software.

For obtaining accurate results and realizing correct simulations, is essential to know the structure of the photovoltaic panel. A typical example of the structure is presented in [18]. Therefore, the main layers are: exterior glass, anti-reflexive coating (ARC), PV cells, ethylene-vinyl acetate (EVA), metal rear contact and polyvinyl fluoride (PVF) film. The thermo-physical properties of these layers are presented in Table 1 [18]. The photovoltaic panels can have different layers, depending on the technology of conception and producer.

For present simulations, the PV panel was considered as a unique layer with thermal characteristics of the PV cells. A heat sink with ribs is connected behind it in order to realize a better heat transfer from the photovoltaic cell. The heat sink is considered to be made from a metal with high conductivity, in this case copper.

The photovoltaic system is the most efficient when the temperature of the cell is about 25 °C. In practice, there are few cases when the conditions to obtain this temperature are assured, determined by the lack of space or climatic conditions. Therefore, the concern to find solutions to reduce the operating temperature of the cells is necessary.

Table 1. Properties of the layers of photovoltaic panel [17]

Layer	Thickness (m)	Thermal conductivity (W/m·K)	Density (kg/m^3)	Specific heat capacity J/kg·K)
1. Glass	0.003	1.8	3000	500
2. ARC	100 x 10^{-9}	32	2400	691
3. PV Cells	225 x 10^{-6}	148	2330	677
4. EVA	500 x 10^{-6}	0.35	960	2090
5. Rear contact	10 x 10^{-6}	237	2700	900
6. PVF	0.0001	0.2	1200	1250

2. Problem description

The paper studies the influence of the operating temperature of a photovoltaic panel during a clear day of summer. The position of the panel is considered vertical, integrated into a ventilated double skin façade (DSF). In this hypothesis, the PV panel is a part of exterior glazing of the double skin façade. The study presents also a solution to enhance the cooling of photovoltaic panel, by attaching a heat sink on its back. The width of double skin façade channel is considered constant, of 0.1 m.

The photovoltaic panel studied in this paper has the following dimensions: L (length) = H (height) = 0.5 m. The cooling of the PV panel is evaluated in case of using a heat sink with ribs, for different heights and angles of the ribs.

The heat sink that is attached at the back of PV panel is realized from a metal with high thermal conductivity, like copper or aluminum. The heat sink is composed from a ribbed wall, with following dimensional characteristics:

h – height of the ribs (0.01...0.05 m);
s – step between ribs (0.05 m);
L, H – length and height of heat sink base (L = H = 0.5 m);
g – thickness of the base of the heat sinks (0.002 m);
g_n – thickness of the ribs (0.002 m);
l_n – length of the ribs (0.48 m).

3. Numerical approach

The geometry of the model, Fig. 2, was realized using ANSYS – Design Modeler. The ribs of the heat sink have circular holes of 0.003 m radius, placed at a distance of 0.03 m one to another. These holes intend to improve the air circulation near the heat sink and to extract more heat from the PV panel. The mesh was realized with different refinement for the heat sink and ventilation channel. Therefore, the minimum size of the cell in the interest domain is about 0.002 m for the heat sink and ribs, and about 0.008 m for the air channel.

The model used to simulate the solar radiation is the specialized tool Solar Ray Tracing from Fluent software. The optical parameters of photovoltaic panel were synthesized as a global absorption coefficient of solar radiation, $\alpha = 0.7$ *[19]*.

The resulting Reynolds (Re) number is about 13100, for the imposed velocity of 1.5 m/s [16]. Therefore, the turbulent flow regime was considered. The numerical simulation was realized using k-ε Re-Normalization Group (RNG) model of turbulence, recommended for air flow inside channels [20].

The turbulence intensity can be estimated as:

$$I = 0.16 \cdot Re^{-\frac{1}{8}} \quad (1)$$

The characteristic values used as input for turbulence model was:

I – turbulence intensity of 4.8 % for the inlet velocity 1.5 m/s;

DH – hydraulic diameter of the channel: 0.166 m.

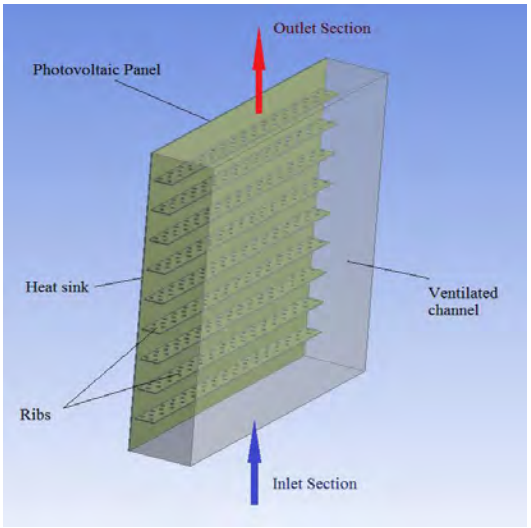


Fig. 2. Geometry of the studied model

Simulations were realized for disadvantageous external temperature of 35 °C. The velocity of the air behind the photovoltaic panel was set at 1.5 m/s [16]. The normal component of solar radiation used in the calculations is ΦS = 500 W/m2, assuming a vertical integration of the PV panel. A low convective heat transfer was considered to the outer surface of photovoltaic panel and the heat transfer coefficient was αconv = 8 W/m2.K.

The continuity, momentum and energy equations were solved using Fluent computational tool. For simulation it was used the control volume method, SIMPLE pressure-velocity coupling and First Order Upwind for equation solver. This method uses a relationship between velocity and pressure corrections to enforce mass conservation and to obtain the pressure field. A fully implicit numerical scheme is employed, in which upwind differences are used for the convective terms and central differences for the diffusion terms. The calculation is iterative, with convergence criteria of 10-6 for the energy equation and 10-3 for the pressure, velocities and continuity equations.

The different cases studied in this paper were realized by modifying the height of ribs from 0.01 m to 0.05 m with the step of 0.01 m. Once the height is growing another row of holes is added on the rib. The inclination of the ribs toward the vertical is also variable. The angles studied in these simulations are of 45°, 90° and 135°, see Fig. 3.

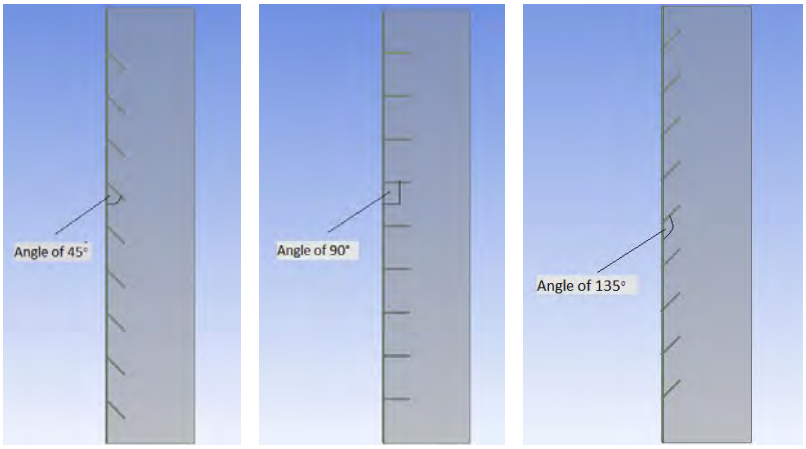


Fig. 3 – Inclination angles of the ribs for studied cases

4. Results

Results of simulations consist of the photovoltaic panel temperature variation depending on the height and angle of the ribs. Figures exported from the ANSYS-Fluent software present temperature spectra, Fig. 4, and velocity magnitude, Fig. 5, for the intermediate case of 0.03 m rib height.

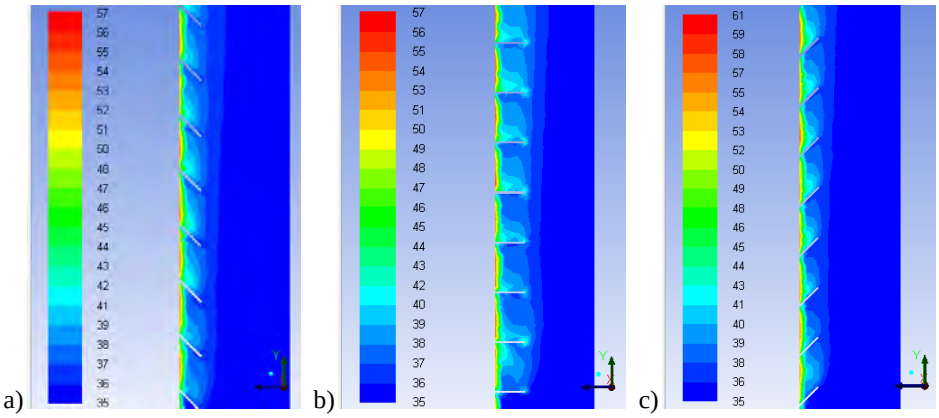


Fig. 4. Temperature spectra for different angles of ribs a) 45 °, b) 90°, c) 135°

The angle of the ribs has an influence on the heat transfer and airflow inside the ventilated channel. A more intense heat transfer is recorded for the angle of 45°, while the case of 135° angle is considered the most disadvantageous. In consequence, the maximum temperature of the photovoltaic panel is greater for the 135°, of about 61 °C, Fig. 4, while in the other two cases it is limited to 57 °C. The same tendency is also registered for the other heights of the ribs studied.

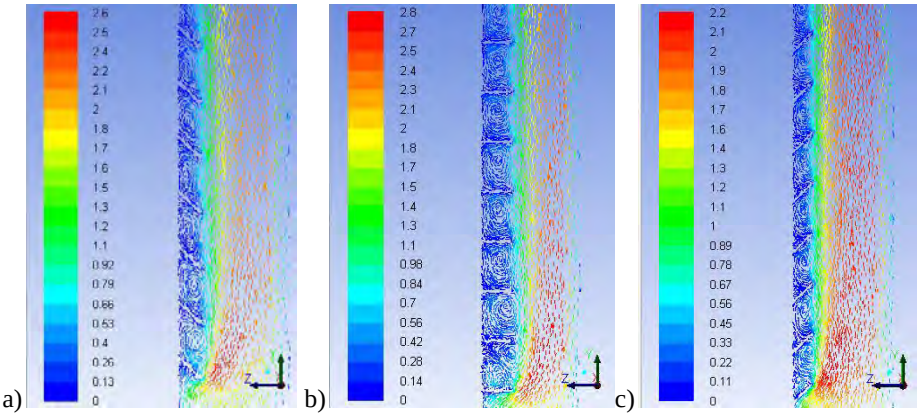


Fig. 5. Velocity magnitude for different angles of ribs a)45 ° b) 90° c) 135°

The cooling of the photovoltaic panel is directly proportional with the height of the ribs and inversely proportional with their inclination angle, Fig. 6. Lower values for operating temperature of the cell are registered for the angle of 45 °. The average temperature of the PV cell, Fig. 6, decreases when the 45° angle is used with about 1 °C comparing to the 135°, for the height of the rib of 0.03 m, while for the last case, when the height is 0.05 m, the drop of the temperature is about 2 °C. The angle of the ribs has a less important influence for low heights and the reversed effect is noticed for the 0.01 m height.

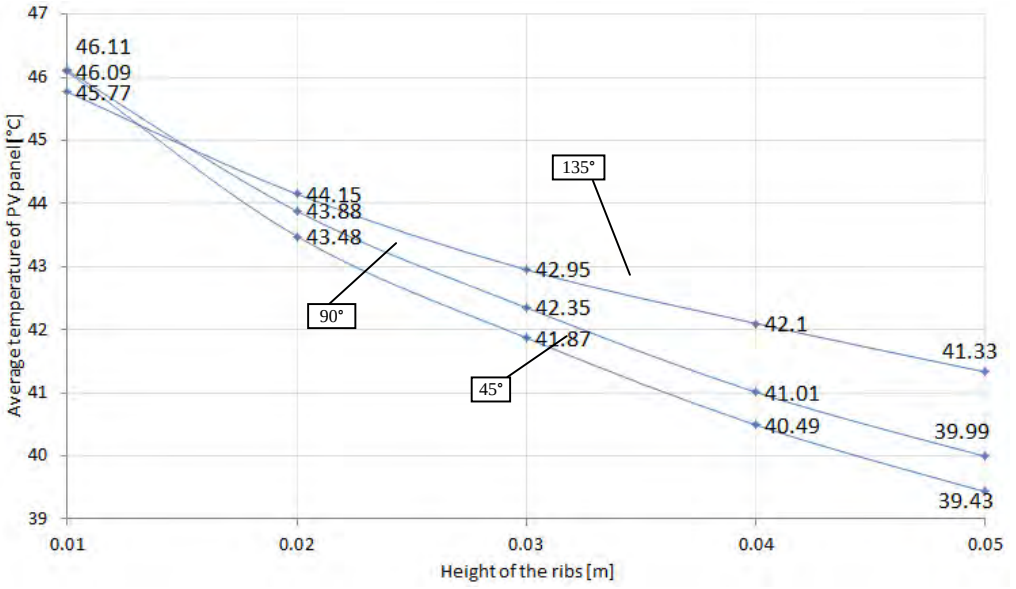


Fig. 6. Variation of average temperature of PV panel depending on the ribs angle and heights

The influence of the heat sink with ribs in reducing the temperature of the panel is presented in Table 2, for the 0.03 m height of the ribs. There are obtained increases of efficiency and higher productions of electric energy, in same conditions of solar radiation.

Table 2. Influence of operating temperature over PV panel efficiency

Case	Angle of ribs	t_p [°C]	*[%] of P_N	η	**P_{elspec} [W/m^2]	S_p [m^2]	P_{el} [W]	Raise over base case [%]
Base***	-	56	86	0.1376	68.8	0.25	17.2	-
h = 0.03 m	45°	41.87	92.5	0.148	74	0.25	18.5	7.55
	90°	42.35	92	0.1472	73.6	0.25	18.4	6.97
	135°	42.95	91.5	0.1464	73.2	0.25	18.3	6.39
Nominal	-	25	100	0.16	80	0.25	20	16.28

* According to [22]

** Incident solar radiation 500 W/m^2

*** Case without ribs

Where: t_p – average temperature of PV panel [°C];
P_N – nominal power produced at 25 °C [W];
η – conversion efficience, $\eta = P_{el}/\Phi_S$;
$P_{elespec}$ – specific electric power [W/m^2];
S – surface of PV panel [m^2];
P_{el} – electrical power produced by the studied PV panel [W].

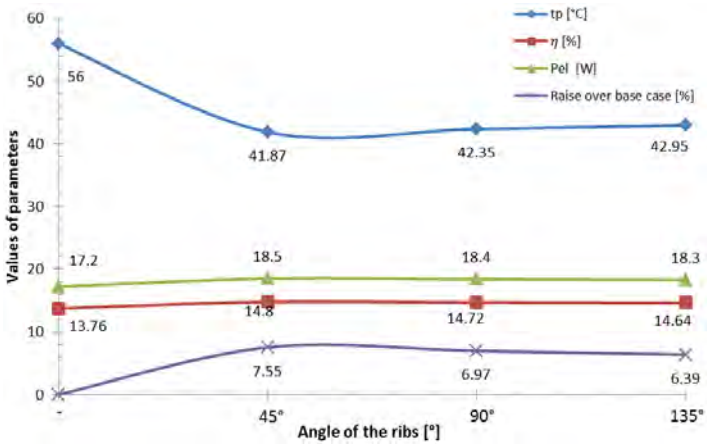


Fig. 7. Variation of PV panel temperature (t_p), efficiency (η), power (P_{el}) and the raise over the base case for height of ribs of 0.03 m

5. Conclusions

The operating temperature of photovoltaic panel has an important influence on its conversion efficiency, Fig. 7. This effect is easiest to be explored through the main parameters of the PV panel: intensity of the current and the voltage of the photovoltaic panel, which are globally expressed as maximum output power. For the studied case, the operating temperature of PV panel reaches about 56 °C, if no ribs are used and the maximum produced power is 86% of the nominal one.

In case of using a heat sink, even for small heights of the ribs, the average temperature of the PV panel is decreasing. According to simulations, the temperature is reduced with at least 10 °C below the value obtained in the basic case, Tab. 2. This aspect is favorable for the conversion efficiency, determining a maximum power produced above 90% of the nominal one.

According to Fig. 7, for the studied configuration, the raise of maximum power produced by photovoltaic panel is from 6.97% to 7.55% comparing to the base case, for angles of the ribs from 90° to 45° respectively.

Taking into account the intrinsic necessity of ventilating the double skin facades during summer, the presented method could represent a cheap and energy efficient solution for cooling photovoltaic panels.

In order to validate these results, an experimental research will be realized in future works.

References

[1] http://www.ctsolarservices.com/ct-solar-services-photovoltaics.html.
[2] http://en.wikipedia.org/wiki/File:I-V_Curve_T.png.
[3] http://www.pvresources.com/portals/0/Images/SolarCells/solarcells4.png.
[4] Fesharaki VJ, Dehghani M, Fesharaki JJ. The Effect of Temperature on Photovoltaic Cell Efficiency, Proceedings of the 1st International Conference on ETEC, Tehran, Iran; 2011.
[5] Borkar DS, Prayagi SV, Gotmare J. Performance Evaluation of Photovoltaic Solar Panel Using Thermoelectric Cooling, International Journal of Engineering Research, Vol. 3, No. 9; 2014, p. 536-539.
[6] Fontenault B. Active Forced Convection Photovoltaic/Thermal Panel Efficiency Optimization Analysis, Rensselaer Polytechnic Institute Hartford; 2012.
[7] http://www.bosch-solarenergy.de.
[8] http://www.yinglisolar.com/en.
[9] http://global.kyocera.com.
[10] http://www.sharp-world.com.
[11] http://www.solar-facts.com/panels/panel-efficiency.php.
[12] FSEC Standard 202-10. Test Method for Photovoltaic Module Power Rating; 2010.
[13] Skoplaki E, Palyvos JA. On the temperature dependence of photovoltaic module electrical performance: A review of efficiency/power correlations, Solar Energy 83; 2009, p. 614–624.

[14] Cuce E, Bali T, Sekucoglu SA. Effects of passive cooling on performance of silicon photovoltaic cells, International Journal of Low-Carbon Technologies; 2011, p. 1-10.
[15] Tonui JK, Tripanagnostopoulos Y. Improved PV/T solar collectors with heat extraction by forced or natural air circulation, Renewable Energy 32; 2007, p. 623–637.
[16] Hudisteanu VS, Mateescu TD, Chereches NC, Popovici CG. Numerical study of air cooling photovoltaic panels using heat sinks, Romanian Journal of Civil Engineering, Vol. 6, No. 1; 2015, p. 11-20.
[17] Hamrouni N, Jraidi M, Chérif A, Solar radiation and ambient temperature effects on the performances of a PV pumping system, Revue des Energies Renouvelables, Vol. 11, No. 1; 2008, p. 95–106.
[18] Armstrong S, Hurley WG, A thermal model for photovoltaic panels under varying atmospheric conditions, Applied Thermal Engineering 30; 2010, p. 1488-1495.
[19] Santbergen R, Optical Absorption Factor of Solar Cells for PVT Systems, ISBN: 978–90–386–1467–0; 2008.
[20] ANSYS Fluent Documentation.
[21] Karvinen A, Ahlstedt H. Comparison of turbulence models in case of three-dimensional diffuser.
[22] http://www.lorentz.de/pdf/lorentz_pvmodules_general_en-en.pdf.

Environmental Engineering and Management Journal December 2020, Vol. 19, No. 12, 2231-2240
http://www.eemj.icpm.tuiasi.ro/; http://www.eemj.eu



"Gheorghe Asachi" Technical University of Iasi, Romania



EXPERIMENTAL ANALYSIS OF INNOVATIVE HEAT EXCHANGER WITH UNIFORM HEAT FLUX USED IN HEAT PUMPS SYSTEMS

Sebastian Valeriu Hudișteanu*, Cătălin George Popovici, Marina Verdeș, Vasilică Ciocan, Nelu-Cristian Chereches, Florin Emilian Țurcanu

Gheorghe Asachi Technical University of Iaşi, Faculty of Civil Engineering and Building Services, 13 Dimitrie Mangeron, Iași, 700050, Romania

Abstract

The study presents the experimental testing of a heat exchanger with uniform thermal flux (HEUTF), used as a cold source in HVAC systems with heat pumps. A water-water heat exchanger is tested, having a special geometry, with uniform thermal flux along the system. The heat exchanger proposed consists of a distributor and a collector, connected to each other by means of 20 staggered copper pipes, being suitable for serving low or medium geothermal sources. The innovation consists in the uniformity of the heat flux along the entire length of the heat exchanger, due to the alternating circulation of the heat transfer fluid between collector and distributor. The work is focussed on offering a replacement to current technical solutions that are characterized by horizontal or vertical polyethylene pipes connected in parallel. Unlike the typical geothermal heat exchangers, when the surface and the depth of digging determines a non-uniform loading of the soil, the present solution induces an improved level of uniformity regarding the thermal load of the storage medium, while the global heat transfer coefficient resulting from the experimental tests has values between 76.9 ... 110.7 $W/m^{2}K$. The proposed solution is highly efficient in terms of maximizing the storage capacity and of decreasing the necessary surface for mounting the source.

Key words: beam of pipes, compact heat exchanger, geothermal sources, heat pump, heat flux

Received: March, 2020; Revised final: May, 2020; Accepted: June, 2020; Published in final edited form: December, 2020

1. Introduction

The field of heat pumping systems has become of interest in European countries since the 1970s, in Switzerland, and the 1980s, in Sweden. During this period, an intense program of analysing the behaviour during the lifetime of these systems has begun (Cazacu, 2016). It was concluded that the most appropriate quantification of heat pump efficiency is given by their coefficient of performance (COP), and with the help of the further studies, research and experimental tests it was progressively increased (Sebarchevici, 2013). Researches on the thermodynamic behaviour of hybrid geothermal heat pump systems (Cazacu, 2016; Pricâ, 2015) has led to the statement that they have superior performance over conventional ones.

The moment when the internal efficiency of the system reached an adequate level of performance coincided with an increase in the number of studies in literature that are focussing on improving the performance of the heat extraction/injection into the storage medium. Studies from University of Technology in Nicosia, Cyprus, 2013 aimed on the geothermal properties of the soil used for heat pump systems, while at the Perpignan Via Domitia University in France, the improvement of geothermal drills with vertical boreholes is analysed by controlling the thermal conductivity of the bentonite used (Cazacu, 2016).

* Author to whom all correspondence should be addressed: e-mail: sebastian.hudisteanu@tuiasi.ro; Phone: +407 46328149

The European Geothermal Heat Pump market reveals the tendency of the countries with stable markets and the development of some new ones (Fig. 1) (Gavriliuc, 2015). The European legislation regarding the field of heat pump systems is not fully resolved yet, having important differences between countries (Popovici and Hudișteanu, 2019). The main reasons why legislation cannot be fully harmonized are the existence of various geological conditions, country development index or financial support programs offered by governments (AG 31-008, 2002; Bonin, 2015; Ekman et al., 2008; EurObserv'ER, 2016; Forsén et al., 2008; NRC, 2004; Rehman, 2011).

The studies from literature are regarding on the systems using geothermal heat pumps equipped with different types of water-water or water-ground heat exchangers (ASHRAE, 1995, 2012, 2013). According to these, one of the most important elements that ensures an optimum operation of the heat pump systems is the geothermal heat exchanger (Gabor et al., 2016; Gavriliuc, 1999, 2016; Neacsu et al., 2010) and the heat storage medium (Klimašauskas, 2020). The main parameter that characterizes geothermal heat exchangers is the global heat transfer coefficient K [W/m^{2}·K] (Sebarchevici, 2013; Gabor et al., 2017), which represents also the main research target of the present study.

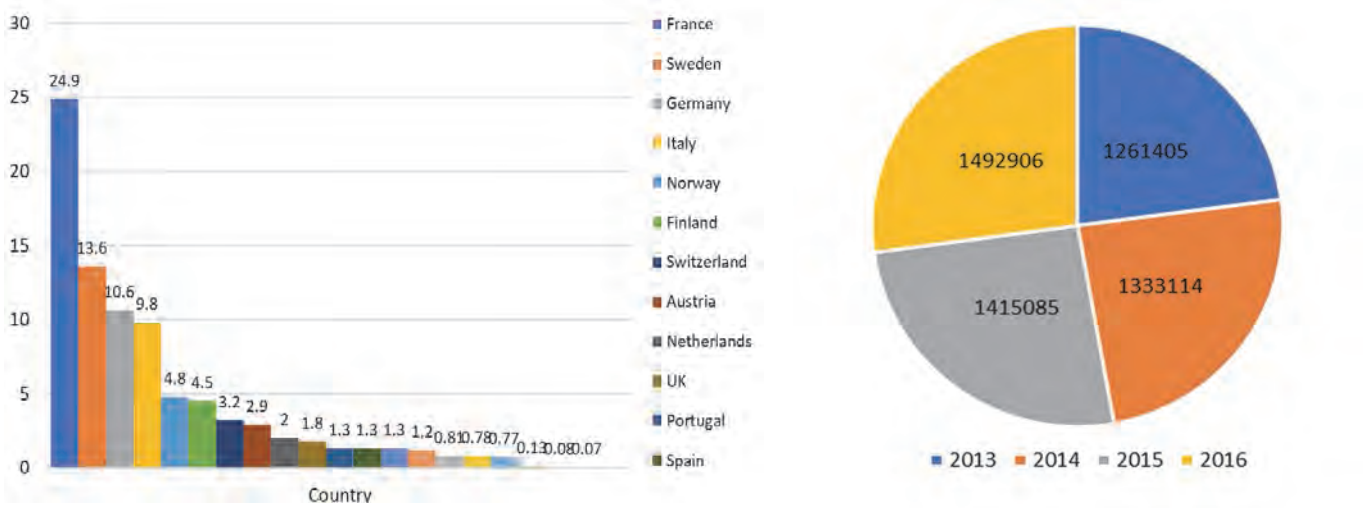
This experimental research presents the analysis of the operating parameters of an innovative heat exchanger with uniform heat flux (HEUTF) that offers a replacement to current technical solutions that are characterized by horizontal or vertical polyethylene pipes connected in parallel (Raymond et al., 2015). The novelty of the research consists in conception of a heat exchanger with a special geometry and achieve, by experimental tests, conclusive data regarding the velocities, flow rates, temperatures and global heat transfer coefficient.

2. Experimental setup

The experimental results are used for determining the heat flux and heat transfer coefficient of the heat exchanger evaluated. The images of the heat exchanger subjected to analysis are presented in the following images in Fig. 2. The main elements of the proposed heat exchanger are presented in Figs. 3-4. The model was validated by preliminary numerical analysis conducted for this special arrangement of the main components, that is used in order to obtain an evenly distributed average temperature of heat exchange over the entire surface of the exchanger (Popovici and Hudișteanu, 2019).

The heat exchanger with uniform thermal flow (HEUTF) integrated as a cold source for heating and air-conditioning systems equipped with heat pumps is a small-scale geothermal heat exchanger with a high thermal conductivity beam of pipes. The analysed heat exchanger has a special geometry, consisting of a distributor (D) and a collector (C), connected to each other by means of 20 copper pipes, Cu15x0.7 mm. Fig. 5 shows an overview of the model analysed and the position of the heat exchanger inside the storage medium. The particularity of this exchanger consists in the circulation of the heat transfer fluid, determined by the configuration of the distributor and the collector which are separated by alternating sectors.

The heat transfer fluid circulation is forced to take place in a strict direction between the inlet and outlet sectors, respectively from top to bottom and from bottom to top, alternatively (Fig. 6). Thus, the average temperature of the heat transfer is evenly distributed throughout the surface of the exchanger.



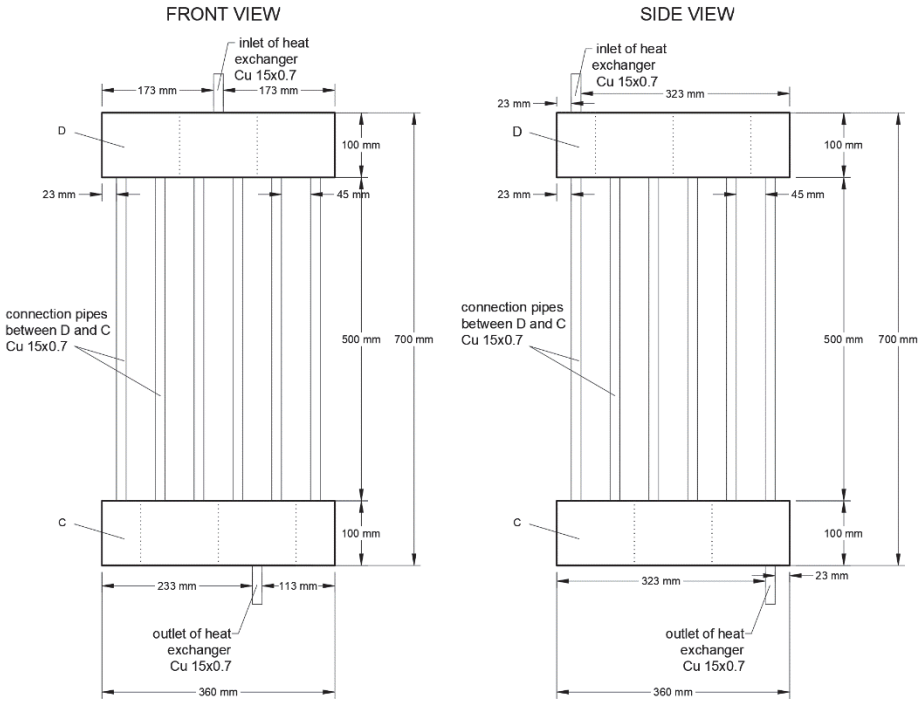
(a) (b)

Fig. 1. (a) Energy produced (TWh) by heat pumps in EU in 2014 (EHPA, 2020),
(b) Number of geothermal heat pump units in operation in EU 2013-2016 (Statista, 2020)



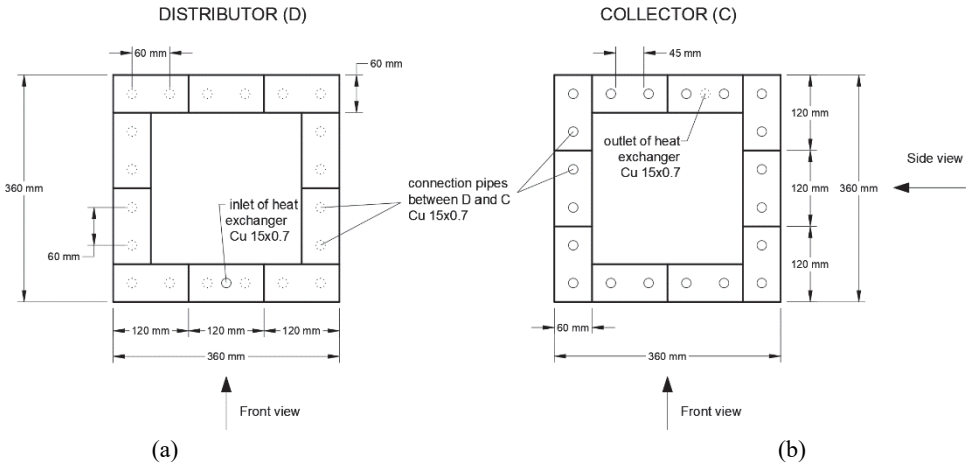
(a) (b)

Fig. 2. Images of the heat exchanger: (a) front view, (b) side view



(a) (b)

Fig. 3. Details of the heat exchanger: (a) front view, (b) side view



(a) (b)

Fig. 4. Details of the heat exchanger: (a) - distributor, (b) collector

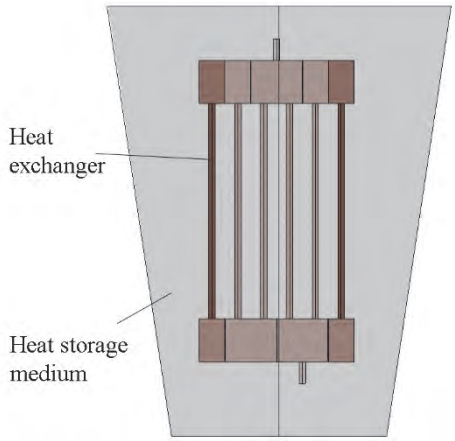
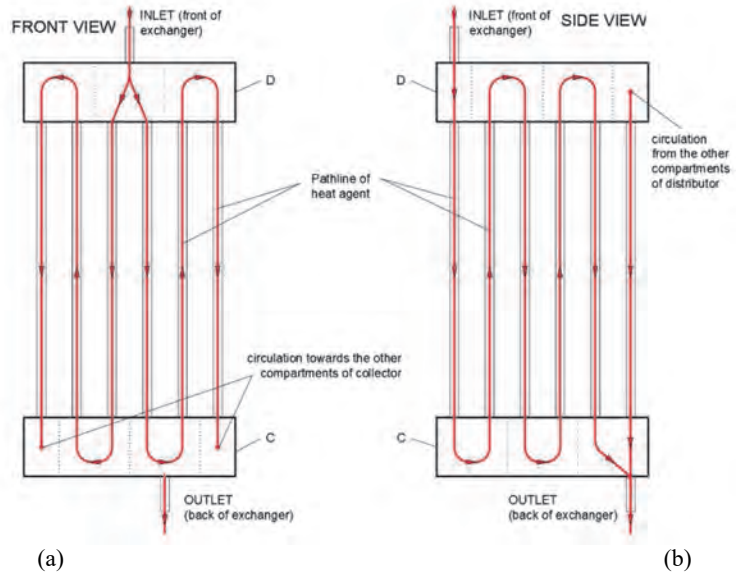


Fig. 5. Position of the heat exchanger inside the storage medium



(a) (b)

Fig. 6. The heat transfer fluid circulation through heat exchanger: (a) front view, (b) side view

The heat exchanger analysed is made of high thermal conductivity material (distributor/collector and pipes made of copper), with a transfer capacity superior to the exchangers made of polyethylene pipes. It is designed to be used as a cold/hot source for low and medium depth, required for systems equipped with geothermal heat pumps with mechanical vapor compression. It works with water as heat transfer fluid between the heat pump and the storage medium used. The heat flux (Q) transmitted by the small-scale heat exchanger is calculated according to the following relationship (Eq. 1):

$$Q = G \cdot \rho \cdot C \cdot (T_{in} - T_{out}) \ [W] \quad (1)$$

where: ρ [kg/m^3] - density of heat transfer fluid; c [J/kg·K] – specific heat of heat transfer fluid; $T_{in} - T_{out} = \Delta T$ [K] – temperature difference at heat pump; G [m^3/s] – volumetric flow rate.

The global heat transfer coefficient (K) is determined using the following mathematical expression (Eq. 2):

$$K = 1/[1/(\pi \cdot \alpha_i \cdot D_i) + (1/2 \cdot \pi \cdot \lambda)) \cdot \ln(D_i / D_e) + 1/\alpha^* \ [W/m^2K] \quad (2)$$

where: λ [W/m·K] – thermal conductivity of the pipes; D_i, D_e [m] - inner, outer diameter of the pipes; α_i [W/m^2·K] - convective heat transfer coefficient from heat transfer fluid to the pipe wall; α^* [W/m^2·K] - convective heat transfer coefficient from pipe wall to the storage medium.

During this study, the HEUTF is used to inject thermal energy into the storage medium (water), but it can be used also to extract thermal energy from soil/water or to recover heat from technological processes. It works with an intermediate heat transfer agent (water), between the heat pump exchanger and the storage medium used. HEUTF represents a heat exchanger with modular construction, designed with variable geometry, with uniform heat transfer and extraction throughout the system.

The uniformity of the thermal flux, which is the main characteristic of the proposed solution, ensures a

balanced loading of the earth mass including the drilling length reduction necessary for the storage medium. The uniformity can be also achieved by series connection of the multiple HEUTF with increasing lengths along the heat transfer fluid circulation. The proposed small-scale heat exchanger is tested in three constructive variants (Table 1), obtained by varying the length of the pipes:

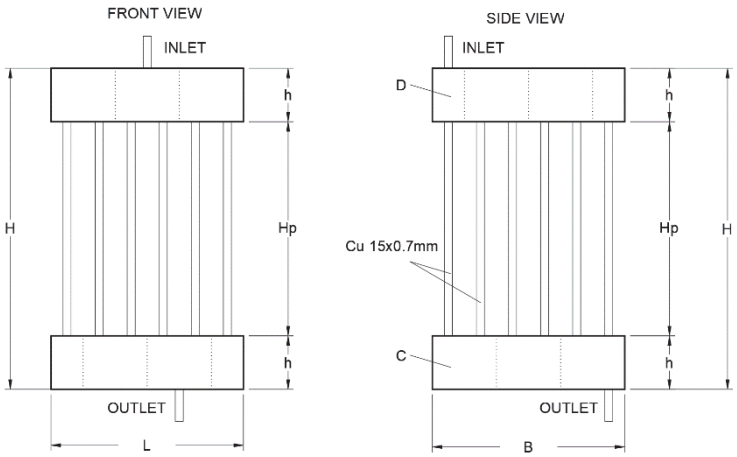
- HEUTF 60: H = 600 mm, H_p = 400 mm;
- HEUTF 70: H = 700 mm, H_p = 500 mm;
- HEUTF 80: H = 800 mm, H_p = 600 mm.

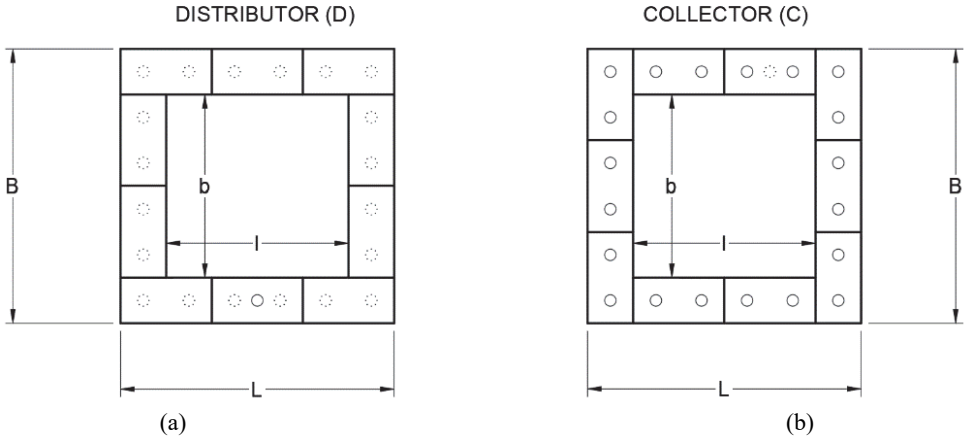
The structure of distributor/collector, both composed of 10 separate sectors for the circulation of the heat transfer fluid is presented in the following image (Fig. 7).

The main purpose of the analysis of the efficiency of the heat exchangers is to determine the global heat transfer coefficient by measuring the inlet and outlet temperatures of the heat transfer fluid, as well as the operating conditions of the heat pump.

The output temperature of the heat transfer fluid from the heat exchanger is the determining factor in the process of extracting/injecting heat from/to the storage medium, quantifying the energy efficiency throughout the system. The technical details of the heat exchange parameters of the 3 models of heat exchangers proposed are recorded in Table 2. In order to verify the energy performance of the proposed solution, an experimental research program was carried out on the small-scale physical model.

Table 1. Dimensions and structure of the heat exchangers analysed

Model	***HEUTF60***	***HEUTF70***	***HEUTF80***
Dimensions			
Dimensions [mm]: – height (H) – width (L) – depth (B)	H = 600 L = 360 B = 360	H = 700 L = 360 B = 360	H = 800 L = 360 B = 360
Material	Copper		
Structure	Distributor (D) Beam of pipes (20 pieces) Collector (C)		



(a) (b)

Fig. 7. Sectors of circulation of heat agent inside (a) distributor (D), (b) collector (C) dimensions of D and C: - outer contour L x B x h [mm]: 360 x 360 x 100; - inner contour l x b x h [mm]: 240 x 240 x 100

Table 2. Technical details of the analysed heat exchangers

Model	***HEUTF60***	***HEUTF70***	***HEUTF80***
Beam of pipes	Cu 15x0.7mm		
	20 pieces		
Pipe length H_p [mm]	400	500	600
Heat exchange surface [m^2]	0.918	1.012	1.106
Volume of the heat exchanger [L]	15.81	16.17	16.52
Mass of empty heat exchanger [kg]	6.17	6.80	7.43
Montage	Vertical		
Inlet/Outlet connection	External cylindrical thread DN15, according to DIN ISO 228/1		
Length of heat transfer fluid path inside the exchanger [m]	8.24	10.25	12.26

The main objectives of the study were:

- determining the functional characteristics of the proposed heat exchangers;
- determining the global heat transfer coefficient of the exchangers;
- establishing the energy efficiency of the exchangers.

The experimental program was performed taking into account the variation of the operating parameters of the heat transfer fluid (temperatures, flow rates), as well as the temperature of the storage medium. The maximum temperatures and flow rates used in the tests for the injection of heat into the storage medium (water) were in the following range:

- inlet temperature of heat transfer fluid: T_{in} = 30....50 ºC;
- heat transfer fluid flow rate: q = 200...500 l/h.

The experimental program was carried out through the separate testing of the 3 proposed heat exchangers, using the experimental set up shown in Fig. 8, whose functional scheme is represented in Fig. 9. The tests were aimed at measuring the operating parameters of the proposed small-scale exchangers and their efficiency. The main components of the system are (Figs. 8-9): 1 - heat exchangers (inside storage tanks), 2 - storage tanks, 3 - rotameter, 4 - heat source - electric heater with circulation pump, 5 – hot water accumulator, 6 - manometer, 7 – safety valve, 8 - distribution pipelines, 9 – backup circulation pump, 10 - valves, ST/1 ... 13 - temperature sensors, D/C – distributor/collector of the system, HP - heat pump, FC - fan coil, DAS - data acquisition station.

The experiments were achieved according to the parameters presented in Table 3. The experimental program included a series of several tests, by varying the parameters of the heat transfer fluid and the regime of heat injection using the proposed small-scale heat exchangers. The characteristics of the main instruments used for measuring temperatures and flow rates are presented in Table 4. All the temperature sensors used together with MS5 Data Logger were supposed to a calibration bath at constant temperature to let the two devices adjust for 30 minutes to the temperature point.

Table 3. The values for the main parameters involved during experiment

Parameter	***Value***
Heat transfer fluid and storage medium	Water
Nominal heat flow rate [kg/s]	0.056
Density of heat transfer fluid [kg/m^3]	995.56
Dynamic viscosity of the heat transfer fluid [Pa·s]	1.0×10^{-3}
Specific heat of heat transfer fluid [J/kg·K]	4110
Initial temperature of heat transfer fluid [°C]	55
Initial temperature of the storage medium [°C]	15
Operating pressure of heat transfer fluid [bar]	0.5...6



Fig. 8. The experimental stand - storage tanks and secondary circuit

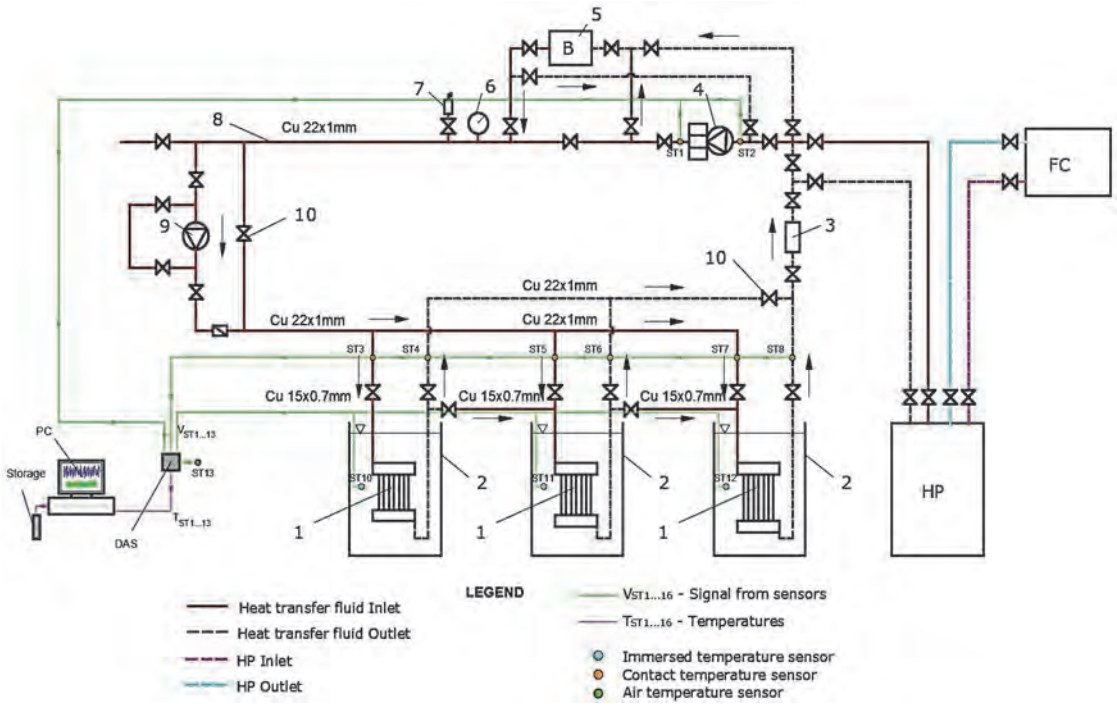


Fig. 9. Functional scheme of the experimental stand

Table 4. The accuracy and range of measuring devices

No.	*Equipment*	*Use*	*Characteristics*
1	Data acquisition system (DataLogger MS5) http://www.comet-datalogger.hu/english/monitoring-system-ms5.htm	Read signal from temperature sensors	16 channels
2	Immersed temperature sensor (Pt1000TG68/0 universal probe) - www.tequipment.net/Comet/SN233/Temperature-Probes/	Measure temperature of storage medium (suspended in water storage tank)	Range from -30 to +150°C Accuracy class of element * ± (0,15 + 0,002 | t |) in °C
3	Contact temperature sensor (PTS350-5/0 surface probe) - www.tequipment.net/Comet/SN182/Temperature-Probes/#description	Measure temperature of heat transfer fluid (attached to pipes)	Range from -30 to +130°C Accuracy class of element * ± (0,15 + 0,002 | t |) in °C
4	Air temperature sensor (Pt1000TG7/0 surface probe) – www.tequipment.net/Comet/SN167/Temperature-Probes/	Measure temperature of outside air (suspended in air)	Range from -30 to +200°C, Accuracy ±(0,15+0,002 |t|)
5	Flowmeter (HFB-2-05) www.dwyer-inst.com/Product/Flow/Flowmeters/In-Line/SeriesHF?Query=HFB-2-05#specs	Measure volumetric flow of heat transfer fluid	Range from 1...19 l/m water Accuracy: 4% FS over the entire field; 2.5% centre third of the measuring range; repeatability: 1% of scale
6	Electric heater www.hydronicsupplies.com.au/wp-content/uploads/2015/04/Laing-Electric-Heaters.pdf	Temperature control of heat transfer fluid	Heating capacity: 2000 W pump A1-150, 230V, 25W constant temperature thermostat with a range of 20°C to 80°C

3. Results and discussion

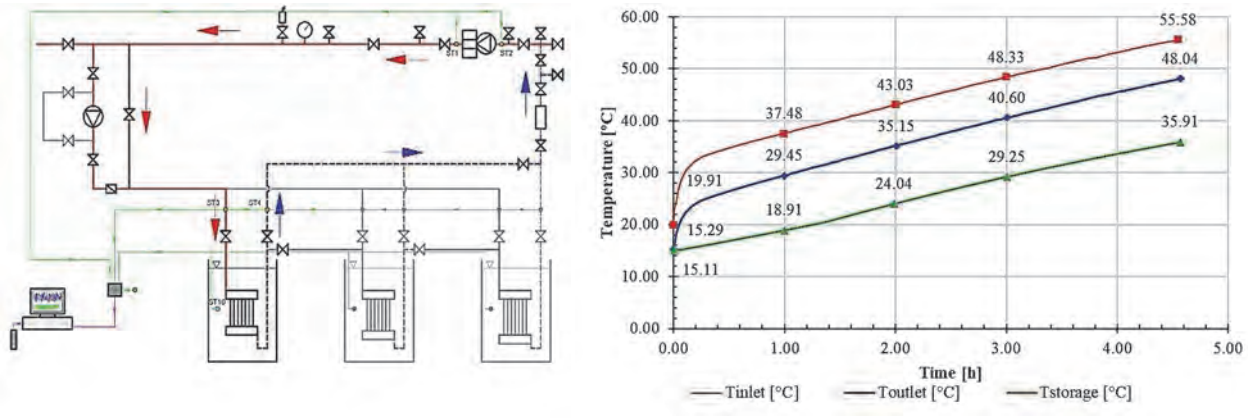
A total of four experiments were conducted in this research. The results presented are based on a number of at least three preliminary repetitive tests for each experiment with approximately the same input parameters, that provided the same trend of the output data. Tests 1, 2 and 3 present the separate operation of each small-scale heat exchanger, and the results are presented in Figs. 10 -12. The duration of experiments varies between 3.5 and 5 hours.

The HEUTF60 and HEUTF70 testing (Figs. 10-. 11) presents similarities in terms of storage temperature variation, while the HEUTF80 (Fig. 12) determines a more accelerated heat transfer as well as an intensified tendency of increasing the temperature of storage medium.

In Test 4, the experimental measurements were performed on the series connection of the proposed small-scale heat exchangers. Thus, in order to obtain the heat flux uniformity, the heat exchangers were successively connected from the smallest one (HEUTF60) at inlet, to the largest one (HEUTF80) at outlet. The results of the experiment are presented in Fig. 13. It was noticed that after some initial fluctuations in the first hours of operation, the

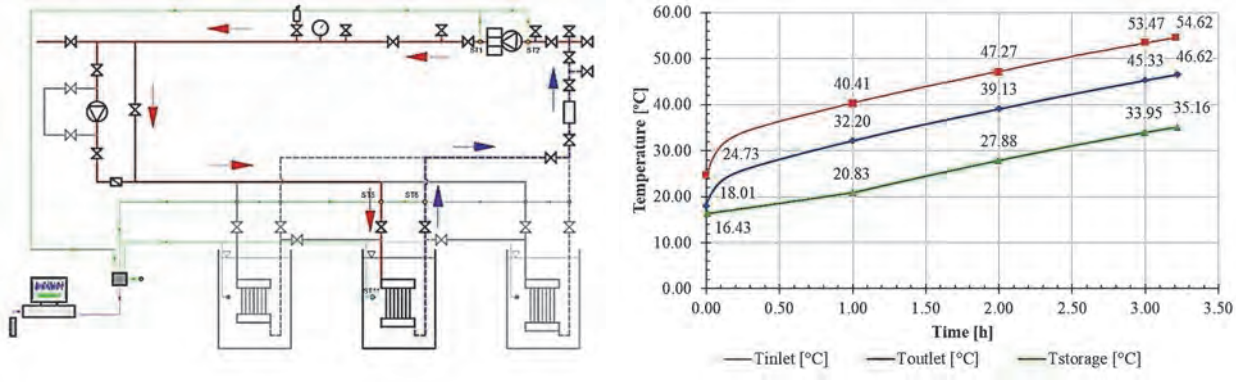
temperatures in all the storage media begin to have approximately equal values (Fig. 13), meaning that the storage media started to be quasi-uniform loaded by the heat exchangers. This represents an important advantage in order to realize the correct dimensioning, forecasting and evaluation of a system to be installed.

The energy performances of the heat exchangers were analyzed from the point of view of the efficiency of the heat transfer, quantified as global heat transfer coefficient. The proposed heat exchangers were analyzed separately and the uniform loading of the storage medium (water) was also found when they are connected in series. Table 5 presents the values of the of the global heat transfer coefficient for each type of small-scale heat exchanger for various operation times (from 1 hour to 3 hours).



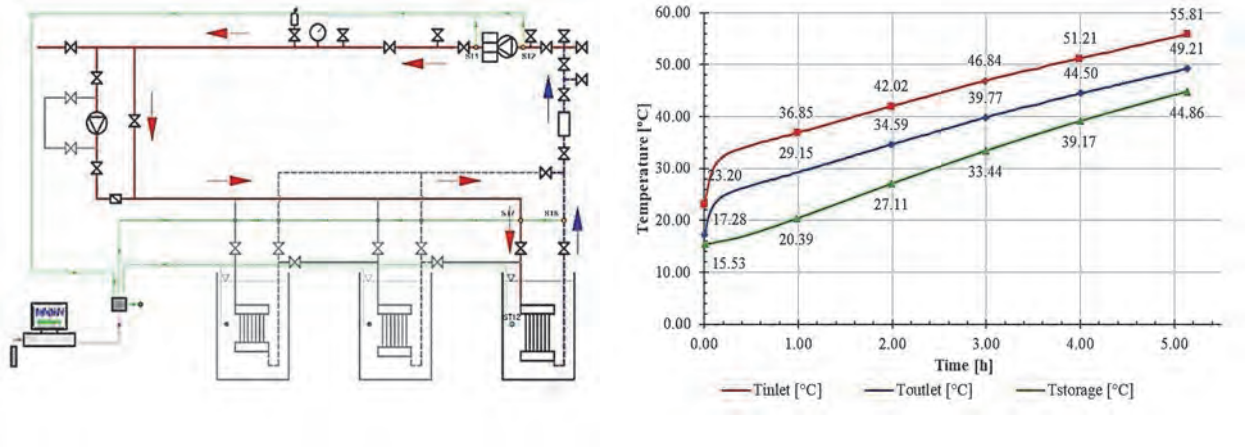
(a) (b)

Fig. 10. Test 1 - Operation of the first heat exchanger (HEUTF60, H = 600 mm, H_p = 400 mm): (a) functional scheme, (b) evolution of inlet, outlet and storage medium temperatures



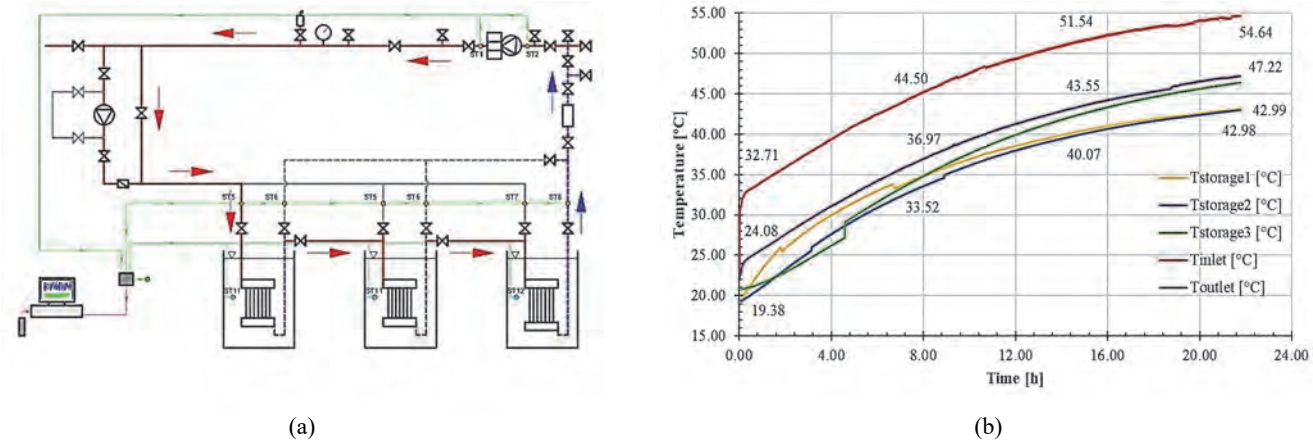
(a) (b)

Fig. 11. Test 2 - Operation of the second heat exchanger (HEUTF70, H = 700 mm, H_p = 500 mm): (a) functional scheme, (b) evolution of inlet, outlet and storage medium temperatures



(a) (b)

Fig. 12. Test 3 - Operation of the third heat exchanger (HEUTF80, H = 800 mm, H_p = 600 mm): (a) functional scheme, (b) evolution of inlet, outlet and storage medium temperatures



(a) (b)

Fig. 13. Test 4 - Analysis of the uniformity of the loading of the storage medium by series connection of the proposed exchangers (HEUTF60, 70, 80): (a) functional scheme, (b) evolution of inlet, outlet and storage medium temperatures

Table 5. The global heat transfer coefficient for each type of exchanger

Model	***HEUTF60***	***HEUTF70***	***HEUTF80***
Pressure loss [bar]	0.024	0.026	0.029
Operating time [h]	1 / 2 / 3	1 / 2 / 3	1 / 2 / 3
Average thermal flow during operation [W]	883.1 / 744.3 / 726.9	910.6 / 776.0 / 744.7	1176.3 / 970.8 / 823.7
Average global heat transfer coefficient during operation [W/m^2·K]	88.0 / 78.2 / 76.9	93.8 / 84.5 / 82.0	110.7 / 105.9 / 103.1

It is found that the global heat transfer coefficient resulting from the experimental tests varies between 76.9...110.7 W/m^2·K during the heat injection in the storage medium, decreasing once its temperature begins to rise. Taking into account the values of the global heat transfer coefficients from literature: 73.28…73.81 W/m^2·K (Neuberger et al., 2014), 100 W/m^2·K (Lamarche, 2019) at similar operating parameters, it is found that this type of exchanger has adequate results in order to represent a viable solution for use in heat pump systems and geothermal sources.

4. Conclusions

The main result of the study is that the proposed heat exchangers (HEUTF) achieve adequate global heat transfer coefficients (76.9 ... 110.7 W/m^2·K) during operation and constant heat flux when they are connected in series, ensuring uniform loading of the storage medium.

The proposed heat exchanger model is very well suited to new buildings with low availability for low-depth groundwater capture, equipped with ground-water or water-water heat pumps. Also, the proposed solution can successfully replace ground energy capture systems characterized by deep drillings (100 to 200 m) at a reduced price and good efficiency.

HEUTF can be also used for existing buildings equipped with cold-water heat pumps in classical variant. The advantage of integrating the proposed model lies in the flexibility, the reduced amount of necessary works or space and the limitation of the intervention area.

There is expected an economic impact of implementing the solution developed on a large scale, at the level of a residential, public, commercial or industrial building for capitalizing the residual or renewable energy resources. Though, the reduction of costs can be achieved by using the proposed heat exchangers with high efficiency of extracting/injecting the thermal energy needed for heating, ventilation and air conditioning systems. The implementation of the analysed solution at the level of a building has a potential of reduced return on investment time, depending on the size and the destination of the consumer.

Given that the heat exchanger with uniform heat flux does not have moving elements and is made by using modern technologies of execution, it is possible to estimate an important operating life and an increased safety in operation.

Acknowledgements

This work was supported by a grant of the Romanian Ministry of Research and Innovation, CCCDI - UEFISCDI, project number PN-III-P2-2.1-CI-2018-1491, within PNCDI III.

References

AG 31-008, (2002), Application guide AG 31-008, *Geothermal heat pump design manual*, McQuay International, Staunton, Virginia, USA.

ASHRAE, (1995), *Commercial/Institutional Ground-Source Heat Pump Engineering Manual*, American Society of Heating, Refrigerating and Air-Conditioning Engineers, Atlanta, USA.

ASHRAE, (2012), *HVAC System and Equipment*, American Society of Heating, Refrigerating and Air-Conditioning Engineers, Atlanta, USA, On line at:

https://www.ashrae.org/technical-resources/ashrae-handbook/description-2017-ashrae-handbook-fundamentals

ASHRAE, (2013), *Handbook Fundamentals*, American Society of Heating, Refrigerating and Air-Conditioning Engineers, Atlanta, USA, On line at: https://www.ashrae.org/technical-resources/ashrae-handbook/description-2017-ashrae-handbook-fundamentals

Bonin J., (2015), *Heat Pump Planning Handbook*, Routledge, New York, USA.

Cazacu I., (2016), *Use of renewable forms of energy in systems equipped with heat pumps* (in Romanian), PhD Thesis, Gheorghe Asachi Technical University of Iași, Romania.

EPHA, (2020), European Heat Pump Association, On line at: https://www.ehpa.org.

Ekman B., Granryd E., Nilsson T., Rolfsman L., (2008), *Handbook on Indirect Refrigeration and Heat Pump Systems*, Melinder A. (Ed.), Svenska Kyltekniska Föreningen, KTF, Kullavik, Sweden, On line at: http://www.cold.org.gr/library/downloads/Docs/library MEMBERS/gr/Handbook%20on%20indirect%20refrigeration%20and%20heat%20pump%20systems.pdf

EurObserv'ER, (2016), *The state of renewable energies in Europe*, Observ'ER, Paris, France, On line at: https://www.eurobserv-er.org/pdf/2016/EurObservER-Annual-Overview-2016-EN.pdf.

Forsén M., Roots P., Bertenstam A.L., (2008), *Market Status for Ground Source Heat Pumps in Europe*, Ground-reach market Status for Ground Source Heat Pumps in Europe, 1-41, On line at: https://ec.europa.eu/energy/intelligent/projects/sites/iee-projects/files/projects/documents/ground-reach_market_status_for_gchp_in_europe.pdf

Gabor T., Dan V., Badila I.N., Tiuc A.E., Sur I.M., (2017), Improving the energy efficiency of residential buildings by using a drain water heat recovery system, *Environmental Engineering and Management Journal*, **16**, 1631-1636.

Gabor T., Dan V., Tiuc A.E., Sur I.M., Badila I.N., (2016), Modelling and simulation of heat transfer processes for heat exchangers used in wastewater treatment, *Environmental Engineering and Management Journal*, **15**, 1027-1033.

Gavriliuc R., (1999), *Heat Pumps - from Theory to Practice*, (in Romanian), MatrixRom, Bucharest, 1-166.

Gavriliuc R., (2015), *Regulatory Aspects Referring to GSHPS Systems*, Conf. of Building Services and Energy Efficiency, Iași, Romania, 7-14.

Gavriliuc R., Cucueteanu, D., (2016), *First Data Base for Ground Source Heat Pumps Systems in Romania*, Romanian Conf. on the Energy Performance of Buildings RCEPB VIII, Bucharest, Romania, 2-3 June 2016.

Klimašauskas M., Šaulys V., Baublys R., Survilė O., (2020), Hydraulic conductivity of drainage ditch backfill with a lime additive in clay soils, *Environmental Engineering and Management Journal*, **19**, 497-504.

Lamarche L., (2019), Horizontal ground heat exchangers modelling, *Applied Thermal Engineering*, **155**, 534-545.

Neacsu S., Eparu C., Albulescu M., Stoica C., Stoica I., (2010), Experimental analysis of soil heat extraction systems, *Environmental Engineering and Management Journal*, **9**, 1407-1410.

Neuberger P., Adamovský R, Šeďová M., (2014), Temperatures and heat flows in a soil enclosing a slinky horizontal heat exchanger, *Energies*, **7**, 972-987.

NRC, (2004), *Heating and Cooling with a Heat Pump*, Natural Resource Canada's Office of Energy Efficiency, On line at: https://www.nrcan.gc.ca/energy/publications/efficiency/ residential/ heating-heat-pump/6817.

Popovici C.G., Hudișteanu S.V., (2019), Numerical analysis of heat exchanger with uniform heat flux used in heat pumps systems, *IOP Conf. Series - Materials Science and Engineering*, **586**, 1-10.

Prică G., (2015), *Research on the optimization of heat pumps that have soil as a heat source* (in Romanian), PhD Thesis, Technical University of Civil Engineering Bucharest, Romania.

Raymond J., Mercier S., Nguyen L., (2015), Designing coaxial ground heat exchangers with a thermally enhanced outer pipe, *Geotherm Energy*, **3**, 1-14.

Rehman U., (2011), *Heat transfer optimization of shell-and-tube heat exchanger through CFD studies heat transfer optimization of shell-and-tube heat exchanger*, MSc Thesis, Chalmers University of Technology, Goteborg, Sweden.

Sebarchevici C., (2013), *Optimization of thermal installations in buildings in order to reduce energy consumption and CO_2 emissions, using heat pump coupled to the ground* (in Romanian), PhD Thesis, Polytechnic University Timisoara, Romania.

Statista, (2020), Global Business Data Platform, On line at: https://www.statista.com/statistics/739745/heat-pumps-in-operation-eu.

FIRE AND ARTIFICIAL INTELLIGENCE (AI): HOW AI ANTICIPATES HUMAN BEHAVIOUR IN FIRE SITUATIONS- CASE STUDY OF THE COLECTIV FIRE

C.-G. Popovici[a], I. Enaru[a,] *, C.-C. Aioanei[a], F.-E. Ţurcanu[a], S.-V. Hudişteanu[a], N.-C. Cherecheş[a], Marina Verdeș[a], Diana-Ana Ancaș[a], V. Ciocan[a]

[a] Technical University "Ghe. Asachi" of Iasi, Faculty of Civil Engineering and Building Servicies, Department Building Sevicies, D. Mangeron 67 Street, 700050, Romania; E-mails: catalinpopovici@climatherm.ro, * iulian.enaru@student.tuiasi.ro, catalin-claudiu.aioanei@student.tuiasi.ro, turcanufemilian@gmail.com, seby_hudisteanu@yahoo.com, cristi_chereches@yahoo.com, verdesmarina2003@yahoo.com, ancas05@yahoo.com, vciocan2005@yahoo.com

Received: 17.12.2023 / Accepted: 20.01.2024 / Revised: 02.02.2024 / Available online: 31.05.2024

DOI: 10.2478/jaes-2024-0009

KEY WORDS: fire, emergency, PyroSim, FDS, simulation, Pathfinder.

ABSTRACT:

The catastrophic fire at Bucharest's Colectiv Club marks a profoundly tragic event in Romania's history, being one of the most significant human-made disasters the country has faced in recent decades. This study seeks to meticulously reconstruct the events of that fateful night through the use of advanced simulation software applications. By doing so, it aims to provide a detailed analysis of the factors leading to the tragedy, which claimed the lives of 64 individuals and caused injuries to 185 others. The objective is to understand better the dynamics and consequences of the fire, potentially leading to improvements in safety protocols and emergency response strategies to prevent such disasters in the future.

1. INTRODUCTION

1.1 Overview

One of the most critical emergency situations, in terms of the number of casualties resulting from its occurrence, is caused by the risk of fire (Chang et al., 2020).

In Romania, according to the statistics of the General Inspectorate for Emergency Situations[1], only in 2022, fires produced the highest number of victims compared to the other disasters that occurred on the territory of our country, both in terms of injuries and deaths. For example, in 2022, out of a total of 43234 fires, a total of 1057 victims resulted, of which a total of 742 people were injured and 315 people died, which, unfortunately, has maintained an upward trend in recent years.

One of the most significant fires regarding the number of victims resulting in our country is the fire that occurred on October 30, 2015, at the Colectiv Club in Bucharest (Figure 1). A fire broke out in a hall of a former factory in Bucharest, where the club was located, with disastrous consequences for the people present, causing 185 injuries and 64 deaths. In this context, this study aims to reconstruct and identify the measures that could have contributed to limiting the number of victims of the fire at the Colectiv Club in Bucharest, according to the provisions of the legislation in force at the time, but also to identify the lessons of good practice to prevent a similar emergency situation in the future (Galhardo et al., 2022).



Figure 1. Image captured during the concert before the fire started

Last but not least, the article also deals with the importance of using simulation software (Pyrosim, Pathfinder) with a focus on the "fire safety" requirement imposed by Law no. 10/1995 on quality in construction, which by their complexity and usefulness have a place in the portfolio of simulators used in the design of important buildings (Urban Habitat Constructions Under Catastrophic Events, n.d.).

2. THEORETICAL CONSIDERATIONS

According to the Control Report regarding the emergency intervention at the fire in the Colectiv Club in Bucharest on the evening of October 30, 2015, carried out by the Prime Minister's Control Corps, the fire at the Colectiv Club in Bucharest was one of the biggest human-made disasters in our country in the last 25 years, which took place on 30. 10.2015, at 10:32 p.m., resulting in 64 deaths (of which 27 people died at the time of the fire and 37 in hospital units) and 146 people injured (Figure 2).

* Corresponding author: Iulian Enaru, iulian.enaru@student.tuiasi.ro, Romania.

The fire that generated such a large number of victims started from some fireworks placed on the poles of the arranged stage, fireworks that came in contact with the polyurethane foam used for soundproofing and generated a fire, which in a very short time developed in the enclosed space where a large number of people were present.



Figure 2. Image from the fire, showing the fire victims and the escape door

In the initial phase, the participants overlooked the seriousness of the situation that was about to occur, as they considered it all part of the artistic program. Still, after the fire had grown in intensity, people began to evacuate the club through the only usable escape route represented by a door with a width of 85 cm. It should be specified that the space had two escape routes, one of which was blocked, and at the time of evacuation, due to panic, the people inside forced this evacuation, managing to evacuate there as well (Figure 3).

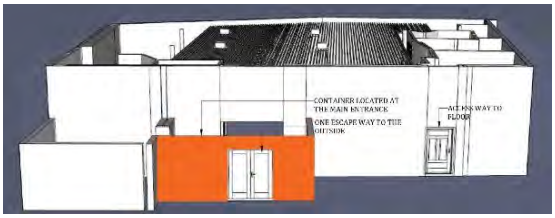


Figure 3. View of the main facade of the Colectiv Club created in PyroSim software

2.1 Reconstitution of the conditions that caused the fire

Using PyroSim simulation software and 3D design software (Allplan), the Colectiv club's geometry was created and adapted according to information found in the media regarding this issue (Figure 4, Figure 5).

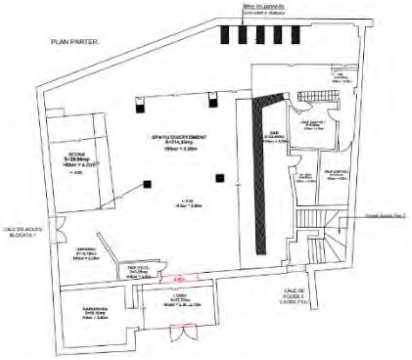


Figure 4. 2D plan of the Colectiv club showing the escape routes, including the blocked one

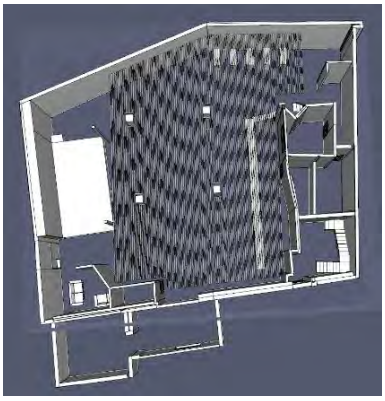


Figure 5. 3D plan of the Colectiv club showing the escape routes, including the blocked one

The chemical and physical properties of the elements that contributed to the initiation and development of the fire were defined using Pyrosim software (FDS) (Halawa, 2020).

The construction materials that initiated and maintained the burning phenomenon were defined, as well as the fireworks in the stage area (which also represent the source of the fire), the highly flammable polyurethane foam (being the first material that ignited) used for sound insulation placed both on the resistance pillars in the stage area and at the top, and the fir wood panels that were placed at the top, on the ceiling (Figure 6, Figure 7) (Costi, 2019).

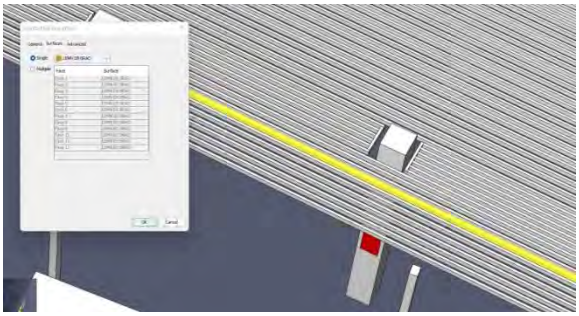


Figure 6. Defining combustible materials in the simulator

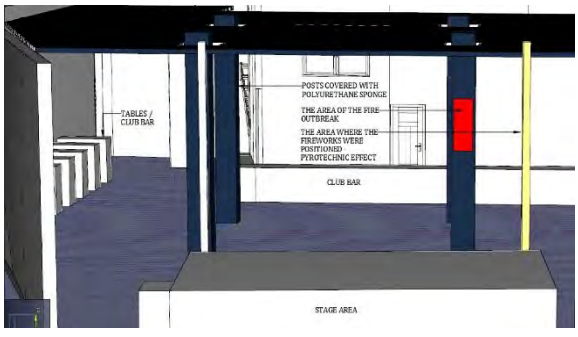


Figure 7. Highlighting the elements that initiated and maintained the fire (fireworks, polyurethane foam and wood)

Figure 7 highlights these three defining elements of the fire at the Colectiv Club. The source of the fire initiation (the fireworks) is materialised on the resistance pole, in the image

having the colour orange. Polyurethane foam is defined according to its chemical properties with the help of the simulator, and it is materialised in the image with blue colour. Last but not least, the wooden panels arranged on the ceiling of the room are defined by the software as having the properties of fir wood, and they can be seen in the image on the upper part (Wikipedia contributors, 2023).

2.2 Computer simulation of the fire

In recent years, there has been a great emphasis on conducting fire safety simulations. However, no such simulator has been created or adapted at the national level, so we use software developed by states with very well-developed "fire safety" requirements. Among the most important simulation software, we mention FDS Pyrosim and Pathfinder (Figure 8, Figure 9). (Nurul Liyana Hanapi , Sabarinah Sh Ahmad, Google Scholar, n.d.)

PyroSim was designed to complement the Fire Dynamics Simulator (FDS) developed by the National Institute of Standards and Technology (NIST) in the US, one of the most comprehensive and powerful simulators in fire research.

The author of the article also used this simulator to study one of the most significant fires in our country, namely the fire in the Colectiv Club.

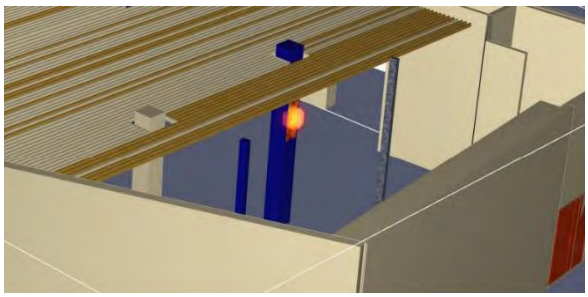


Figure 8. Fire initiation (virtual simulation



Figure 9. Fire initiation and delayed reaction of people (virtual simulation)

According to the videos taken at the scene, the occupants' delayed reaction to realising that what was happening at that moment was not part of the artistic moment but a real danger led to a general panic among those present, with all heading for the only available escape route from the club (Figure 10, Figure 11).

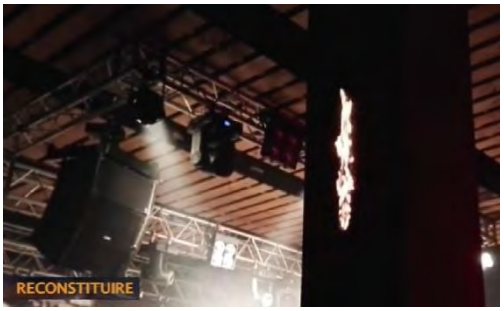


Figure 10. Fire initiation (actual situation)



Figure 11. The initiation of the fire and the lack of reaction from the participants

As seen in Figure 10, although the fire had started and was already taking on proportions, the people present did not react to what was happening and were unaware of the imminent danger to which they were exposed (Figure 12, Figure 13).

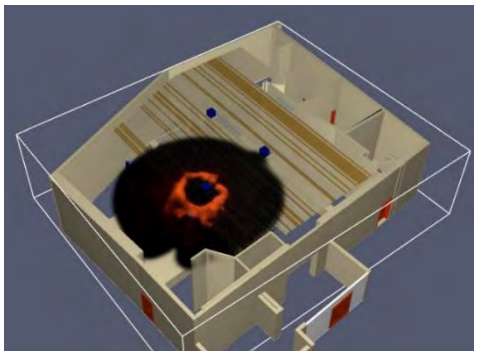


Figure 12. Fire development inside the club (virtual simulation)

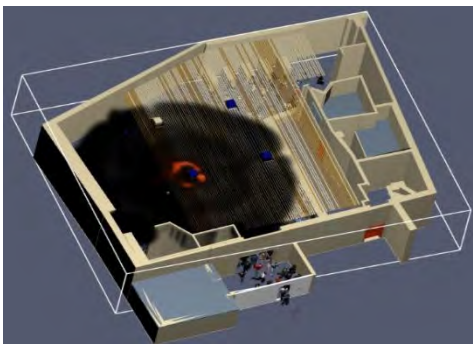


Figure 13. Development of the fire inside the club and start of evacuation of people (virtual simulation)

The escape route not being adequately dimensioned to evacuate the total number of flows present at the time inside the club, respectively dimensioned according to the provisions of the Normative on fire safety of constructions, Indicative P118/99 for "crowded rooms", led to situations where people were unable to evacuate themselves, thus leading to the injury and subsequent death of some of the occupants (Figure 14 - 17).



Figure 14. Fire development inside the club (actual situation)



Figure 15. Congestion created during evacuation (actual situation)

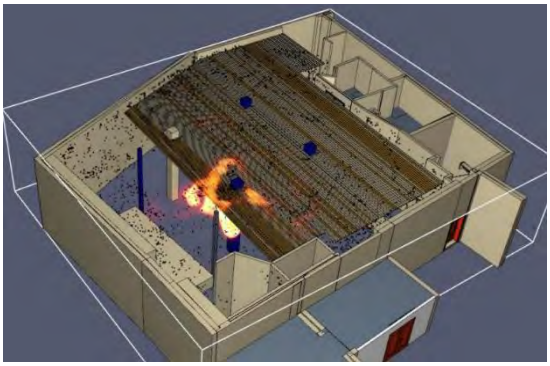


Figure 16. Burning of combustible elements at the top with burning droplets



Figure 17. Burning of combustible elements at the top with burning droplets (actual situation)

The most important causes of the death of the people present were the inhalation of harmful substances from the fire and the burns caused by burning droplets generated by the polyurethane foam on the ceiling (Figure 18, Figure 19).

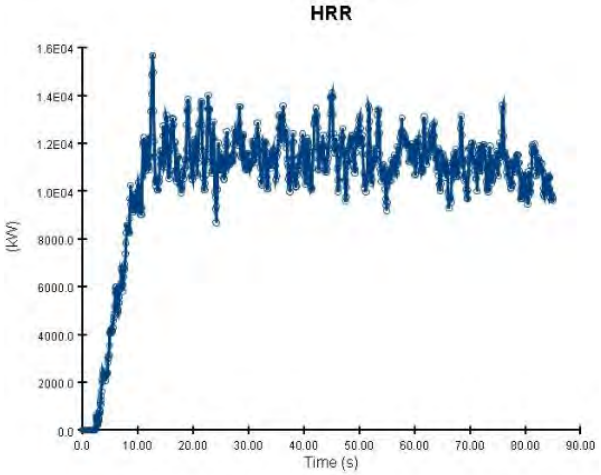


Figure 18. HRR (heat release rate)

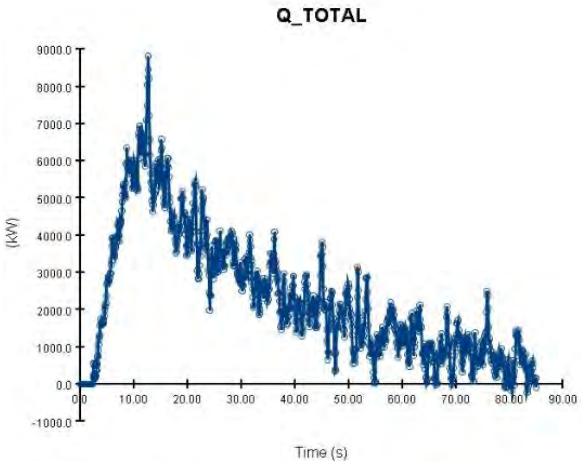


Figure 19. Total rate of released heat

2.3 Computer simulation of the evacuation of persons

Regarding the evacuation and the conditions in which it was carried out at the time of the tragedy at Colectiv, we can note that at that time, there were cumulative factors that made it

difficult to evacuate the users, factors that seriously violated the normative provisions in force at that time.

The Colectiv Club operated in a building of a former factory in Bucharest initially used for production and/or storage, and later changed its use to commerce.

The space in which the tragedy occurred was used for commercial purposes and also fulfilled the conditions of a crowded hall, given that it had an area of approximately 400 square meters and there were 364 people inside at the time of the fire.

According to the provisions of the normative acts at that time, namely H.G. no. 1.739 of December 6, 2006, for the approval of the categories of constructions and facilities that are subject to approval and/or authorisation regarding fire safety, the space where the club operated had the obligation to obtain the certificate, respectively the fire safety authorisation. Still, it worked without a fire safety authorisation.

In the first stage of this chapter, we will analyse, using the Pathfinder simulator, the deficient way in which the evacuation of users from the crowded hall. In the second stage, we will specify the mandatory fire safety measures that had to be respected by the space.

We will conduct a simulation highlighting the importance of a second escape route in such a situation (Figure 20, Figure 21).



Figure 20. Distribution of people inside the club



Figure 21. Distribution of people inside the club before the fire started – stage area

The Pathfinder application, a simulator specially designed to identify shortcomings and aspects likely to make it difficult to evacuate users in an emergency, helped achieve a more uniform and realistic distribution of the people present (Figure 22, Figure 23).



Figure 22. Distribution of people inside the club before the fire started - dance and stage area



Figure 23. Distribution of people inside the club before the fire started - bar area

2.3.1 Evacuation of persons in a real situation: In what follows, it is analysed and highlighted how the evacuation was carried out in actual conditions on a single escape route with a door width of 85cm. Regarding the speed and priority factors: all users in the simulation have the same priority; in the first simulation (with an escape route), the speed of the users is variable, having values between 1.10 m/s and 1.50 m/s (Figure 24, Figure 25).



Figure 24. Distribution of persons at T=0 seconds

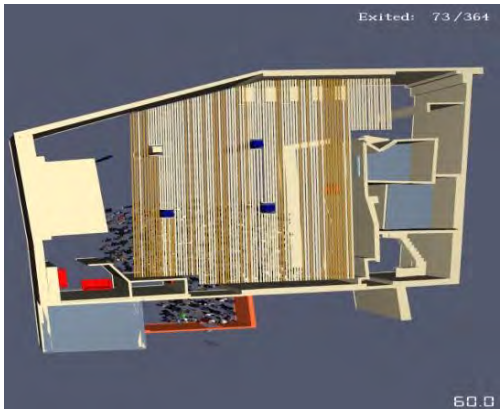


Figure 25. Evacuation of persons at T=60 seconds

We can observe at this point that at T=60 seconds from the moment the participants became aware of the danger, only a number of 73 people managed to evacuate from the interior, being a too small number of people who managed to evacuate, thus increasing the danger of injury and death of the occupants. (Figure 26 - 29).

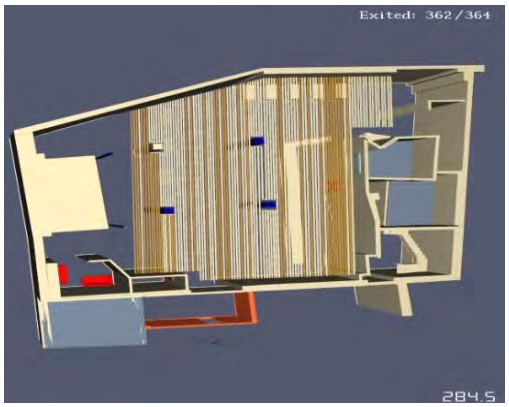


Figure 26. Evacuation of all persons at T=284.5 seconds

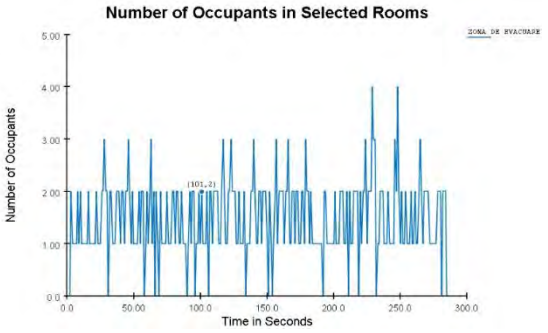


Figure 27. Evacuation flows (persons/second) per escape route

We can see from the simulation that only after 284.5 seconds, all 364 users would have been able to evacuate, which is a very long time, and the only escape route did not allow evacuation in a shorter time, resulting in the injury and death of a considerable number of occupants.

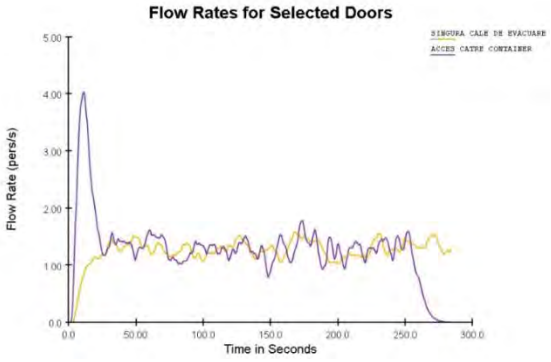


Figure 28. Evacuation zone selection rate

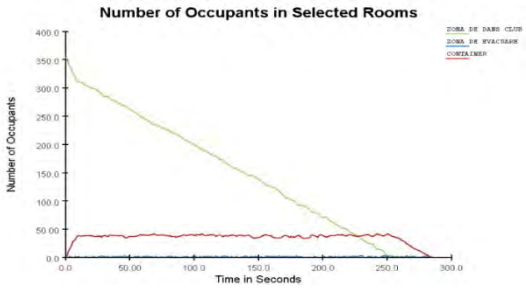


Figure 29. Number of occupants in selected areas and evacuation time

2.3.2 Evacuation of of persons in the proposed situation: Given that it cannot be established and that there is no technical expertise to determine the fire resistance of the building of which the Colectiv club was part, we consider in this article that it has the degree of fire resistance II. According to the provisions of art. 4.1.30 of the Building Fire Safety Normative, Indicative P118/99, the space analysed belongs to the category of S2-type crowded halls.

Also, within the same normative in art. 2.6.12 and art. 4.1.41, in force since 1999, clearly states that ensuring at least two separate and carefully located escape routes is mandatory.

Taking into account the level of fire stability of the construction, which was established above to be II, and the fact that the crowded hall is of type S2, it follows according to table 4.1.43 of the Normative on fire safety of constructions, Indicator P118/99, the fact that the capacity of an evacuation stream is 65 persons (Figure 30).



Figure 30. Creation of two judiciously distributed escape routes - (proposed situation)

The determination of the number of exhaust flows is done according to the following formula, provided by Normative P118/99:

$$F = \frac{N}{C} \quad (1)$$

where:
F = number of flows;
N = number of persons to pass through the escape route;
C = normalised evacuation capacity of a stream.
The results in the relation will be rounded up to the next integer.
N = 364 persons;
C = 65 persons.
F = 364/65 = 5.75 ~ **6 flows**

The calculation resulted in the need to ensure a number of 6 evacuation flows, which in the present article have been achieved by providing two evacuation routes arranged as far as possible diametrically opposite, each with a width of 1.60 m, a width that ensures the evacuation of 3 streams. Then, using the Pathfinder simulator, evacuation from the crowded hall will be carried out, respectively the time taken to evacuate all occupants will be checked, compared to the actual situation (Figure 31-34).

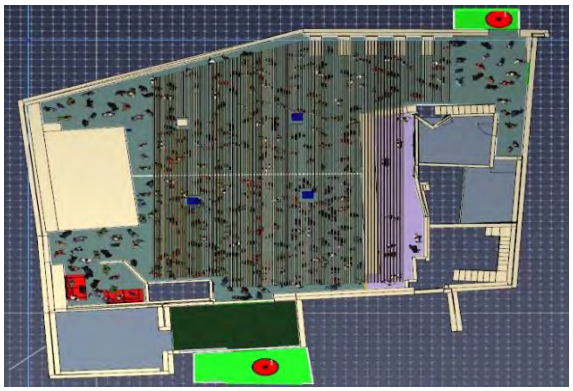


Figure 31. Construction of two diametrically opposed evacuation paths of 3 flows each (160 cm)



Figure 32. Distribution of people at T=0 seconds on the two escape routes

Regarding the speed and priority factors: all users in the simulation have the same priority; in the second simulation (with two escape routes), the speed of the users is variable, having values between 1.10 m/s and 1.50 m/s;

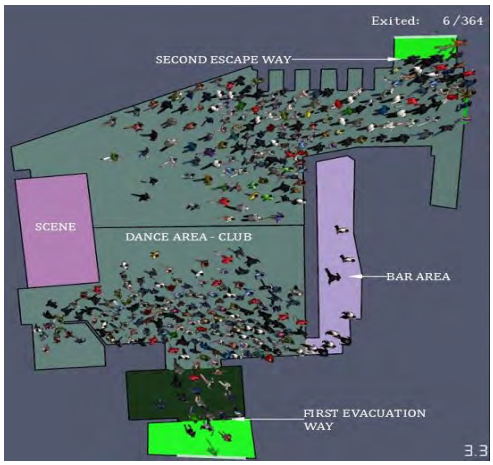


Figure 33. Movement of users to escape routes



Figure 34. Distribution of people at T=60 seconds on the two escape routes

We can see at this point that at T=60 seconds from the moment the participants became aware of the danger, a number of 331 people managed to evacuate from the inside.

At the same time, we can observe that at T=72.8 seconds, through two escape routes with a width of 1.60 m (6 escape flows), all users managed to evacuate, which in the actual situation was completed in a longer time (T =284.5 seconds) (Figure 35 – 38).



Figure 35. Evacuation of all persons at T=72.8 seconds on the two escape routes

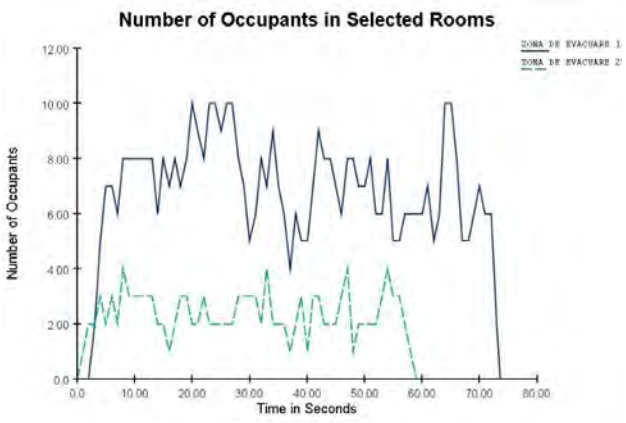


Figure 36. Evacuation flows (persons/second) per escape route

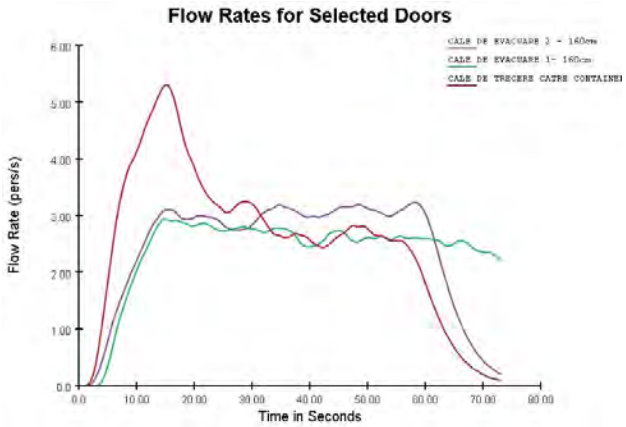


Figure 37. Selection rate of evacuation areas (two escape routes)

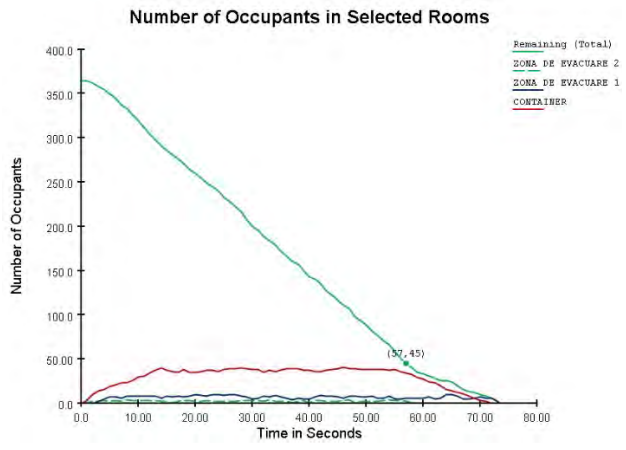


Figure 38. Number of occupants in selected areas and evacuation time

Analyzing these aspects, we can easily conclude that an adequately dimensioned alternative escape route would result in the safe evacuation of the users or significantly decrease the number of fire casualties.

2.4 Technical reference

- **Density:** In this context, density likely refers to the measure of how crowded or concentrated occupants are in a particular area within a mesh or grid. It could be represented as a numerical value.
- **Contour Mesh:** A contour mesh is a representation of a two-dimensional surface where contours or lines connect points of equal value. In this case, it's used to calculate density at various vertices.
- **Vertex:** In a mesh or grid, a vertex is a point or node that defines the corners or intersections of polygons or cells. Each vertex can be associated with a specific location.
- **Density Radius Parameter:** This parameter seems to be a user-defined value that determines the distance around each vertex within which nearby occupants are considered when calculating the density. It sets the scope of influence for occupants on the vertex's density calculation.
- **Occupants:** These are objects or entities within the system, and their positions and interactions are used to compute the density. Occupants can be individuals, particles, or any relevant entities.
- **Intersection Area:** This term suggests that when an occupant partially falls within the circle (defined by the density radius) around a vertex, the portion of the occupant's presence within that circle contributes to the vertex's density calculation based on the area of overlap or intersection

The described concept appears to be a method for determining the density at various points (vertices) in a mesh, where the presence and positions of occupants within a certain radius of each vertex influence the density value. It allows for a more detailed and localized calculation of density, considering partial contributions from occupants when they are only partially within the influence area.

This type of calculation can be useful in various fields such as urban planning, traffic simulation, environmental modeling, and more, where understanding how crowded or concentrated certain areas are is important for analysis and decision-making.

- **Speed**: Speed typically refers to the rate at which an object or entity moves. In your context, it likely indicates how fast each occupant is moving.
- **Occupant**: These are individuals or entities that occupy certain positions in your simulation or system.
- **Vertices of the Contour Mesh:** The vertices represent the points or nodes within the contour mesh, which is used for density calculations, as mentioned earlier.
- **Distance *ri*:** This is a parameter that defines a specific distance within which the occupant's speed is applied to the vertices of the contour mesh. It sets the range of influence for the occupant's speed.

$$s_v = max_{1 \le x \le n}(s_x \frac{r_i - d_x}{r_i}) \quad (2)$$

where:

n: this represents the count of occupants within a 2-dimensional radius of ri surrounding the position of the vertex. It essentially quantifies the number of occupants within a certain circular area centered at the vertex;

s_x: this denotes the current speed of a specific occupant, denoted as x. It represents how fast the particular occupant is moving;

d_x: this refers to the 2-dimensional distance from the vertex to the position of the specific occupant x. It quantifies the spatial separation between the vertex and the position of the given occupant;

- **Normalized speed** value per vertex can be determined using the following formula or method. While the specifics of the calculation may vary, the general approach involves some form of normalization to standardize the speed values across different vertices. Normalization typically involves scaling values to a common range or standardizing them based on certain criteria. This process ensures that the speed values are relative and comparable across the entire dataset or mesh. Normalization can help in understanding the relative significance of speeds at different locations or vertices within the mesh.

$$s_v = max_{1\le x\le n}\left(\frac{s_x}{s_{xmax}} * \frac{r_i - d_x}{r_i}\right) \quad (3)$$

where:
s_{xmax}: the maximum speed of occupant x;

- **Time to Exit:** This is the calculated value at each vertex, representing the time it takes for an occupant to exit from that location. It's based on the minimum time calculated among all occupants within a certain radius.

$$tte_v = max_{1\le x\le n}\left[(t_{exit} - t_{curr}) * \frac{r_i - d_x}{r_i}\right] \quad (4)$$

where:
x: the variable representing different occupants, the formula considers the minimum time calculated among all occupants;

t_{exit}: this is the exit time for occupant x, which is the time required for that occupant to reach the exit;

t_{curr}: the current contour calculation time, indicating the point in time when the contour value is being calculated;

s_{xmax}: the maximum speed of occupant x, which determines the occupant's speed capability.

3 CONCLUSIONS AND DEVELOPMENT PERSPECTIVES

This emergency is a lesson in the importance that has to be given about "fire safety" in our country.

According to the Building Fire Safety Normative, Indicative P118/99, the club was meeting the conditions of a "crowded hall". Its surface area was approximately 400 square meters, and more than 400-500 people were present at the time. Also, the equipment with fire extinguishing installations and the construction measures were very precarious and did not correspond to the required regulations for crowded halls.

This fire was a "zero" point in terms of legislation in Romania, leading to the initiation and approval of "*Government Decision no. 915 of 3 November 2015 on the establishment of criteria for stopping the operation or use of constructions or facilities caused by serious violation of the fire safety requirement in terms of endangering the lives of occupants and intervention forces, failure to ensure the stability of load-bearing elements, respectively limiting the spread of fire and smoke inside the building and to the surroundings*", a normative act based on which the operation of a building or installation may be stopped if a severe violation of the essential requirement "fire safety" is found, thus leading to the tightening of fire prevention controls by the structures of the General Inspectorate for Emergency Situations.

Last but not least, a necessary element that should be implemented as a development and innovation perspective for this fundamental "fire safety" segment is using fire simulators to verify the usefulness of passive and active fire safety systems and measures for specific buildings. These simulators have proven successful in countries with a strong emphasis on fire research.

References

Chang, L., Zhong, M., Song, S., Xia, F., Tian, X., Yang, Y., & Zeng, L. (2020). Experimental and numerical study on critical ventilation velocity for confining fire smoke in metro connected tunnel. Tunnelling and Underground Space Technology, 97, 103296. https://doi.org/10.1016/j.tust.2020.103296.

Galhardo, A., Viegas, J. C., & Coelho, P. J. (2022). The influence of wind on smoke propagation to the lower layer in naturally ventilated tunnels. Tunnelling and Underground Space Technology, 128, 104632. https://doi.org/10.1016/j.tust.2022.104632.

Urban habitat constructions under catastrophic events. (n.d.), Google Books: https://books.google.ro/books?hl=en&lr=&id=Q9XKBQAAQBAJ&oi=fnd&pg=PA201&dq=CFPA-E+No+19:2009+Fire+safety+engineering+concerning+evacuation+from+buildings.&ots=RFxkZ-Vq8T&sig=xA6hHqRY_UVbONapNPzIk5k7QWM&redir_esc=y#v=onepage&q=CFPA-E%20No%2019%3A2009%20Fire%20safety%20engineering%20concerning%20evacuation%20from%20buildings.&f=false, view at 10.11.2023.

Mei, F., Tang, F., Ling, X., & Yu, J. (2017). Evolution characteristics of fire smoke layer thickness in a mechanical ventilation tunnel with multiple point extraction. Applied Thermal Engineering, 111, 248–256. https://doi.org/10.1016/j.applthermaleng.2016.09.064.

Law no. 307 12/07/2006 - Legislative Portal. (n.d.). https://legislatie.just.ro/Public/DetaliiDocumentAfis/73657, view at 10.11.2023.

Wikipedia contributors. (2023, December 24). Colectiv nightclub fire. Wikipedia; https://en.wikipedia.org/wiki/Colectiv_nightclub_fire, view at 10.11.2023.

St. frt. MÜLCEA Alin, St. Fort. AIOANEI Cătălin-Claudiu, Scientific Coordinator: Conf. univ. dr. Eng. Col. DARIE Emanuel, "Alexandru Ioan Cuza" Police Academy, Faculty of Firefighters - Qualitative Simulation of Fire at the Club Colectiv. Comparison with the provisions of the norms in force regarding the evacuation of persons, the XIIIth edition of the Conference of the Students of the Firefighters Faculty - SIGPROT 2016 - Emergency Situations Management.

Simulation of the evacuation of users in case of fire at the Colectiv club, Romanian Journal of Civil Engineering, Volume 9 (2018), Number 2, authors: Gabriel Prigoreanu, Ion Anghel, Micu Cristian-Andrei.

Building fire safety normative, Indicative P118/99.

Normative Fire Safety of Buildings, Extinguishing Systems, Indicative P118/2-2013.

Normative Fire Safety of Buildings, Fire detection, signalling and alarm systems, Indicative P118/3-2015.

Numerical Simulation Evaluation of Fire Spreading in a Building Using Fire Dynamics Simulator (FDS); I. Enaru, N.-C. Chereches, S.-V. Hudişteanu, E.-F. Ţurcanu, Ana Diana Ancas, Marina Verdeş, C.-G. Popovici and V. Ciocan.

Labiba, M.A., Mofreh M N., Abdel-Salam A Zoklot, Ahmed Abdel Gawad, 2018 , *Simulation of Smoke Propagation and Evacuation Plans in Underground Tunnels and Stations,* Proceedings of the Thirteenth International Conference of Fluid Dynamics, 21-22 December 2018, Ciro, Egypt, ICFD13-EG-6103.

Law No.10 of 18/01/1995 on quality in construction - updated, Original text published in the Official Gazette of Romania, Part I, No. 12 of 24 January, 1995, Bucharest, Romania.

Guide on fire fighting techniques and tactics - ISU 01.

Guide on fire fighting techniques and tactics ISU 04.

Nurul Liyana Hanapi, Sabarinah Sh Ahmad, Norhati. - Google Scholar (n.d.): https://scholar.google.com/scholar?hl=en&as_sdt=0%2C5&q=Nurul+Liyana+Hanapi+%2C+Sabarinah+Sh+Ahmad%2C+Norhati+Ibrahim%2C+Azli+abd+Razak%2C+Nor+Merlisa+Ali%2C+Suitability+of+Escape+Route+Design+for+Elderly+Residents+of+Public+Multi-storey+Residential+Building+%2C+2017%2C+Pertanika+J.+Soc.+Sci.+%26+Hum.+25+%28S%29%3A+251+%E2%80%93+258.&btnG=#d=gs_cit&t=1712528494763&u=%2Fscholar%3Fq%3Dinfo%3AVZ01Q8XHrUQJ%3Ascholar.google.com%2F%26output%3Dcite%26scirp%3D0%26hl%3Den, view at 10.11.2023.

Halawa, T. (2020). Numerical simulation of the evacuation process and smoke propagation due to a fire in a road tunnel with transverse ventilation system. Journal of Thermal Science and Engineering Applications (Print), 13(3). https://doi.org/10.1115/1.4047523.

NUMERICAL SIMULATION OF IMPROVING THE EFFICIENTY OF PHOTOVOLTAIC THERMAL PANELS

C.-G. Popovici [a], G. Filipescu[a] , N.-C. Chereches [a]*, S.-V. Hudișteanu [a], E.-F.Țurcanu [a], Ana Diana Ancas [a] , Marina Verdeș [a], P. V. Roșu[a]

[a] Technical University "Ghe. Asachi" of Iasi, Faculty of Civil Engineering and Building Servicies, Department Building Sevicies, D. Mangeron 67 str.,700050, Romania; E-mails: catalin-george.popovici@academic.tuiasi.ro, george.filipescu@student.tuiasi.ro, *nelu.chereches@academic.tuiasi.ro, valeriu-sebastian.hudisteanu@academic.tuiasi.ro, florin-emilian.turcanu@academic.tuiasi.ro, ana-diana.ancas@academic.tuiasi.ro, marina.verdes@academic.tuiasi.ro, rosupetru@yahoo.com

Received: 22.01.2024 / Accepted: 14.02.2024 / Revised: 26.02.2024 / Available online: 31.05.2024

DOI: 10.2478/jaes-2024-0010

KEY WORDS: green energy, photovoltaic thermal panels, numerical simulation, Ansys Software.

ABSTRACT:

The need to optimize the operation of photovoltaic modules inevitably arises with the development of green energy production technology. In order to achieve a good technological yield, durability and efficiency in production, continuous studies and innovations are required. This study focuses on simulating the operation of water-cooled and uncooled PV modules in order to understand the temperature-dependent PV operation. This cooling module consists, in the first phase, of a copper coil through which water circulates, and in the second phase, of a coolant distributor/collector system. The module is attached to the lower surface of the photovoltaic panel, respectively to the teller foil layer. For this simulation we used the Ansys software package (Discovery, Fluent and Space Claim).

1.INTRODUCTION

One of the most widespread renewable energy technologies is the use of photovoltaic (PV) systems, which convert solar radiation into usable electrical energy (Hu J. et. al. 2016; Yau YH et. al. 2016, Markvart T. 2020). This renewable energy production technology is pollution-free during operation, mitigates global warming issues, reduces operational costs, and requires minimal maintenance compared to other renewable energy technologies (Wang Y. et.al. 2006; Bhubaneswari P. et. al.2011).

In the world, there are significant concerns about a potential energy crisis, and the majority of countries still rely on conventional sources of energy production (Pomares-Hernandez C et.al.2021; Kannan N. et.all. 2016) The situation, exacerbated by the world's population growth and industrial progress, has led to an increased demand for energy, causing significant environmental problems due to the intensive exploitation of fossil fuels. In this context, interest in renewable energy sources such as solar or wind energy has grown (Pomares-Hernandez C. et.al.2021; Rauf A. et al. 2018; Robles A. Et.al. 2018).

The development of the present cooling module was conceived for its application on any type of rigid photovoltaic panel. The study includes simulations, taking into account the dimensional characteristics of the most commonly used photovoltaic modules available on the market. Such a method is designed to reduce both the time and cost of maintaining photovoltaic systems, as the cooling prolongs the system's lifespan. This aspect of durability has a positive impact on the environment by reducing costs and production, thereby lowering pollution, optimizing operational efficiency, and reducing harmful emissions into the atmosphere. Moreover, the obtained thermal energy from this cooling process can be stored for future use in domestic or industrial settings, further reducing the direct consumption of electricity required for thermal energy.

Despite the numerous advantages of PV technology, this conversion system faces climate-related challenges, such as hail, dust, and surface operating temperature, which can negatively affect the system's efficiency (DaSilva RM et al. 2010). External climatic parameters, such as wind velocity, ambient temperature, relative humidity, accumulated dust, and solar radiation, are the most common natural factors that influence the surface temperature of a photovoltaic module (Elbreki A.M. et. al.2016). Generally, for every 1°C increase in the temperature on the PV module's surface, there is a 0.5% reduction in efficiency (Kumar K. Et.al. 2007, Chandrasekar, M et al. 2015). As a result of the temperature rise, not all the absorbed solar energy by the photovoltaic cells is converted into electrical energy. To comply with the law of energy conservation, the remaining solar energy is transformed into heat (Tahar M. et. al. 2022). The consequences of this heat loss lead to an overall reduction in conversion efficiency. To make this renewable energy production technology the best solution, it is necessary to improve the efficiency of solar energy conversion systems (Reddy, S.R. et al. 2015). To turn it into a

* Corresponding author: Nelu-Cristian Chereches, e-mail: nelu.chereches@academic.tuiasi.ro

viable solution, different means of addressing this temperature issue must be found, resulting in an overall increase in conversion efficiency (Wang Y. et.al. 2006; Bhubaneswari P. et. al.2011).

2. CASE OF STUDY

The present study aims to calculate the temperature distribution on the surface of a photovoltaic panel under fixed ambient temperature and solar radiation conditions. The solar radiation has been chosen to be 1000W/m2K. Two types of active cooling methods were used: one with a serpentine cooling system and the other with a distributor/collector cooling system. Additionally, the simulation also includes the baseline scenario without any cooling. The inlet temperature of the cooling agent is set to be 20°C, and the thermal agent's circulation velocity. The system was simulated at 0.1; 0.3; 0.5; 0.7; and 0.9 m/s for each of the two cooling systems, as well as for the non-cooling scenario. This resulted in 11 simulations that were compared to understand which type of active cooling is more suitable under these conditions compared to the system without cooling. The data extracted from these simulations were provided a clearer understanding of this phenomenon. The PV surface has a size of 2m² and was subjected to uniform solar radiation over its entire surface.

The simulation results highlights the temperature distribution on the PV surface, the temperatures obtained at the PV surface, and the water temperatures at the outlet of the cooling circuit (for cases with cooling).

For this simulation and numerical analysis study, a standard photovoltaic panel with dimensions of 2000/1000mm was used, composed of the following layers:

- Cover and protective layer made of glass
- EVA layer 1 (ethylene-vinyl acetate)
- PV cells
- EVA layer 2
- Tedlar film (polyvinyl fluoride (PVF) film)

The materials used are the most commonly used in the photovoltaic panel industry, and their physical parameters such as thermal conductivity, density, thickness, and specific heat have been respected.

In constructing the photovoltaic panel, the weighted average of the physical parameters for each layer based on its thickness was considered. This resulted in a unique, compact, and homogeneous layer referred to as the 'PV layer', with specific characteristics (Table 1), which were introduced as calculation parameters for the simulation.

Layer material	Thickness (m)	Thermal Conductivity (W/m°C)	Specific Heat (J/kg°C)	Density (kg/mc)
PV	0,0045	14,44	885,73	2447,11

Table 1. Properties and Dimensions of the Material in the PV Layer Composition

The photovoltaic panel was constructed taking into account real specifications using the Ansys 2023 R1 and R2 student version software package. The limitation in this version was in the Meshing phase, where the calculation nodes and points cannot exceed 500,000 nodes. Generally, this is not a problem; the simulation can proceed smoothly with a level of calculation detail accepted in the research field. The geometry was created using the SpaceClaim program, which is integrated into the same Ansys package.

Fig. 1 and Fig. 2 represent a cross-sectional view of the photovoltaic panel created using the SpaceClaim software.

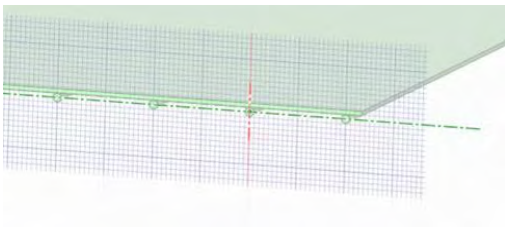


Figure 1. PV Cross-Section, 3D Top View

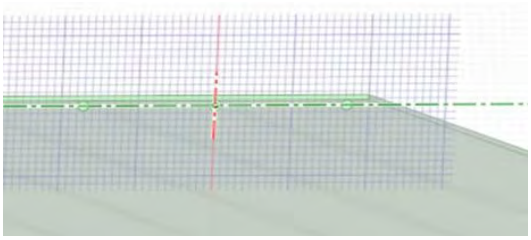


Figure 2. PV Cross-Section, 3D Bottom View

Fig.3 and Fig.4 represent the view in X-Z axis view of the PV with Serpentine Cooling respectively the PV with Distributor/Collector Cooling.

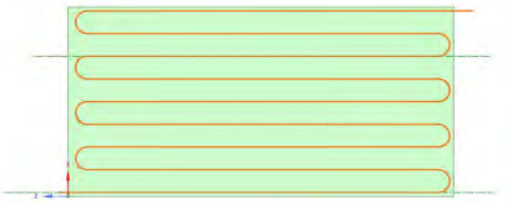


Figure 3. Lower X-Z Axis View of PV with Serpentine Cooling

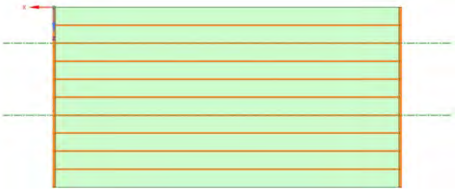


Figure 4. Lower X-Z Axis View of PV with Distributor/Collector Cooling

In Fig. 5-7 is presented the model of the frame used in the PV geometry; it was created using the Ansys Discovery program, version 2023 R1.

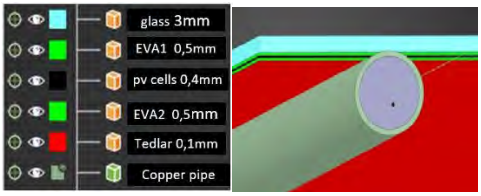


Figure 5. View of the Component Layers of PV

The system involves facilitating heat exchange between the photovoltaic panel and water through an installation composed of Copper pipes with diameters of Dn10mm (for the serpentine cooling system) and Dn16mm (the collector and distributor are constructed using Dn16mm pipes, while the circuits are built with Dn10mm pipes), directly attached to the Tedlar film exposed at the bottom of the PV panel.

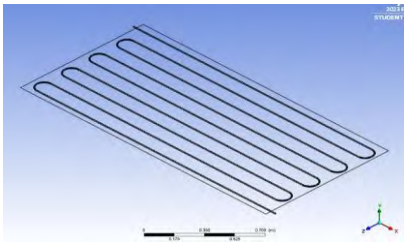


Figure 6. View of the Component Layers of PV

The serpentine cooling system consists of a sequence of 9 copper pipes with a diameter of Dn10mm, Fig. 8. The distance between the pipes is 101mm, and they are consecutively connected to each other through bends with a radius of 55mm. The total length of the serpentine is 18m.

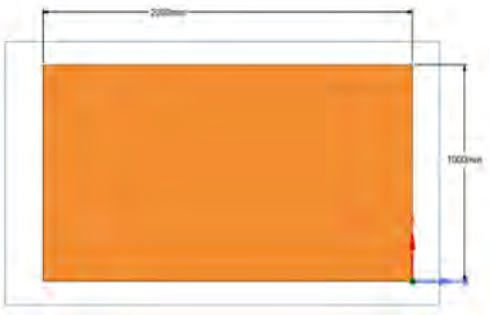


Figure 7. PV Dimensions

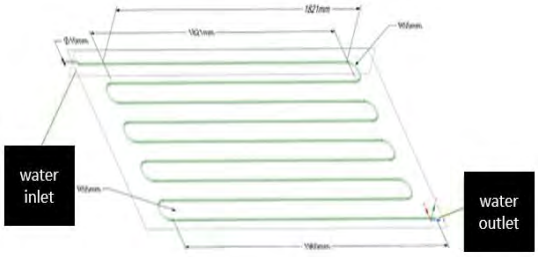


Figure 8. Dimensions of the Serpentine Cooling System

The dimensions of the distributor/collector cooling system are present in Fig. 9, and the distance between the secondary pipes, namely 101mm, is maintained.

The distance between the main pipes (distributor and collector) is 2018mm. This geometry is the only possible configuration to maintain the same physical attachment characteristics to the Tedlar film. Under these conditions, the volume of water in the secondary pipes is preserved and precisely corresponds to the same equivalent volume as in the serpentine pipes.

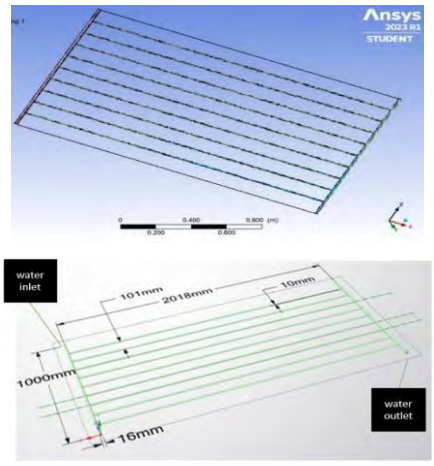


Figure 9. Geometry and Dimensions of the Distributor/Collector Cooling System

3. NUMERICAL SIMULATION

The numerical simulation was performed using the Ansys Workbench 2023-R1 program, student version. The geometry was created with the same CAD program, specifically the three-dimensional (3D) subdivision in SpaceClaim, followed by the Meshing phase, settings, solution, and results carried out with Ansys Fluent, a computational fluid dynamics (CFD) tool capable of physical modeling and simulation.
In this project, the numerical simulation for the operation of the same photovoltaic panel includes 3 cases:

- 3.1 Simulation of PV operation without cooling (G1)
- 3.2 Simulation of PV operation with serpentine cooling system (G2)
- 3.3 Simulation of PV operation with distributor/ collector cooling system (G3)

3.1. Simulation of PV operation without cooling

The numerical simulation for the case of the photovoltaic panel without cooling was possible with the following input parameters:

- Solar power: 1000W/m²
- Air density: constant
- Heat transfer air-PV: through conduction
- PV thermal resistance: negligible the calculation processes were set to 1000 iterations.

PV Characteristics:

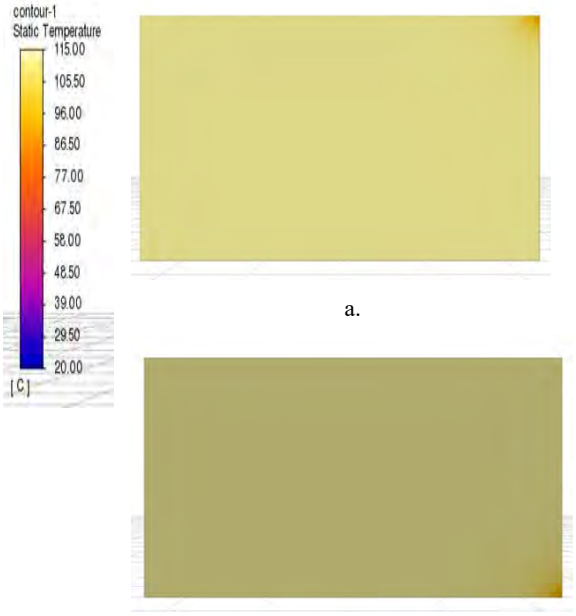
- Material: Mixed (glass, eva1, PV cells, eva2, tedlar)
- Mixed PV layer thickness: 0.0045 m
- Mixed material density: 2447.11 kg/m³
- Specific heat: 885.73 J/kg°C
- Thermal conductivity: 14.44 W/m°C.

The results obtained from the numerical simulation for the photovoltaic panel without cooling are presented in Table 2.

Photovoltaic panel 2000/1000 mm without cooling system					
V_{H2O} (m/s)	T_{H2Oint} (°C)	T_{H2Oout} (°C)	T_{minPV} (°C)	T_{maxPV} (°C)	T_{medPV} (°C)
NO	NO	NO	64,5	112,3	88,4

Table 2. Data from Numerical Simulation of PV Without Cooling

In Fig. 10, the temperature contour on the surface of the photovoltaic panel can be observed for the color spectrum set within the range of 20...110°C. The maximum temperature of the PV panel is at 112.3°C. The average temperature is 88.4°C. The minimum temperature is 64.5°C.



a.

b.

Figure 10. a. Front; b.Bottom View of PV in the Numerical Simulation Without Cooling

3.2. Simulation of PV operation with serpentine cooling

The numerical simulation for the case of the photovoltaic panel with serpentine cooling system was possible with the following input parameters:

- Solar power: 1000W/m²
- Air density: constant
- Heat transfer air-PV: through conduction
- Heat transfer PV-water: through convection and conduction
- PV thermal resistance: negligible
- Water inlet temperature: 20°C
- Water circulation velocity: 0.1...0.9 m/s

The results obtained from the numerical simulation for the PV operation with the serpentine cooling system are presented in Table 3.

Photovoltaic panel 2000/1000 mm with serpentine cooling system					
V_{H2O} (m/s)	T_{H2Oint} (°C)	T_{H2Oout} (°C)	T_{minPV} (°C)	T_{maxPV} (°C)	T_{medPV} (°C)
0,1	20	90,5	55,9	105,3	78,8
0,3	20	44,2	37,5	54,1	44,9
0,5	20	34,8	32,7	42,7	37,1
0,7	20	30,6	30,5	37,5	33,5
0,9	20	28,33	29,1	34,6	31,5

Table 3. Data from Numerical Simulation of PV with Serpentine Cooling

In Fig. 11, the temperature contour on the surface of the photovoltaic panel can be observed for the color spectrum set within the range of 20...110°C. The water circulation velocity ranges from 0.1 to 0.9 m/s.

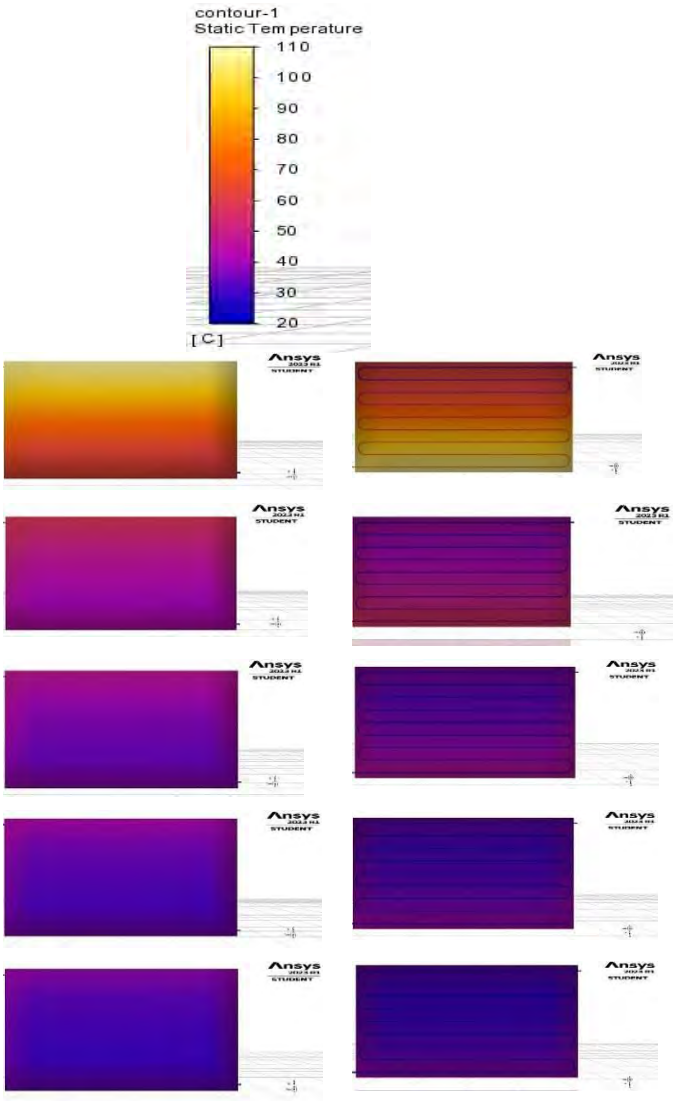


Figure 11. PV with Serpentine Cooling, with the Cooling Agent Circulation at 0.1...0.9 m/s

3.3. Simulation of PV operation with distributor/collector cooling

The numerical simulation for the case of the photovoltaic panel with distributor/collector cooling system was possible with the following input parameters:

- Solar power: 1000W/m²
- Air density: constant
- Heat transfer air-PV: through conduction

- Heat transfer PV-water: through convection and conduction
- PV thermal resistance: negligible
- Water inlet temperature: 20°C
- Water circulation velocity: 0.1...0.9 m/s

The results obtained from the numerical simulation for the PV operation with the distributor/collector cooling system are presented in Table 4.

Photovoltaic panel 2000/1000 mm with distributor/collector cooling system					
V_{H2O} (m/s)	T_{H2Oint} (°C)	T_{H2Oout} (°C)	T_{minPV} (°C)	T_{maxPV} (°C)	T_{medPV} (°C)
0,1	20	79,8	45,8	84,2	64,9
0,3	20	47,5	37,8	57,0	45,8
0,5	20	38,3	33,7	49,2	39,9
0,7	20	34,5	31,2	45,2	36,6
0,9	20	32,5	29,8	42,5	34,5

Table 4. Data from Numerical Simulation of PV with Distributor/Collector Cooling

In Fig, 12, the temperature contour on the surface of the photovoltaic panel can be observed for the color spectrum set within the range of 20...110°C. The water circulation velocity ranges from 0.1 to 0.9 m/s.

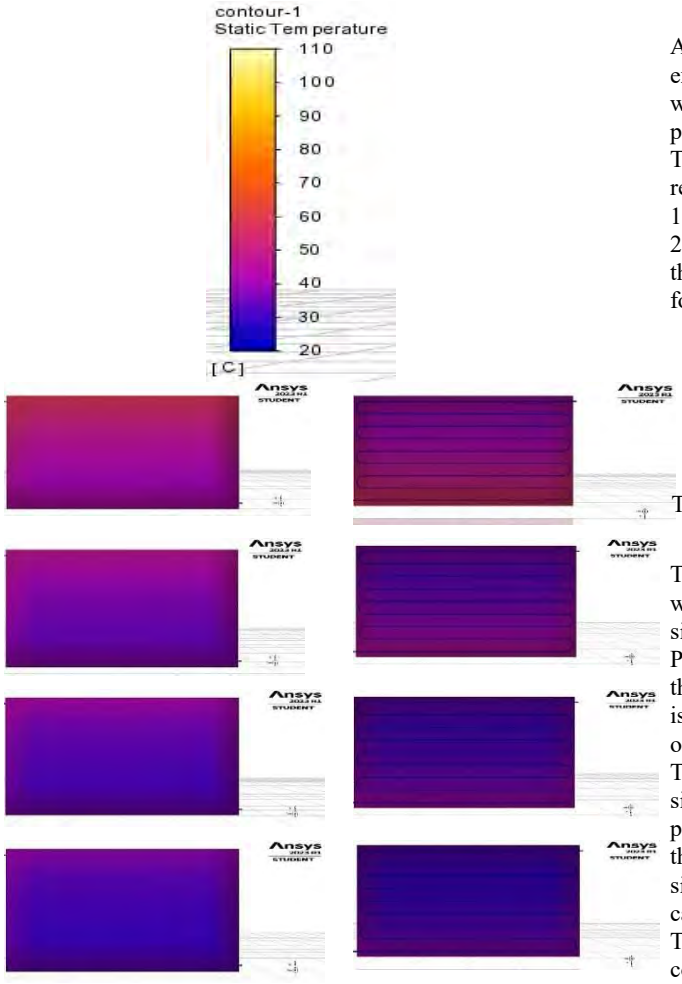


Figure 12. PV with Distributor/Collector Cooling, with the Cooling Agent Circulation at 0.1...0.9 m/s

4. COMPARATIVE STUDY

A total of 11 simulations were conducted. The thermal potential available on the surface of the photovoltaic panels was extracted, including:

- PV without cooling
- PV with serpentine cooling
- PV with distributor/collector cooling

In the following chart (Fig. 13), the temperature dynamics for the PV system without cooling can be observed.

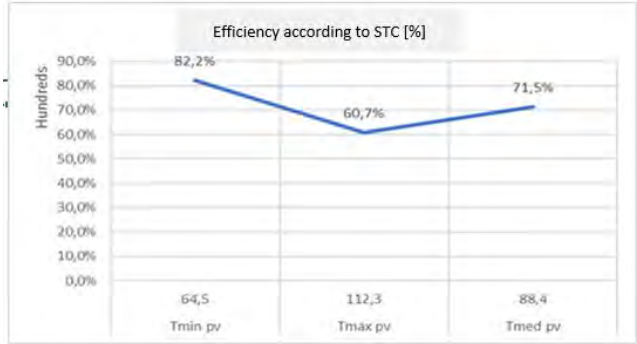


Figure 13. Distribution of PV temperatures for the System Without Cooling

According to the study it is mentioned that for an average external temperature of 25°C and solar radiation of 1000W/m², with uniform and direct exposure of the PV panel to the sun, the photovoltaic cells offer maximum electrical power production. This test is referred to as Standard Test Condition (STC). As a result of this conducted study, it was observed that for every 1°C increase in the photovoltaic panel's temperature above 25°C, there is a reduction in efficiency by 0.45%. Based on these findings and considering the STC test, we can extract the following calculation from Table 5.

		Efficienty according to STC (%)
$Tmin_{PV}$	64,5	82,225
$Tmax_{PV}$	112,3	60,715
$Tmed_{PV}$	88,4	71,47

Table 5. PV Efficiency according to STC - PV Without Cooling

The temperatures obtained during the operation of the PV without cooling reach excessively high levels, leading to a significant decrease in its performance. As seen in Fig. 13, the PV efficiency for the resulting average temperature reaches a threshold of 71%. A reduction to two-thirds of the PV capacity is considerable. It is well-known that the operating temperature of photovoltaic panels is crucial in electricity production. Therefore, at such temperatures obtained in this initial simulation, the capacity to produce electricity by the photovoltaic panel decreases dramatically. Taking into account the maximum temperature obtained from the numerical simulation, the efficiency reduction approaches half. The capacity to produce energy by PV is reduced by up to 60%. This parameter should be considered more, especially concerning the maximum temperature, to verify the functioning under the most adverse conditions.

In the domain of PV operation with serpentine cooling, as shown in Fig. 14, the graph of temperatures obtained from the numerical simulation is presented. Similarly, I consider the obtained maximum temperatures as preliminary data to ensure the logical operation of PV under the most adverse exterior climatic conditions. At the beginning of each serpentine cooling cycle, for each of the five allowed circulation velocities considered, a maximum temperature is observed. In the velocity domain from 0.1 m/s to 0.5 m/s, the maximum temperature obtained does not match the STC efficiency calculation. In this case, the resulting temperatures are too high. In the rest of the approached velocity domain, given the forced circulation of the cooling agent and better distribution on the PV surface, the operating temperatures are lower and even optimal in terms of efficiency.

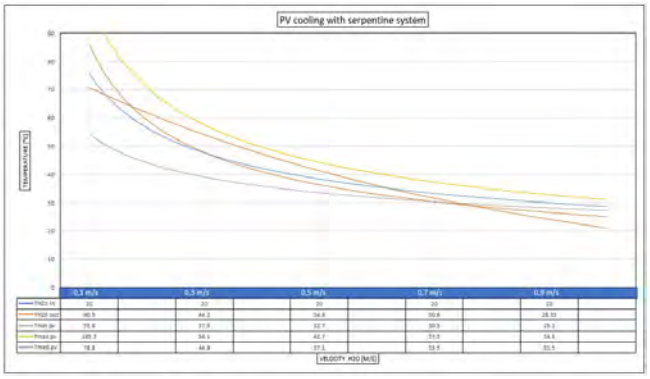


Figure 14. Distribution of PV Temperatures for the Serpentine Cooling System

Table 6, according to the STC test, we extract the following calculation for the efficiency of the PV system with serpentine cooling.

Velocity of cooling agent (m/s)	0,1	0,3	0,5	0,7	0,9
$Tmin_{PV}$(°C)	55,9	37,5	32,7	30,5	29,1
STC(%)	86,095	94,375	96,535	97,525	98,155
$Tmed_{PV}$(°C)	78,8	44,9	37,1	33,5	31,5
STC(%)	75,79	45,79	94,555	96,175	97,075
$Tmax_{PV}$(°C)	105,3	105,3	42,7	37,5	34,6
STC(%)	63,865	63,865	92,035	94,375	95,68

Table 6. Calculation of PV efficiency with Serpentine Cooling according to STC

Fig. 15 illustrates the efficiency of the photovoltaic panel with serpentine cooling, depending on the temperature extracted from the numerical simulation for the five cases of coolant circulation velocity. It is evident that for all temperatures, minimum, average, and maximum, the PV efficiency increases with decreasing temperatures. As expected, the maximum efficiency of PV is achieved at the minimum temperatures obtained on its surface, reaching 98.1%. However, the maximum temperature reached, 105°C, is not favorable in terms of efficiency, and it rapidly decreases the system's reliability over time.

Regarding the PV cooling system with distributor/collector, Fig. 16 displays the graph of temperatures obtained from the numerical simulation. The maximum temperatures obtained serve as preliminary data to ensure the logical operation of PV under the most extreme external climate conditions. At the beginning of each cooling cycle with the distributor/collector, for each of the five allowable circulation velocitys considered, a maximum temperature is observed. In the range of velocitys from 0.1 m/s to 0.3 m/s, the maximum temperature obtained does not match the STC efficiency calculation, indicating that the resulting temperatures are too high. However, in the rest of the velocity range considered, due to the forced circulation of the cooling agent and a uniform and constant distribution over the entire PV surface, the operating temperatures are lower.

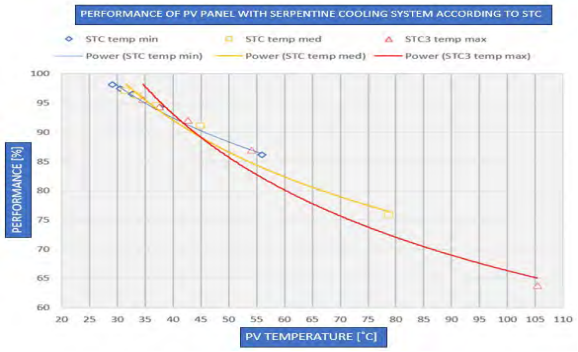


Figure 15. Efficiency of the PV with serpentine cooling according to STC at the obtained temperatures

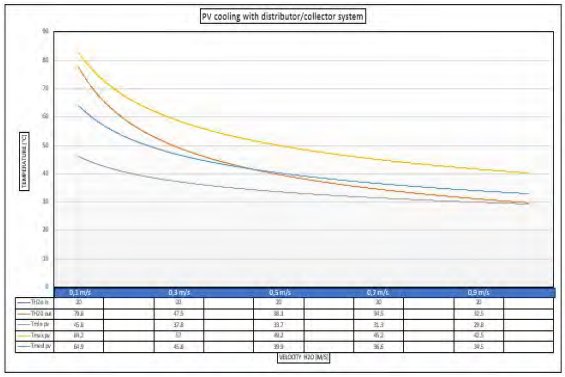


Figure 16. Distribution of temperatures for the PV system with distributor/collector cooling

In Table 7, according to the STC test, we extracted the following calculation for the efficiency of the PV system with distributor/collector cooling.

Velocity of cooling agent (m/s)	$Tmin_{PV}$ (°C)	STC1(%)	$Tmed_{PV}$ (°C)	STC2(%)	$Tmax_{PV}$ (°C)	STC3(%)
0,1	45,8	90,64	64,9	82,045	84,2	73,36
0,3	37,8	94,24	45,8	90,64	57,0	85,6
0,5	33,7	96,085	39,9	93,295	49,2	89,11

0,7	31,3	97,175	36,6	94,78	45,2	90,91
0,9	29,8	97,84	34,5	95,725	42,5	92,125

Table 7. PV Efficiency Calculation with Distributor/Collector according to STC

In the graph (Fig. 17), we can observe the efficiency of the photovoltaic panel with distributor/collector cooling, based on temperature, extracted from the numerical simulation for the five cases of cooling agent circulation velocitys. It is evident for all temperatures, minimum, average, and maximum, that the PV efficiency increases with decreasing temperatures. As expected, the maximum PV efficiency is achieved at the lowest temperatures obtained on its surface, reaching 97.8%. The maximum temperature obtained does not exceed 85°C.

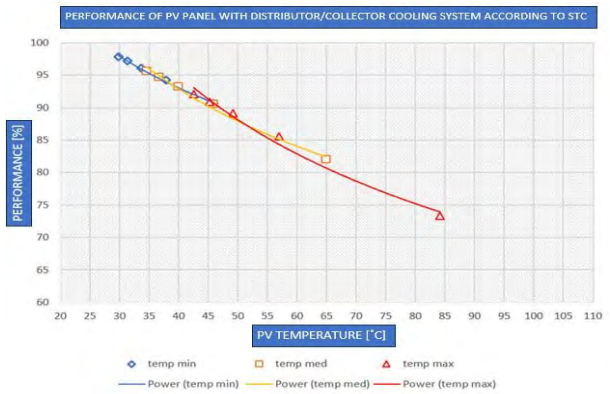


Figure 17. PV Efficiency with Distributor/Collector Cooling - Temperature Dependency

4. CONCLUSIONS

1. In the domain of minimum temperature, in the case of operation without a cooling system, the minimum operating temperature of the PV is high, reaching 64.5°C, considering its distribution over a very small surface. The most favorable minimum PV temperature is obtained with the distributor cooling system at a velocity <0.5 m/s. This results in a better distribution of the cooling agent over the PV surface, leading to improved operating efficiency. Additionally, the cooling water in this case has a higher temperature, making it suitable for thermal energy storage in a secondary system. On the other hand, the cooling system with a serpentine is more effective for velocitys >0.5 m/s. However, the water distribution in this case is not as uniform, resulting in some areas of the PV being better cooled than others. This thermal non-uniformity can have a negative impact on the system's durability, reliability, and energy production, as unevenly functioning photovoltaic cells may experience premature aging.

2. In the domain of average temperature, in the case of operation without a cooling system, the average operating temperature of the PV is 88.4°C. With cooling systems, we observe that the serpentine cooling system achieves lower temperatures at velocitys >0.5 m/s compared to the distributor cooling system. At velocity <0.5 m/s, the distributor cooling system manages to exchange heat more efficiently, resulting in lower temperatures and higher efficiency for the entire PV system.

3. In the domain of maximum working temperature of the system, in the case of simulations without cooling, the minimum temperature obtained on the PV surface remains relatively high at 112°C. It was illustrated the temperature evolution for all three cases analyzed for each of the cooling agent circulation velocitys (excluding PV without cooling). This high temperature can significantly affect the system's efficiency, leading to a considerable decrease in productivity. However, for systems with cooling, the situation improves. Lower temperatures are achieved, and the distributor cooling system works better at velocitys <0.3 m/s. This is due to the uniform distribution of the cooling agent, and the circulation velocity is well suited for this case. At velocitys >0.3 m/s, the continuity is maintained, and the distribution is equally good, resulting in acceptable temperatures and increased efficiency. In the case of serpentine cooling, the disadvantage lies in the non-uniform temperature distribution on the PV surface, but we observe areas with better cooling at velocitys >0.3 m/s. This is due to the fact that a higher cooling agent circulation velocity facilitates more favorable heat exchange at the beginning of the cooling circuit. Thus, a significant temperature discrepancy is observed between two halves of the PV, with one being better cooled than the other. This is undesirable as the system is not thermally balanced, and PV materials and cells may experience unequal transformations over the entire surface, leading to decreased efficiency and reliability over time. The cooling agent's outlet temperature is crucial as it results from a heat exchange process with the PV surface. A higher cooling agent temperature leads to better heat exchange and, consequently, better cooling.

4. In Fig. 18, there is presented the graph of cooling agent operating temperatures for all three simulation cases, i.e., no cooling system and systems with cooling. Lower PV operating temperatures and better system functionality and reliability are achieved. Cooling agent temperature is studied for cases G2 and G3, where the cooling system is involved. At velocitys <0.3 m/s, an advantage of the serpentine system is observed, thanks to its slow, one-directional flow of the cooling agent. At velocitys >0.3 m/s, the distributor/collector cooling system compensates effectively because the cooling agent is distributed through multiple paths, resulting in simultaneous heat exchange. As expected, a better heat exchange benefits the photovoltaic system's operation, durability, and reliability.

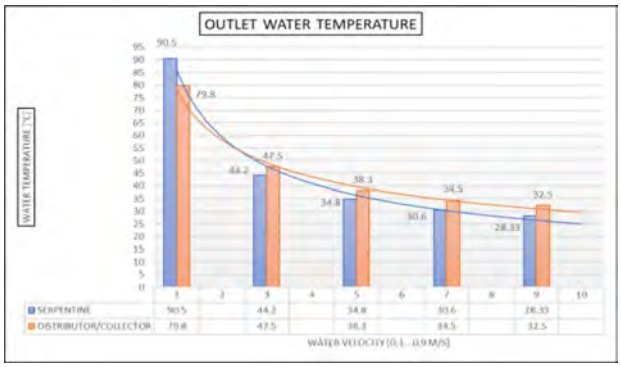


Figure 18. Cooling agent outlet temperature graph

As already evident, in this simulation, we numerically identified this thermal potential. The benefits of improved heat exchange are reflected in the efficient operation, durability, and reliability of the photovoltaic system, as well as the available thermal potential. Thermal energy storage is possible, and there are numerous approaches in this regard. The advantage lies in reducing the environmental impact in the field of electricity and thermal energy production through this hybrid electro-thermal system, optimizing electricity and thermal consumption, reducing fossil fuel consumption, minimizing the environmental impact, reducing assembly and maintenance periods for photovoltaic-thermal (hybrid) systems, and ultimately reducing costs.

References

Hu J, Chen W, Yang D, Zhao B, Song H, Ge B, *Energy Performance of ETFE cushion roof integrated photovoltaic/thermasystem on hot and cold days,* 2016, Appl Energy,173:40–51.

Yau YH, Lim KS. *Energy analysis of green office buildings in the tropics-Photovoltaic system*. Energy Build 2016; 126:177–93

Markvart, T. Solar Electricity, 2nd ed.; John Wiley & Sons: Chichester, UK, 2000.

Wang Y, Zhou S, Hou H, *Cost and CO2 reductions of solar photovoltaic power generation in China: perspectives for 2020*, 2006, Renew Sustain Energy Rev 20 14;39:370–80. Reserve de indiu conform USGS Mineral Commodity Summaries.

Bhubaneswari P, Iniyan S, Goic R, *A review of solar photovoltaic technologies*, 2011, Renew Sustain Energy Rev 15:1625–36.

Da Silva RM, Fernandes JLM, *Hybrid photovoltaic/thermal (PV/T) solar systems simulation with Simulink/Matlab,* 2010, Sol Energy 2010;84:1985–96.

Elbreki AM, Alghoul MA, Al-Shamani AN, Ammar AA, Yegani B, Alsanossi , Aboghrara M, Rusaln MH, Sopian K, *The role of climatic-design-operational parameters on combined PV/T collector performance: a critical review*, 2016,Renew Sustain Energy Rev ,57:602–47.

Kumar K, Sharma SD, Jain L, *Standalone Photovoltaic (PV) module outdoor testing facility for UAE Climate*, 2007, Submitted to CSEM-UAE Innovation Centre LLC.

Chandrasekar, M.; Rajkumar, S.; Valavan, D. *A review on the thermal regulation techniques for non integrated flat PV modules mounted on building top*. Energy and Buildings 2015, 86, 692-697.

Pomares-Hernández, C.; Zuluaga-García, E.A.; Escorcia Salas, G.E.; Robles-Algarín, C.; Sierra Ortega, *J. Computational Modeling of Passive and Active Cooling Methods to Improve PV Panels Efficiency*, 2021, Appl. Sci. , 11, 11370.

Kannan, N., Vakeesan, D, *Solar energy for future world—A review*, 2016, Renew. Sustain. Energy Rev. 62, 1092–1105. [CrossRef].

Rauf A, Liu X, Amin W, Ozturk I, Rehman O.U, Sarwar S, *Energy and ecological sustainability: Challenges and panoramas in belt and road initiative countries*, 2018, Sustainability, 10, 2743. [CrossRef].

Robles Algari, C., Rodríguez Álvarez, O, *An overview of the renewable energy in the World, Latin America and Colombia*, 2018, Espacios, 39, 1–16.

Tahar, M., Rosli, N., *Simulation Study of Cooling System for Photovoltaic Panel Using Ansys M.S.M*, 2022, Journal of Modern Manufacturing Systems and Technology (JMMST) vol. 6, issue 2, 26 – 33.

Reddy, S.R.; Ebadian, M.A.; Lin, C.X. A review of PV-T systems: Thermal management and efficiency with single phase cooling. International Journal of Heat and Mass Transfer 2015, 91, 861-871.

Available online at www.sciencedirect.com

ScienceDirect

Energy Procedia 85 (2016) 416 – 424

Energy Procedia

Sustainable Solutions for Energy and Environment, EENVIRO - YRC 2015, 18-20 November 2015, Bucharest, Romania

Influence of various angles of the venetian blind on the efficiency of a double skin facade

Catalin George Popovici[a], Vasile Valerica Cirlan[a], Theodor Dorin Mateescu[a], Nelu-Cristian Chereches[a]*, Sebastian Valeriu Hudisteanu[a]

[a]*Faculty of Civil Engineering and Building Services, "Gheorghe Asachi" Technical University of Iasi, 13 Dimitrie Mangeron, Iasi, 700050, Romania*

Abstract

The present study analyses the effect of solar protection arrangements on thermo-aeraulic regime inside a double-glazed facade coating (DFC), forced ventilated channel and under imposed working conditions. The facade has been considered being with "full South" guidance, exposed to normal solar radiation, with constant intensity. The "Venetian blinds" protection type has been investigated in optimum assumptions on the basis of previous researches [9], with regard to its positioning at 1/4th of the width of the channel, near exterior glazing and forced ventilation, under constant flow rate of 1260 m^3/h. The opening angle of the blinds, as the sole variable parameter, has been amended in succession between 0° and 90°. Solar protection influence analysis has been carried out by numerical simulation, with the specialized computing program ANSYS-Fluent, laying down, for each opening angle of blinds, variation diagrams of air streams temperatures and velocity along the width and along front panel channels.

© 2016 The Authors. Published by Elsevier Ltd. This is an open access article under the CC BY-NC-ND license (http://creativecommons.org/licenses/by-nc-nd/4.0/).

Peer-review under responsibility of the organizing committee EENVIRO 2015

Keywords: Façade channel; solar protection; blinds angle; radiation; numerical analysis

1. Introduction

Recent technological developments have entailed glass as a highly used material for buildings envelope, due to its multiple and complex functions which transform glazing in an active component regarding from thermal, optical and electrical points of view [1].

* Corresponding author.
E-mail address: cristi_chereches@yahoo.com

1876-6102 © 2016 The Authors. Published by Elsevier Ltd. This is an open access article under the CC BY-NC-ND license (http://creativecommons.org/licenses/by-nc-nd/4.0/).
Peer-review under responsibility of the organizing committee EENVIRO 2015
doi:10.1016/j.egypro.2015.12.222

As far as functional-constructive point of view, double glazed façade arose out of the necessity of protecting a curtain wall by placing in front of it a glass surface. The envelope thus formed influences on the thermo-aeraulic behavior of the hole building – directly or indirectly - based on the connection manner applied between the two glazed surfaces and with inside and outside environments, and also, based on the ventilation solution chosen for the intermediate channel [2].

The two transparent glass elements, placed at a certain distance, form a channel where an air flow circulates [3] and inside which, as applicable, a shading system can be integrated, in order to control the heat quantity acquired from solar radiation [4, 5].

The main function of this system is to improve thermal protection during winter, by passive recovery of the solar energy and exhaust excessive heat accumulated during warm season [6].

The special importance of this system as far as buildings energy efficiency is concerned justifies the technical and scientific interest for thoroughgoing study and acknowledgment of functional outlines and solutions improvements.

In this regard, in the specialized literature are presented results of studies and researches carried out by teams of specialists all over the world that clarifies many of the issues of great interest, such as:

- recommended functional organizational design, geometry and dimensions;
- ventilation methods and functional scenarios;
- energy and comfort efficiency;
- calculation models;
- experimental testing on small scale or natural models and others.

Analyzing behavior of DFC equipped with solar protection is important as it allows identification of various phenomena that influence on system's efficiency [7, 8].

Thermal-aeraulic behavior of the façade depends equally on the geometry of the façade, the characteristics of its components, the ventilation system and the air flow regime inside the façade channels [5].

The main objective of the study was to determine, by numerical modeling, the optimum opening angle of solar protection type venetian blinds blades in relation to dynamic insulation efficiency (ε).

As in a previous study [9], in which the optimum position of the blinds inside the façade channel had been analyzed, resulting that, during summer conditions, maximum efficiency is achieved when blinds are closer to exterior glazing, the present study was developed taking into consideration the above mentioned conclusions.

Numerical analysis has been elaborated for a double glazed façade having the characteristics accordingly with experimental setup, Table 1, inside the laboratory of Building Services Engineering Department, Technical University "Gheorghe Asachi "of Iasi – Fig. 1 [10].

Table 1. Thermo-physical properties of components

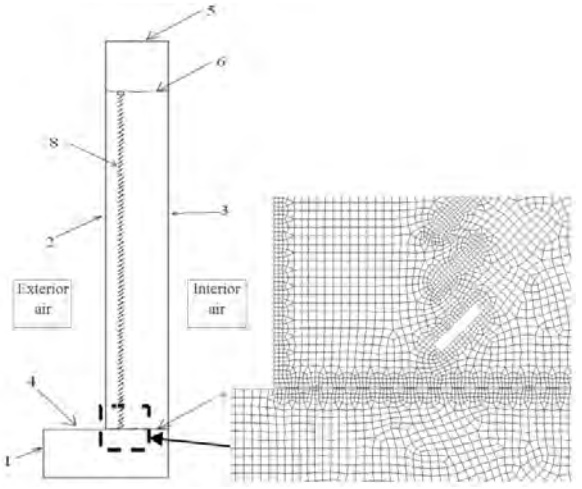
Component element	Density ρ [kg/m^3]	Specific heat cp [J/kg·K]	Thermal conductivity λ[W/m·K]	Absorption index, a	Refractive index, τ	Reflection index, r
exterior glazing	2 500	670	5.3	0.11	0.82	0.07
air	1.225	1 006.43	0.0242	0	1	0
racks steel	8 030	502.48	43	0.65	0*	0.35
blinds aluminum	2 719	871	202.4	0.76	0*	0.24
interior glazing	2 500	670	1.4	0.18	0.69	0.13

*during simulation, solar protection has been considered as semi-transparent surface with refractive coefficient assimilated with the corresponding percentage of free surface resulted for the blades angle.

Main characteristics of the model are:

- dimensions- 2.1 m height, 1.5 m length, 30 cm channel width;

- façade channel consisting of one exterior simple glass (2) of 6 mm thickness and one interior double glazed type window (3) with 27 mm thickness, made of 2 layers of glass of 6 mm respectively 5 mm thickness and 16 mm air interspace;
- Venetian type blinds (8) – made of horizontal metallic adjustable blades of 25 mm width and 22,5 mm interspaces;-positioned at 1/4 D behind exterior glazing;
- Air flow balancing grilles, with 50% obscuration rate, mounted along the façade channel at both at supply and exhaust in/out of the channel (6 and 7).



a) b)

Legend:
1 – supply;
2 – exterior glazing;
3 –interior glazing;
4 – entrance box;
5 – exhaust;
6 – superior grille;
7 – inferior grille;
8 – blinds;

Fig. 1. Description of the geometry (a) and the mesh (b) of the model

2. Modeling hypothesis

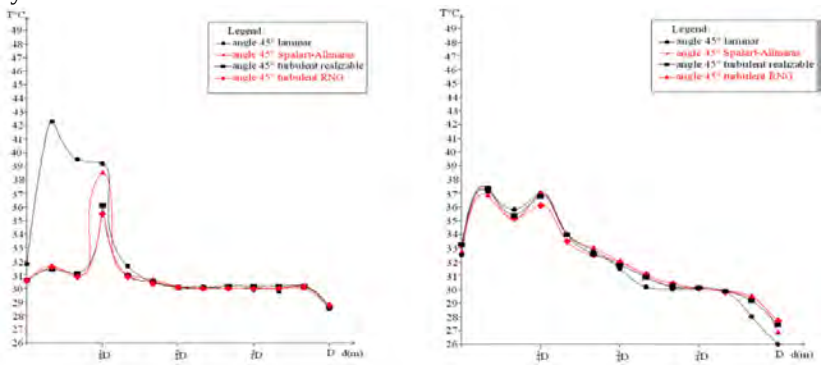
Modeling was carried out under permanent regime, for blades inclination angels of 0°, 30°, 45°, 60°, under the following hypotheses:

- direct solar radiation intensity imposed on exterior glass of the façade : 285 W/m^2;
- diffuse solar radiation intensity: 82 W/m^2;
- outside air temperature, T_e : 30°C (which is the inlet temperature for simulated cases) and convective heat transfer coefficient from the façade with exterior air, α_{ve} : 24 W/m^{2o}C;
- inside temperature, T_i : 25 °C and convective heat transfer coefficient from the façade with interior air, α_{vi} : 8 W/m^{2o}C;
- forced convection, with constant flow rate of 1260 m^3/h, according to the average velocity of 0.5 m/s at the inlet section and turbulence intensity of 4.7 %.

Numerical simulations were conducted with the program ANSYS-Fluent [12] based on control volumes method and using SIMPLE algorithm [13]. For meshing, has been used a non-uniform and rectangular mesh which has maximum face size of 0.0035 m, 96333 elements, 99301 nodes and 195779 faces. The height of the first cell, near the exterior and interior glass is 1.75 mm and the number of the prism layers in the boundary layer is 4.

In order to choose an appropriate model of turbulence were tested and analyzed different turbulence models (k-ε realizable, k-ε RNG and Spalart-Allmaras) and additionally the laminar model, for the opening angle of 45° (Fig. 2). Temperature variations were represented in Fig. 2 and we can observe that is no notable difference between the different turbulence models. Thus, it was chosen the use of k-ε realizable in all cases of study, which is widely used in computational fluid dynamics and validated for classical cases of turbulence flows including the channels with obstacles and layer flows [12].

For radiation, Discrete Ordinates model (DO) which solves the radiative transfer equation for a finite number of discrete solid angles, was adopted to simulate the radiation, being the only model where solar direct and diffuse radiation is mentioned. Calculation is iterative, having convergence limit of 10−6 for temperature and 10−4 for pressure and velocity.



a) supply section, 10 cm above inferior grille (H=0,10m); b) exhaust section, 10 cm beneath superior grille (H=2m)

Fig. 2. Temperature variations for turbulence models simulated

3. Results interpretation

Results are presented as velocity and temperatures spectra (Fig. 3), graphs variations (Fig. 4 and 5) and velocity vectors (Fig. 6), in the vertical median section of the facade, at H=0.10 m; H=1.05 m; H=2.00 m (10 cm upstream and downstream the supply/exhaust section and half façade), with a 2.5 cm step alongside façade width.

Analyzing the results given by the four versions of blades opening, we can underline the following aspects:

General

- Blinds blades opening induce local and transversal circulations between channels, comparatively more intense alongside the supply and exhaust section due to disruptive effect of distribution grilles (Fig. 3) and the spread difference between pressure and temperature;
- For opening angles of 45° and 60° transversal circulations are dominant.

Temperature related

- Temperature values differ along the façade, as they are obviously higher inside exterior channel and decreasing as we focus towards the glazing inside the interior channel;
- Temperature variation inside control sections is relatively uniform inside the interior channel unrelated to opening angles and more pronounced inside the exterior channel (Fig. 4);

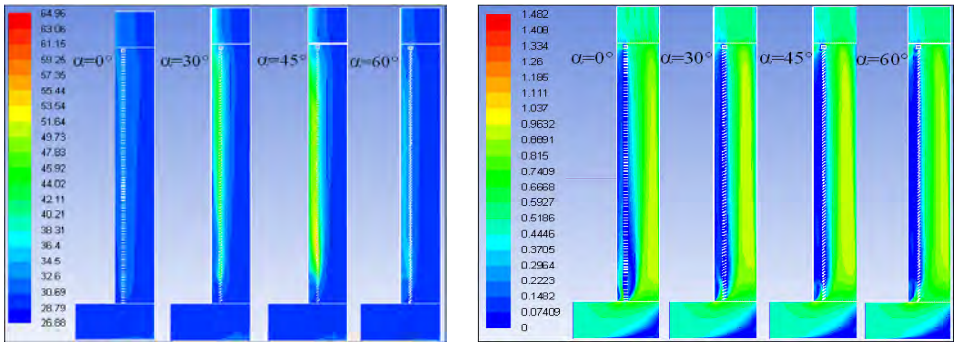
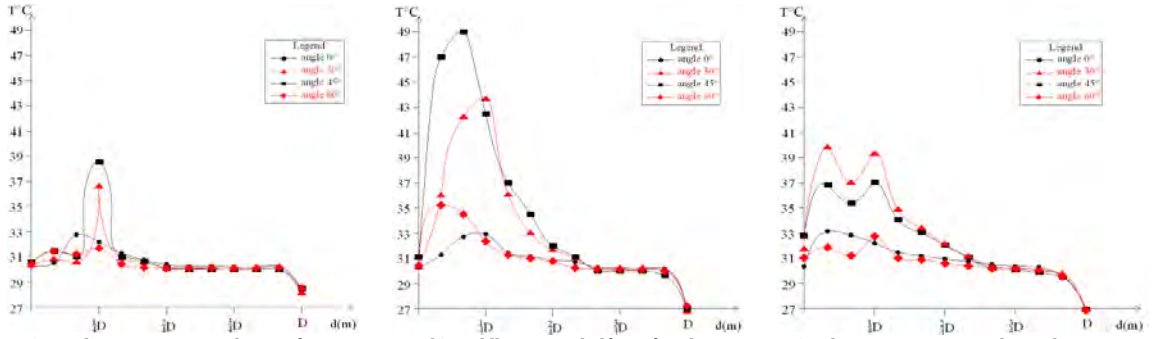


Fig. 3. Temperature (°C) and velocity spectrum (m/s)

- - Solar protection acts like a barrier for the radiative flow accumulating heat and reducing the air heating effect inside the channel and alongside interior glazing for opening angles wider than 30°;
- Maximum temperature along blinds is registered at 45° opening, reaching 65°C, when the minimum value is reached at 0° opening angle;
- Temperature specters are correlated with velocity specters as they are inversely proportionate;
- For all angles, inside glazing temperatures vary between 27 to 29°C, and outside glazing temperatures vary between 30 to 34°C;
- Air temperatures vary between 30 to 31°C in the axis of inside channel and between 31 to 40°C inside exterior channel.

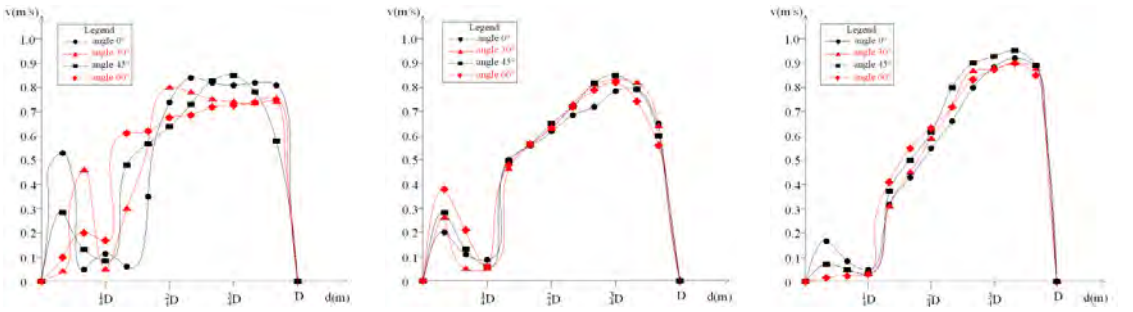


a) supply section, 10 cm above inferior grille (H=0,10m); b) middle section, halfway facade (H=1,05m); c) exhaust section, 10 cm beneath superior grille (H=2m).

Fig. 4. Temperature variation along channel width related with blinds opening angle

Velocity related

- Velocities vary alongside façade with significantly higher values inside the interior channel;
- Medium velocity values are between 0.52 m/s and 0.58 m/s for all sections inside the interior channel and between 0.10 m/s and 0.18 m/s inside exterior channel, (Fig. 5);
- Along control sections maximum values of velocities are registered along channel axis reaching up to 0.5 m/s inside exterior channel, respectively 1.0 m/s inside interior channel and decrease towards glazing and protection section;



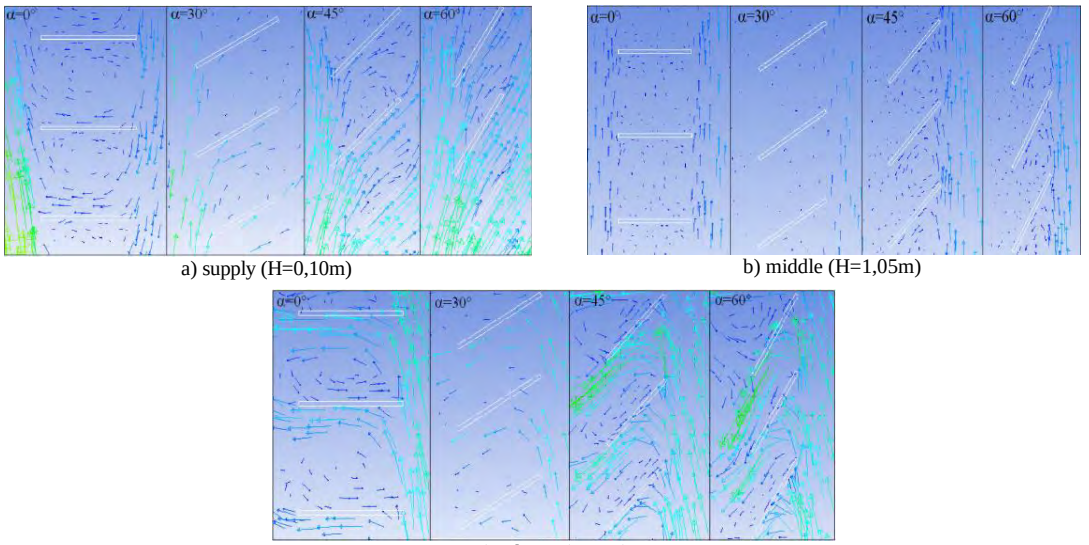
a) supply section, 10 cm above inferior grille (H=0,10m); b) exhaust section, 10 cm beneath superior grille (H=2m) c) middle section, halfway facade (H=1,05m);

Fig. 5. Velocity profiles

Mass transfer related

- Presence of sunscreen facade induces local turbulence and mass transfer between its channels, as shown in Fig. 5;
- Phenomenon intensity and direction of movement is influenced by the opening angle and the gap position control section temperature / pressure between the two channels;

- In the supply area the flow lines indicate transfer from the exterior to the interior channel;
- In the middle area are recorded, especially local circulation phenomena between blades, proportional to the opening angle;
- In the exhaust area the mass transfer is increases from the inner channel to the outer channel.



a) supply (H=0,10m) b) middle (H=1,05m)

c) exhaust (H=2m)

Fig. 6. Velocity spectrum recorded between blades

Table 2. Dimensionless numbers and convective heat transfer coefficients inside façade channel

No.	Façade configuration	Blade angle	V_{med} [m/s]	T_{med} [°C]	Re	Pr	Nu	α_v [W/m^2°C]	α_p [W/m^2 °C]	α_k [W/m^2 °C]
1	Exterior channel	0	0.182	31.96	1 316.6	0.77	6.43	24	2.31	0.56
		30	0.103	38.72	745.10	0.77	4.08	24	1.45	0.35
		45	0.108	45.71	781.27	0.77	4.24	24	1.66	0.37
		60	0.023	34.21	166.38	0.77	1.23	24	1.93	0.10
2	Interior channel	0	0.718	30.6	14 232.7	0.77	43.20	8	2.31	1.34
		30	0.740	32.03	14 668.79	0.77	44.26	8	1.45	1.37
		45	0.763	32.22	15 124.72	0.77	45.36	8	1.66	1.40
		60	0.728	30.43	14 430.92	0.77	43.68	8	1.93	1.35

For each blinds study position, dimensionless numbers, Re, Pr, Nu, values had been calculated, as well as convective heat transfer coefficients at surface bounding elements (Table 2) for the two façade channels related on flowing regime and surfaces temperatures, for each opening blades angles, where: αv, αp, αk represents convective heat transfer coefficients respectively from glass surfaces to exterior and interior air (αv), at the surface of the blades (αp) and from glass surfaces to air inside the channels (αk).

Convective transfer coefficient varies between 0.10 and 0.56 (W/m2K) for exterior glazing. The highest value of the convective exchange coefficient is registered at blades opening angles of 45°, reaching 1.40 (W/m2K), as for other angles, convective heat exchange coefficient remains steady around values between 1.37 (W/m2K) and 1.34 (W/m2K).

As far as interior glazing is concerned, coefficient value increases starting to 0° opening angle up to 45°, when it reaches the maximum value, followed by a decrease around de 60° angle.

4. Dynamic insulation efficiency

For comparative and quantifies assessment of energetic effect of the blinds over thermal regime inside DFC susceptible to overheat during summer regime, dynamic insulation efficiency has been calculated, for each blades opening angle. Dynamic insulation efficiency is defined as ratio between heat flow of exhausted air and (Q_r) and total heat flow supplied inside the protected area (Q_{inc}).

$$\varepsilon = \frac{Q_r}{Q_{inc}} \tag{1}$$

Due to variable thermal regime, induced in the two compartments of façade by solar protection presence, total flow exhausted, Q_r, has been determined as sum of partial flows.

$$Q_{rc1} = m_{vc1} \cdot c_p \cdot \Delta T_{c1} \tag{2}$$

$$Q_{rc2} = m_{vc2} \cdot c_p \cdot \Delta T_{c2} \tag{3}$$

where: m_{vc1} –mass exhausted airflow from the exterior channel; m_{vc2} –mass exhausted airflow from inside interior channel; c_p – air specific heat; Δt_{c1} – temperature difference between supply and exhaust air from the exterior channel of the facade; Δt_{c2} – temperature difference between supply and exhaust air from the interior channel of the facade.

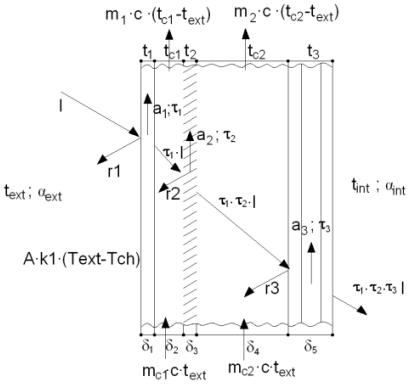
Thermal flow received from the external environment supplied in the protected area, by radiation and convection (Fig. 7), in double skin façade respectively is determined by the following equation:

$$Q_{inc} = \Pi \tau_i \cdot A \cdot I + k_{glo} \cdot \left(T_{ext} - T_{\text{int}}\right) + Q_{rc1} + Q_{rc2} \tag{4}$$

Where: $\Pi\tau_i$ – intermediate surfaces transmittance product; k_{glo} – global heat transfer coefficient; t_{int} – inside air temperature, in the protected space; t_{ext} - outside air temperature; I- global solar radiation component, normal along façade surface; A - façade surface.

$$k_{glo} = \frac{1}{\Sigma R_i} = \frac{1}{\frac{1}{\alpha_{ext}} + \frac{1}{\alpha_{\text{int}}} + \Sigma \frac{\delta_i}{\lambda}} \tag{5}$$

where R_i represent the thermal-conductive-convective and radiative transfer trough façade elements.



$$\varepsilon = \frac{\sum_{i=1}^{2} m_i c \cdot \left(t_{ci} - t_{ext}\right)}{A\left[k_{glob} \cdot \left(t_{ext} - t_{\text{int}}\right) + \prod_{j=1}^{3} \tau_j\right] I + \sum_{i=1}^{2} m_i c \cdot \left(t_{ci} - t_{ext}\right)}$$

Fig. 7. Energy flow schema along the facade

Table 3 presents consecutive values of solar protection calculated, accordingly with blades opening angle, Eq. (1).

Table 3. Dynamic insulation efficiency

No.	Angle of blinds	$\Pi\tau_i \times A \times I$ [W]	k_{glo} [W/m^{2}K]	m_{vc1} [kg/s]	m_{vc2} [kg/s]	Δt_{c1} [K]	Δt_{c2} [K]	Q_{rc1} [W]	Q_{rc2} [W]	Q_r [W]	Q_{inc} [W]	ε [%]
1	0°	632.70	0.077	0.0106	0.2269	2	0.9	21.33	205.52	226.85	859.73	26.4
2	30°	208.77	0.076	0.0057	0.2327	6.9	1.6	39.58	374.71	414.29	623.86	66.4
3	45°	158.12	0.070	0.0039	0.2716	5.9	1.2	23.15	328.01	351.17	509.83	68.9
4	60°	88.56	0.076	0.0023	0.2381	1.7	0.5	3.93	119.81	123.77	189.73	65.2

Dynamic insulation efficiency reaches the maxim value of 68.9% for an opening angle of 45°, and 26.4% for 0°, which can be stated that the blinds offer the best protection for an opening blades angle of 45 degrees. Mass air flow determined inside the façade channels (mvc1 and mvc2) was studied according with average velocities for the chosen modeling hypothesis.

Incident solar radiation values over intermediate surfaces had been calculated according to glazing refraction indexes τi.

Solar protection has been considered as a semi-transparent surface, reflection index being assimilated with free area ratio with regard to blades opening.

$$\tau = \frac{H - n \cdot b \cdot \sin\beta}{H} \tag{6}$$

where: n – number of blind blades; b – blade width; H – total height of solar protection; β – opening blinds blades angles.

5. Conclusions

In this paper, the influence of various angles of the venetian blind was studied in order to determine the efficiency of the double skin façade. The results consist of the optimum opening angle of solar protection.

Solar protection efficiency is directly proportional with air flow velocity inside façade channel and inversely with blades opening angle.

Opening blinds blades angles analysis for the interior surface of DFC reveals that the optimum opening angle is at 45 degrees, when the dynamic insulation efficiency reaches the maxim value of 68.9%.

References

[1]. Perez-Grande I., Meseguer J., Alonso G., Influence of glass properties on the performance of double-glazed façades, Applied Thermal Engineering 2005; 25: 3163-3175

[2]. Chan A. L. S., Chow T. T. , Fong K. F., Lin Z., Investigation on energy performance of double skin façade in Hong Kong Building, Energy and Environmental Technology Research Unit 2009; 41: 1135-1142

[3]. Padet J., Principes des transfer convectifs, Polytehnica, Paris, France; 1997.

[4]. Ye P., Harrison S.J., Oosthuizen P.H., Naylor D., Convective Heat Transfer from a Window with Venetian Blind: Detailed Modeling, Refrigerating and Air- Conditioning Engineers (ASHRAE) Transactions 1999; 105: 1031-1037

[5]. Safer N., Modeling of double-skin facades types equipped with sunscreens: multiscale approaches, (in french language), Institut National des Sciences Appliquées de Lyon, Centre de Thermique de Lyon (CETHIL), France, PhD Dissertation, 2006.

[6]. Arons D., Properties and Applications of Double-Skin Building Facades, Massachusetts Institute of Technology (MIT), USA; 2000

[7]. Hossein G., Mohammad G., Mahdi S., Meisam M., Mohammad M., Analytical solution for energy modeling of double skin facades building, Energy and Buildings 2012; 50: 158-165

[8]. Romila C., Popovici C. G., Cherecheș N.-C., Reduction of building energy consumption using ventilated façades, Environmental Engineering and Management Journal 2012; 4: 806-811

[9]. Cirlan V. V., Mateescu T., Chereches N. C., Popovici C., Location of this sunscreen in channel of double skin facades in relation to their energy eficiency, (in romanian language), 48th National Conferences of Building Services, Sinaia 2013: 105-113
[10]. Grigoraş C., Mateescu T., Cotorobai V., Chereches N.C., Experimental and numerical study on the influence of radiative flux on the thermodynamic behavior of a double-skin facade, (in romanian language), 47th National Conferences of Building Services, Sinaia 2012: 331-340
[11]. Pasut W., De Carli M., Evaluation of various CFD modelling strategies in predicting airflow and temperature in a naturally ventilated double skin façade, Thermal Engineering 2012; 37 : 267-274
[12]. Fluent Inc. Fluent user's manual, 2013
[13]. Safer N., Woloszyn M., Roux J.J., Three-dimensional simulation with a CFD tool of the airflow phenomena in single floor double-skin façade equipped with a Venetian blind, Solar Energy 2005, 79(2):193-203

Available online at www.sciencedirect.com

ScienceDirect

Energy Procedia 112 (2017) 434 – 441

Energy Procedia

Sustainable Solutions for Energy and Environment, EENVIRO 2016, 26-28 October 2016, Bucharest, Romania

Innovative solutions for geothermal heat exchangers

Cătălin George Popovici[a], Teodor Mateescu[a], Răzvan Luciu[a], Ionela Cazacu[a]*

[a]*Faculty of Civil Engineering and Building Services, "Gheorghe Asachi" Technical University of Iasi, 13 Dimitrie Mangeron, Iasi, 700050, Romania*

Abstract

Common types of geothermal heat exchange, the surface and the depth is characterized by demanding uneven ground. Uniformity thermal load of the massive and efficiency may be a solution in the sense of optimizing energy storage capacity and therefore reduced surface / volume of land used.

A solution atypical geothermal heat exchanger, shallow, variable spatial geometry using cylindrical or tapered, which compared with geothermal drilling or pilots, presents significant recovery in terms of thermal capacity of the ground.

For the spiral pipe conducted with constant diameter is maintained disadvantage loading / unloading uneven ground. The situation is radically altered when using the spiral geometry of tapered or cylindrical modular charge transfer areas to which it is directly proportional to the reduction in temperature of the work and its evolution, leads to a transfer of that charge / discharge uniformly. From a functional perspective and energy, this solution is obvious superior to any surface or deep usual, the heat transfer in the heat exchanger is variable. The novelty of the proposed solution is a favorable argument optimizing surface geothermal exchanger used in making reversible heating / cooling with solar energy.

© 2017 The Authors. Published by Elsevier Ltd. This is an open access article under the CC BY-NC-ND license (http://creativecommons.org/licenses/by-nc-nd/4.0/).

Peer-review under responsibility of the organizing committee of the international conference on Sustainable Solutions for Energy and Environment 2016

*Keywords:*geothermal heat exchangers;variable spatial geometry;numerical simulation.

* Corresponding author. Tel.: +40-0767309066.
E-mail address:cazacuionela@ymail.com

1876-6102 © 2017 The Authors. Published by Elsevier Ltd. This is an open access article under the CC BY-NC-ND license (http://creativecommons.org/licenses/by-nc-nd/4.0/).

Peer-review under responsibility of the organizing committee of the international conference on Sustainable Solutions for Energy and Environment 2016
doi:10.1016/j.egypro.2017.03.1102

1. Introduction

Social and economic progress leads to the use of traditional energy resources are exhaustible problem involving organized use consumption on the entire chain of production, distribution and consumption, the problem presented extensively Boian, and others in 2006 [4]. Fridleifsson and others show the importance of using geothermal energy using heat pumps as an alternative to traditional technologies [10]. PraktischeNutzungVonErdwärne and others presents the data available on the European market for geothermal heat pump reveals an interesting picture, which shows the existence of stable markets and develop new ones [1]. Fridleifsson I.B shows scientific development in European countries in the field of heat pumps in general and especially geothermal pumps: Switzerland, Sweden, Germany, France, Italy. [11]

Bluc I. describes the evolution of the temperature at the soil surface, representing the most important factor in warming the earth's surface [3] - the ability to transfer and heat storage is determined by the characteristics of the soil thermo-dependent spatial structure of constituents and volume share of its studied the problem and Fleige H. [9]. J. R. Edwards describes how heat transfer: conduction, convection and radiation, due to the temperature difference between the parties concerned. The main goal of the thermal analysis is to determine the water temperature and operating conditions of the heat pump [6]. Determining factor in the process of extracting heat from the ground is the outlet temperature of the working fluid heat exchanger, causing energy efficiency throughout the system.

In literature there are many models for functional characterization of systems, including those developed by Ph.Ackerer and M.A.Bues [2]. Progress programs and computer equipment led to solve differential equations of heat transfer, obtaining solutions with high precision. An example is the model presented by P. Brousseau, M. Lacroix [5]. Eskilson P and Gérard Magnin describe how to transfer heat from the ground through geothermal heat exchangers, surface and depth, characterized by requiring uneven ground. [7], [8]. The heat transfer to the soil is carried out with heat exchangers made of tubes or loops through which a working fluid, these may be horizontal or vertical. Common types of geothermal exchange, both the surface and the depth is characterized by non-uniform application of the soil, uniform thermal load of soil represent a efficient solution for storage capacity and reduction of land area needed for installation of heat exchangers.

The paper presents a constructive concept - functional and numerical simulation results of the machine ground heat exchanger used to build the type of geothermal equipped with reversible heat pumps. This exchange geothermal is subject the patent file - OSIM A 2016/00061.

2. Material

Geothermal exchanger proposed is made of modules in series with variable geometry, is an innovative solution that enables optimization thermal and current economic solutions.

Modular transfer distribution and sizing of the surface it is inversely proportional to the temperature difference, provides uniform heat flux along the device and therefore stored heat load is balanced.

Using the execution of materials with high thermal conductivity - copper, brass or steel significantly increases the overall heat transfer coefficient and thus reduce heat transfer area needed, positive impact on the amount of land needed for development of sources colder.

From the point of view of construction, geo modular heat exchanger with variable geometry, can be done in two ways:

- Cylindrical modules - rectangular ring section and flow baffle
- Modules cylindrical with constant diameter (D) and variable height (Hi) made of bundles of pipes whose side surface is the surface heat transfer.

All variants are embedded in devices made with sand of the stock heat with thermos -controlled grain size and characteristics, the large diameter drilling (pilot) or holes, isolated environment.

Sizing is based on seasonal and thermal stress as compared with the operating system serviced.

The calculation is performed properly heat exchangers heat accumulation.

a). b). c).

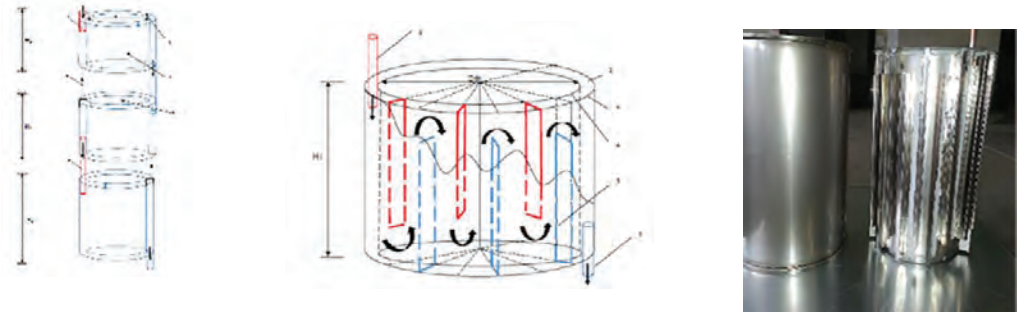


Fig. 1. The modular geothermal heat exchanger a) assembly, b) detail, c) picture

By integrating differential equations of heat transfer and thermal balance

- $w_1(T_{11} - T_{12})\,d\tau = w_2\,d\theta = KS\Delta T_m\,d\tau$ (1)

With the notations:

$$w_1 = Co(\rho c)_1,\ w_2 = V(\rho c)_2, \varepsilon = \frac{K_s}{w_1} \quad (2)$$

Relationships resulting calculation:

- Required surface heat exchangers

$$S_{nec} = \frac{w_1}{K} ln\left[1 - \frac{w_2}{w_1 \tau_{loading}} ln \frac{T_{11} - \theta_{initial}}{T_{11} - \theta_{final}}\right] \quad (3)$$

-Temperature working fluid out of the exchanger at the moment:

$$T_{12} = \theta - \frac{\theta - T_{11}}{e^{\varepsilon}} \quad (4)$$

- During loading stock

$$\tau_{loading} = \frac{w_2}{w_1} \cdot \frac{1}{1 - e^{-\varepsilon}} ln \frac{T_{11} - \theta_{initial}}{T_{11} - \theta_{final}} \quad (5)$$

- Temperature in storage at a time τ:

$$\theta_\tau = T_{11} - (T_{11} - \theta_{initial}) e^{-\frac{w_1}{w_2}(1 - e^{-\varepsilon})\tau} \quad (6)$$

These systems are generally designed both for winter and for summer. The amount of heat injected into the ground in the hot season is significantly higher than that to be extracted in winter, thermal equilibrium is achieved by the correct sizing of the power for heating load .Therefore it should be adopted bivalent concept using excess heat from the hot season for hot water or for other uses and providing a thermal sources to cover additional requirements under winter.

The proposedsolutionhastheadvantagethattheoperationaimstosource control compensation on an annualbasis, resulting in reduced land arearequired for settingheatexchangers.

3. Method

To analyze the efficiency of a geothermal exchanger with variable geometry was carried out numerical modeling of the thermal behavior of some modules in series diameter D_m = 0,425m and 1,00m lengths imposed, 1,25m and 1,50m in different operating regimes with flow and temperature extremes adequate quantities of heat pumps type REHAU - GEO 7 and GEO 37, respectively G = 1,3mc / h and 7,2mc / h, $T_{tour} = 35^0$C.

Sand were used the following parameters ρ = density of 1800Kg /m^3, coefficient of thermal conductivity λ = 14 kcal / m^0C, the average temperature $\theta_2 = 10^0$C.

- diameters - Di = 0.40 m , De=0.45 m = , D_m = 0,425 m
- specific areas of transfer : $A=\pi(D_i + D_e) = 2{,}67m^2/ml$
- the number of channels with the angle at center 30^0= 12pcs.
- vertical cross-sectional area of the channel $\omega = 0{,}0028m^2$
- the equivalent diameter d equivalent d_{eq}=0,0594m

Table 1. Appropriate arrangements relating to the two types of hydraulic pumps follows:

Size feature	Symbol	MU	Numerical values related	
			GEO 7	GEO 37
Heating water flow	G	m^3/h	1,3	7,2
The flow rate in the vertical channels	v	m/s	0,064	0,354
Reynolds criterion	Re	-	2904	16,066
Nusselt criterion	Nu	-	75,36	177,2
Prandtl criterion	Pr	-	9,4	9,4
Convective transfer coefficient	α	$Kcal/m^2\,^0C$	634,4	1492
Global heat transfer coefficient	K	$Kcal/m^2\,h\,^0C$	81,42	87,9
How I	H	m	1,0	1,0
	T_{11}	^0C	35	35
	T_{12}	^0C		
How II	H	m	1,25	1,25
	T_{21}	^0C		
	T_{22}	^0C		
How III	H	m	1,50	1,50
	T_{31}	^0C		
	T_{32}	^0C		

The numerical simulation was carried out in the modeling ANSYS - FLUENT.

Fluent software is a code CFD (Computational Fluid Dynamics), which was developed for solving the equations of heat transfer and flow characteristics using the finite volume. This method is based on the spatial integration of the equations of conservation, turning them into algebraic equations which are solved by the physical sequentially analyzed.

Numerical modeling:

The CFD uses numerical technique to solve equations governing the flow in various types of geometries depending on the boundary conditions; reduce the number of experiments required and deliver results that would be difficult to determine experimentally. Working assumptions and boundary conditions.

The working hypotheses for the primary are:

Boundary conditions:

Upon entering the exchanger: - live: $v_z = v_y = v_0$; (7)

- setpoints: $T = T_0$

On leaving the exchanger: $\frac{\partial v_x}{\partial y} = \frac{\partial v_y}{\partial y} = \frac{\partial T}{\partial z} = 0$ (8)

The input parameters:

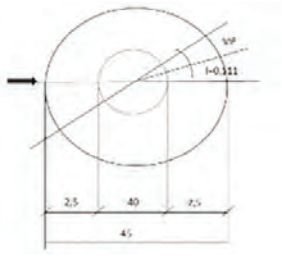
For determining the performance of the heat exchanger analyzed, there were used the following relationships:

$$\alpha_{nf} = \frac{Nu \cdot \lambda}{d_e} \quad (9)$$

where:

Reynolds: $R_e = \frac{v \cdot d_{eq}}{\vartheta}$ (10)

Prandtl: $P_r = \frac{C_p \cdot \eta}{\lambda}$ (11)

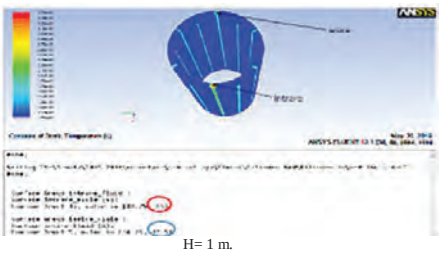


Dm = 0,425
d_{eqiv}= 0,0594
ω= 0,002775
G= 1,3 mc/h
v = 0,064m/s
A = 2,669m^2/mc

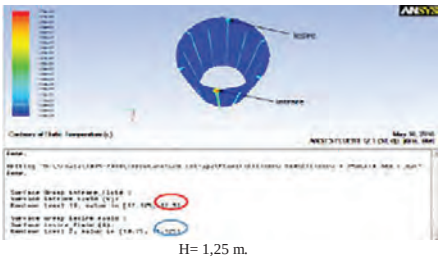
Fig. 2. Details of calculation

Following numerical modeling, it can analyze and visualize temperature and speed spectra corresponding cases studied:

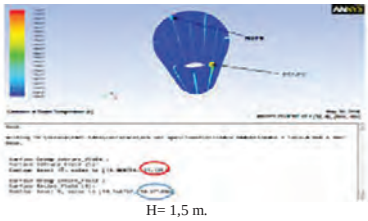
v	H	Ti	Te
m/s	m	°C	
0,36	1	35,00	**17,50**
	1,25	**17,50**	11,125
	1,5	11,125	**10,225**



H= 1 m.



H= 1,25 m.



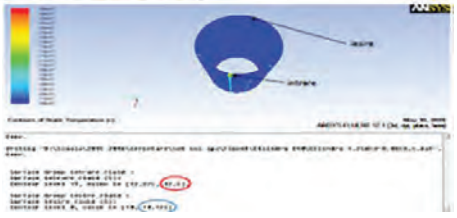
H= 1,5 m.

Fig.3 -Case 1 - GEO 37:

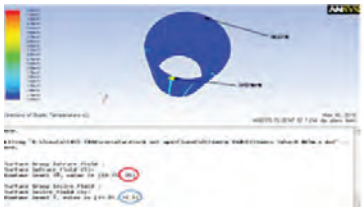
v	H	Ti	Te
m/s	m	°C	
0,065	1	35,00	**12,50**
	1,25	**12,50**	10,125
	1,5	10,125	**10,00**



H= 1 m.



H= 1,25 m.



H= 1,5 m.

Fig. 4. Case 2 - GEO 37

It considered the characteristic length: $R_e = \frac{vl}{\vartheta}$ and $\alpha = \frac{\lambda}{e} Nu$, the equivalent diameter (d_{eq})

$$\omega = e \times l \cong 0{,}008 \tag{12}$$

$$d_{eq} = \sqrt{\frac{\omega}{0{,}785}} = 0{,}059456\ m \tag{13}$$

$$Rh = \frac{d_{eq}}{4} = 0{,}01486 \tag{14}$$

$$v = \frac{G}{2 \cdot 3600} \cdot \frac{1}{\omega} = 0{,}064\ m/s \tag{15}$$

$$Re = \frac{v \cdot d_{eq}}{\vartheta} = 2904 \tag{16}$$

$$Pr = 9{,}4 \tag{17}$$

$$Nu = 0{,}666 \cdot Re^{\frac{1}{2}} \cdot Pr^{\frac{1}{3}} = 113 \tag{18}$$

$$K = \frac{1}{\frac{1}{\alpha} + \frac{\delta}{\lambda_C} + \frac{1}{\alpha^*}} \tag{19}$$

$$\alpha^* = \frac{1}{\rho_{granules}} \left[0{,}06 \frac{2\lambda_s \cdot \lambda_{cu}}{\lambda_s + \lambda_c} + 0{,}94 \lambda_{air}\right] = 93\ Kcal/m^{2\,0}C \tag{20}$$

$$\alpha = \frac{\lambda}{d_{eq}} Nu = 951 Kcal/m^{2\,0}C \tag{21}$$

$$K = 84{,}69 Kcal/m^{2\,0}C \tag{22}$$

Heatbalance of thedifferentialequation:

$$-G \cdot \rho \cdot c \cdot dt = K(T - \theta) \cdot A\ dH \tag{23}$$

$$-\int_{T_1}^{T_2} \frac{dt}{T - \theta} = \frac{K \cdot A}{G \cdot \rho \cdot c} \int_0^H dH \tag{24}$$

$$\ln(T-\theta)/_{T_2}^{T_1} = \frac{KA}{G \cdot \rho \cdot c} => \frac{T_1 - \theta}{T_2 - \theta} = e^{\frac{KAH}{G\rho c}} \tag{25}$$

$$T_2 = \theta + \frac{T_1 - \theta}{e^N} \tag{26}$$

With: $N = \frac{K \cdot A \cdot H}{G \cdot \rho \cdot c} = 0{,}173H$ (27)

It requires: - temperatures: $T_{tour} = 35^0C$, $T_{back} = 15^0C$, $\theta = 10^0C$

- length of the first section H= 1,0 m
- temperature input $T_{11} = T_{back} = 35^0C$

- the temperature at the output of the first module

Result:

$$T_{12} = \theta + \frac{T_{11} - \theta}{e^N} = 35^0C \tag{28}$$

- output temperature of al- II module

L= 1,25m

$$T_{22} = \theta + \frac{T_{21} - \theta}{e^N} = 126{,}9^0C \tag{29}$$

- output temperature of al- third way

L= 1,50m

$$T_{32} = \theta + \frac{T_{31} - \theta}{e^N} = 23^0C \tag{30}$$

If required output temperature module output temperature IV, of al- II module $T = 15^0C$

H4 required length is determined from the relationship (26)

$$e^N = \frac{T_{i1} - \theta}{T_{i2} - \theta} = e^{0{,}173 H_i} \tag{31}$$

Namely: $0{,}173H_4 = \ln \frac{T_{41} - \theta}{T_{42} - \theta}$ (32)

$$H_4 = \frac{1}{0{,}173} ln \frac{23 - 10}{15 - 10} = 5{,}5m \tag{33}$$

Integrated form of the equation (23)

$$G \cdot \rho \cdot c\ (T_{1i} - T_{2i}) = K \cdot A(\overline{T_i} - \theta) H_i \tag{34}$$

Equivalencefollows:

$$H_i \frac{T_i-\theta}{T_{1i}-T_{2i}} = \frac{G\cdot\rho\cdot c}{K\cdot A} = \text{constant} \quad (35)$$

Or: $\frac{H_1}{H_2} = \frac{\overline{T_2}-\theta}{T_{21}-T_{22}} \cdot \frac{T_{11}-T_{12}}{\overline{T_1}-\theta}$ (36)

Namely: $H_2 = H_1 \frac{\overline{T_1}-\theta}{\overline{T_2}-\theta} \cdot \frac{T_{21}-T_{22}}{T_{11}-T_{12}}$ (37)

It requires the input temperature of the module II respectively: $T_{21} - T_{22} = 5^0C$

$$\overline{T_1} = 33^0C \quad (38)$$

$$T_{11} - T_{12} = 4^0C \quad (39)$$

$$\overline{T_2} = 28{,}5^0C \quad (40)$$

And: $H_2 = 1{,}55m$ (41)

It is considered the characteristic length l=Rh

$$R_e = \frac{vRh}{\vartheta} = 738 \quad (42)$$

$$\text{Nu} = 38 \quad (43)$$

$$\alpha = \frac{\lambda}{R_h} Nu = 1266 \text{ Kcal}/m^{2\,0}C \quad (44)$$

$$\text{K} = 86{,}99 \text{ Kcal}/m^{2\,0}C \quad (45)$$

$$\text{N} = \frac{K\cdot A\cdot H}{G\cdot\rho\cdot c} = 0{,}178H \quad (46)$$

For $H_1 = 1{,}0m$, $T_{11} = 35^0C$ result:

$$T_{12} = \theta + \frac{T_{11}-\theta}{e^N} = 30{,}9^0C \quad (47)$$

Module II: $H_2 = 1{,}25m$, $T_{22} = 26^0C$ (48)

Module III: $H_3 = 1{,}50m$, $T_{32} = 22^0C$ (49)

For $H_4 = 5m$, $T_{41} = T_{32} = 22^0C$ (50)

Result: $T_{42} = 14{,}9^0C$ (51)

Consequently, to reduce the flow temperature T tour = 35 la T back = 15 is a formal exchange of modules in total length: $H_{total} = \sum_1^n H_i = 8{,}75\ m$ (52)

Or: $H_{nec} = ln\frac{T_{tour}-\theta}{T_{back}-\theta} = 9{,}0\ m$ (54)

4. Conclusion

According to the characteristics of the source cold -ground, and consumer characteristics, modular variable geometry exchanger is sized properly.Compared to the usual solutions of land area needed is much lower, the exchanger is recommended in bivalent systems for climate (heating / cooling) of the building.Numerical simulation results validate the analytical calculation model proposed.

Connecting three modules in specifiedconditions, was seen as the last exchanger output temperature is approximately equal to soil temperature, so downloading was done completely, same case was for charging source for the hot season when demand for cooling heat is much lower.

The novelty of the proposed solution is a favorable argument optimizing surface geothermal exchanger used in making reversible heating / cooling with solar energy.

References

[1] BFE - Geothermie, PraktischeNutzung Von Erdwärne, Swiss Federal Office for Energy, BERN, 1998, 23 P.; Geothermal Heat Pumps, Ubeg.
[2] Ph.Ackerer; M.A.Bues, Simulation numerique du transfert de chaleur dans un milieu poreux sature Et Non-Sature
[3] Bluc I.- Elemente de fizicaconstrucțiilor, UniversitateaTehnica,,GH. Asachii" Iași, 1995.
[4] Boian, I., Fota, Pompeletermicedinperspectivadezvoltăriidurabile. Instalațiipentruconstrucțiișieconomia de energie. Iași, EdituraCermi, 2006.
[5] Brousseau P., Lacroix M., Numerical simulation of a multi-layer latent heat thermal energy storage system, International Journal of Energy Research 22, 1998, p. 1–15.
[6] Edwards R. J., Typical Soil Characteristics of Various Terrains, 15.02.1998.
[7] EnergyCities, Gérard Magnin, Seminaire pompes a chaleur geothermiques, Mode de captajegeothermique, 09.11.2010. pag. 20-28.
[8] Eskilson P., Thermal analysis of heat extraction boreholes, Doctoral thesis, Department of Mathematical Physics, University of Lund,

Sweden, 1987.
[9] Fleige H., Horn R., Field experiments on the effect of soil compaction on soil properties runoff interflow and erosion, 2000.
[10] Fridleifsson, I.B. Bertani, R. Huenges, E. Lund, J.W. Ragnarsson, A. Rybach, L. The possible role and contribution of geothermal energy to the mitigation of climate change, IPCC Scoping Meeting on Renewable Energy Sources, Hohmeyer, O. Trittin, T. (eds.), 2008, pp.
[11] Fridleifsson I.B., Geothermal energy for the benefit of the people, European Summer School on Geothermal Energy Applications, Oradea, 2001.

Available online at www.sciencedirect.com

ScienceDirect

Energy Procedia 112 (2017) 360 – 365

Energy Procedia

Sustainable Solutions for Energy and Environment, EENVIRO 2016, 26-28 October 2016, Bucharest, Romania

HVAC system functionality simulation using ANSYS-Fluent

Cătălin George Popovici*

Faculty of Civil Engineering and Building Services, "Gheorghe Asachi" Technical University of Iasi, 13 Dimitrie Mangeron, Iasi, 700050, Romania

Abstract

The aim of the study is to simulate the functionality of a HVAC system in different situations, summer and winter time, using specialized software ANSYS-Fluent. A 2D building model was realized and simulating the internal conditions represented the main elements of the study.
There are studied the indoor air temperature and air velocity in different conditions. The results are presented as graphs/plots and spectra of interest parameters. HVAC system functionality simulation using ANSYS-Fluent is providing important results for the studied scenario.
© 2017 Published by Elsevier Ltd. This is an open access article under the CC BY-NC-ND license (http://creativecommons.org/licenses/by-nc-nd/4.0/).
Peer-review under responsibility of the organizing committee of the international conference on Sustainable Solutions for Energy and Environment 2016

*Keywords:*indoor climate; HVAC system; numerical simulation; ANSYS Fluent

1. Introduction

Studies regarding the simulation of air flow inside buildings and the effects over indoor climate are gaining more and more importance in literature [1, 2]. Mostly, these analysis are achieved using specialized tools for transient [3] or steady [4] state. Interest also exists in studying the influence of the outside air circulation over interior climate [5, 6] is analyzed. Another field of development is the medical one, where this type of approach provides preliminary information on the surgery or emergency ward climate [7, 8]

* Corresponding author. Tel.: 0722540571
E-mail address: catalinpopovici@climatherm.ro

1876-6102 © 2017 Published by Elsevier Ltd. This is an open access article under the CC BY-NC-ND license (http://creativecommons.org/licenses/by-nc-nd/4.0/).
Peer-review under responsibility of the organizing committee of the international conference on Sustainable Solutions for Energy and Environment 2016
doi:10.1016/j.egypro.2017.03.1067

The functionality of the HVAC system and other building services is a very important target for all type of buildings and even more for locations with high density of people. The present study is analyzing the HVAC system functionality, in steady state conditions, for a college amphitheater, being also available for a conference hall. The capacity of the audience is about 100 people, distributed as 12 people on 8 rows. Each row is placed on a higher step than previous one – Fig. 1.

Nomenclature

p - Pressure (Pa)
α - convective heat transfer coefficient (W/m^{2}K)
v - Overall velocity vector (m/s)
t - Time (s)
ρ - Density (kg/m^3)
τ - Shear stress (Pa)
g - Gravitational acceleration (m/s^2)
F - Force vector (N)
E - Total energy (J)
h - Enthalpy (J/kg)
h^0- Standard state enthalpy of formation (energy/mass, energy/mole)
J - Mass flux; diffusion flux (kg/m^2-s)
S_h- Source of heat added
S_m- Source of mass added to the continuous phase
T_{ext} - temperature of external air (°C)

a b

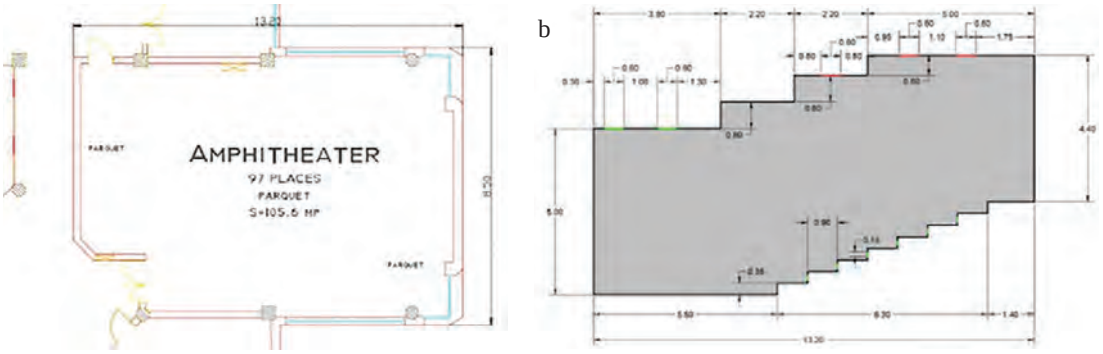


Fig. 1 – Geometry of the amphitheater a) plan; b) longitudinal section

The air conditioning of the hall is realized using an independent HVAC system, double flux. The introduced airflow is equal with the evacuated one, thus the ventilation system is balanced.

2. Case description

The treated air is introduced by the aid of a total 4 inlet grilles of 0,6mx0,6m placed at ceiling and 24 inlet grilles of 0,15mx0,5m placed at risers - Fig. 2. The evacuation of the air is realized by 6 outlet grilles of 0,6mx0,6m placed at ceiling.

There are two studied cases, the functionality of HVAC system during winter and during summer season respectively. For winter season, the system was designed for a 2100 m^3/h airflow, while in summer it is 3100 m^3/h.

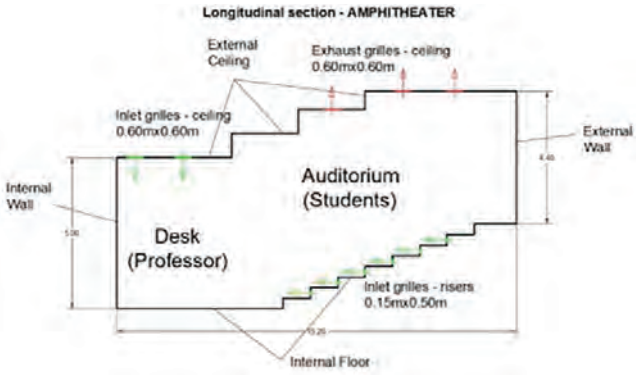


Fig. 2 – Longitudinal section – position of inlet and outlet grilles

3. Modeling HVAC system

The simulations are achieved in steady state regime, using turbulent flow and k-ε model, appropriate for evaluation of airflow and heat transfer inside closed domains [9]. The results obtained refers to the temperature and velocity data inside the amphitheater. Performing numerical simulations carried out by CFD tool, ANSYS-Fluent, the differential equations of heat transfer and fluid mechanics were solved [10]:

Momentum equation:

$$\frac{\delta}{\delta t}(\rho\vec{v}) + \nabla\cdot(\rho\vec{v}\vec{v}) = -\nabla p + \nabla(\bar{\bar{\tau}}) + \rho\vec{g} + \vec{F} \quad (1)$$

Energy conservation:

$$\frac{\delta}{\delta t}(\rho E) + \nabla\cdot(\vec{v}(\rho E + p)) = -\nabla\cdot(\sum_j h_j J_j) + S_h \quad (2)$$

Conservation of mass:

$$\frac{\delta p}{\delta t} + \nabla\cdot(\rho\vec{v}) = S_m \quad (3)$$

The mesh of the model was realized using ANSYS-Meshing, with refinements near walls. The geometry of the building is a simplified one, for the longitudinal section only, assuming a 2D model. The mass flow for each grille was determined taking into account that Fluent uses an auxiliary virtual dimension of 1 m long [10].

The boundary conditions at inlet sections are the temperature of the conditioned air and the mass flow inlet equivalent to airflow of HVAC system. Temperature of treated air is about 20 °C during winter and 24 °C in summer. For external walls, a convective heat transfer was considered with α = 24 W/m^{2}K, T_{ext} = -18 °C in winter and α = 12 W/m^{2}K, T_{ext} = 35 °C in summer. The walls are made of reinforced concrete insulated with 20 cm expanded polystyrene.

The turbulence was modelled using semi-empirical model k-ε, considered adequate for simulating air flow inside large domains [10].

4. Results

The results are presented comparatively for the two studied cases. The qualitative data are revealed by contours of velocity and temperature - Fig.3, Fig, 5. Also there are presented charts for different representative heights – Fig. 4, Fig. 6, or velocity vectors – Fig. 7.

a b

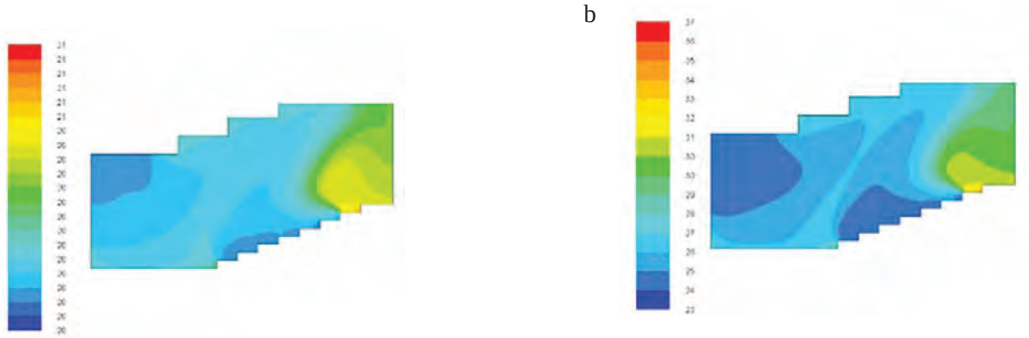


Fig. 3 – Temperature [°C] spectra: a) winter season b) summer season

The distribution of temperatures for both cases is highlighted in Fig. 3, the higher temperatures during summer season being determined by the inlet air temperatures, external heat transfer and internal gains from people.

a b

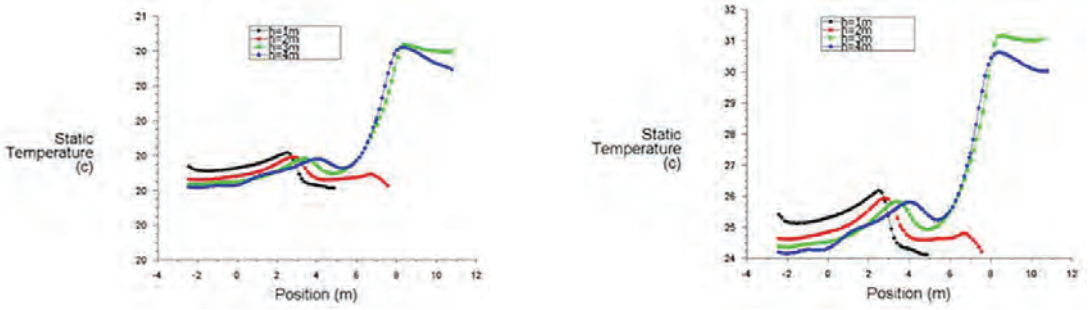


Fig. 4 – Temperatures [°C] at different heights: a) winter season b) summer season

Numerical values for the same parameters can be noticed in Fig. 4 that represents the distribution of temperatures at different height in longitudinal section. The elevation planes were selected as h = 1 m, 2 m, 3 m and 4 m, that are the most relevant from the point of view of human comfort. During winter season, temperatures are placed in very narrow interval, from 20 °C to 21 °C, while in summer, due to thermal gradient they lay on 24-42 °C gap.

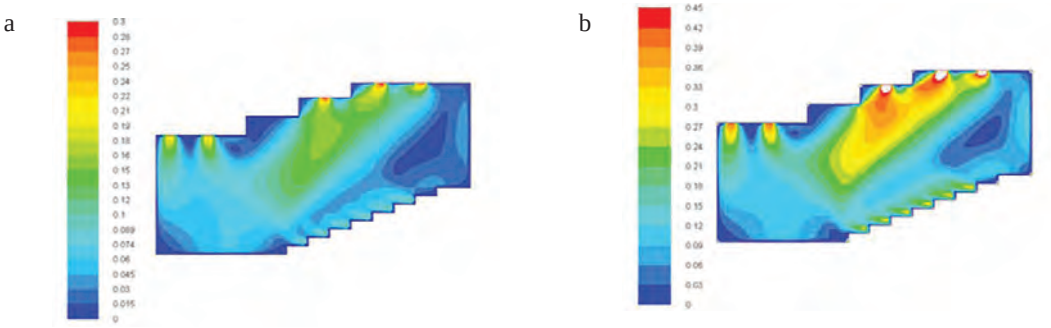


Fig. 5 - Velocity spectra: a) winter season b) summer season

The velocity spectra are almost similar for both seasons, caused by the same strategy of ventilation used during winter and summer. The only difference is recorded on maximum air velocities that are higher on summer.

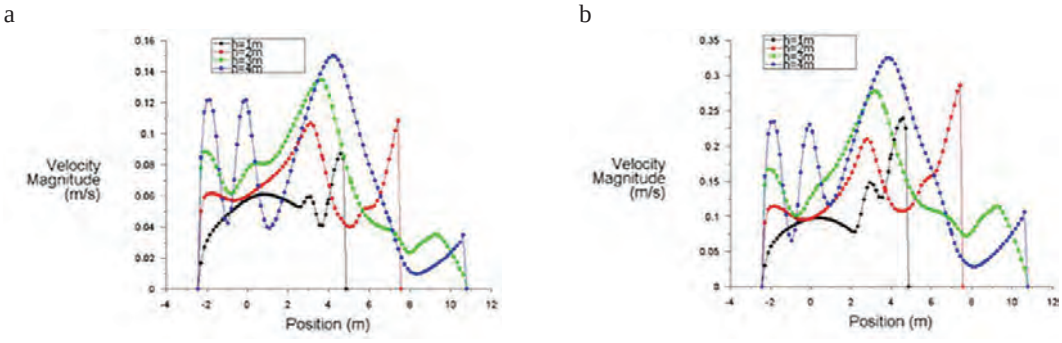


Fig. 6 - Velocity at different heights: a) winter season b) summer season

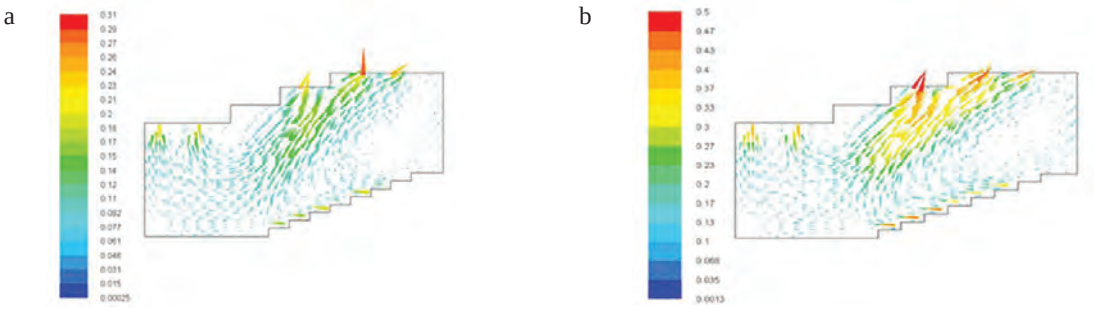


Fig. 7 – Velocity vectors: a) winter season b) summer season

Analyzing Fig. 6 and Fig. 9, it can be noticed that maximum values of velocity in both seasons are far and away compared to the uncomfortable ones. Thus, in winter the maximum velocities in occupied zone are about 0.15

m/s and for summer they are about 0.3 m/s.

5. Conclusions

The study aimed to simulate HVAC system functionality in different situations, summer and winter time, using specialized software ANSYS-Fluent. The realization of 2D building model and simulation of external and internal conditions it represents the main elements of simulation.

As general conclusion, it can be stated with certainty that the recently implemented HVAC system reaches its task and provides adequate comfort conditions inside the amphitheater during both seasons.

The average velocities, are slightly bigger during summer season, due to higher airflows required. However, this effect doesn't affect the occupants, because they are lower than the comfort ones.HVAC system functionality simulation using ANSYS-Fluent is providing important results for the studied scenario.

This type of analysis can be used for pre-examination of the future projects in order to obtain functional systems and verify the all requirements for the HVAC installation. The results can be used in further analysis for determining the correlations to the main comfort indicators, PMV and PPD.

References

[1] Thiyagarajan GM, Raj Kumar S. Velocity optimisation using computational fluid dynamics as a tool in leed rated building to reduce energy consumption. Journal of Chemical and Pharmaceutical Sciences; 2015, p. 142-145.

[2] Popovici CG, Hudișteanu SV.Numerical simulation of HVAC system functionality in a socioculturalbuilding, Procedia Technology 22; 2016,p. 535–542.

[3] Gustafsson M, Dermentzis G, Myhren JA, Bales C, Ochs F, Holmberg S, Feist W. Energy performance comparison of three innovative HVAC systems for renovation through dynamic simulation, Energy and Buildings82; 2014, p.512–519.

[4] MohammadshahiS, Ahmadabadi MN, Nematollahi O. Improvement of ventilation and heat transfer in Shavadoon via numerical simulation: A traditional HVAC system, Renewable Energy96; 2016, p. 295–304.

[5] Mahu R, Popescu F, Ion IV. CFD Modeling Approach for HVAC Systems Analysis. Chemical Bulletin of "Politehnica" University of Timisoara; 2012, p. 69-73.

[6] Bhaskoro PT, Gilani SI, Aris MS.Simulation of energy saving potential of a centralized HVAC system in an academic building using adaptive cooling technique, Energy Conversion and Management 75; 2013, p. 617–628.

[7] Peri A, Fernandes PM, Vishwanadha C. Numerical simulation of air flow in a general ward of a hospital. IJRRAS 8; 2011, p. 400-444.

[8] Balocco C, Petrone G, Cammarata G, Vitali P, Albertini R, Pasquarella C. Indoor Air Quality in a Real Operating Theatre under Effective Use Conditions. Biomedical Science and Engineering; 2014, p. 866-883.

[9] Schwarz W, Marchal T. Innovation in Building Design through Engineering Simulation. ANSYS, Inc.; 2009.

[10] ANSYS-Fluent, Theory Guide.

Available online at www.sciencedirect.com

ScienceDirect

Procedia Technology 22 (2016) 535 – 542

Procedia Technology

9th International Conference Interdisciplinarity in Engineering, INTER-ENG 2015, 8-9 October 2015, Tirgu-Mures, Romania

Numerical simulation of HVAC system functionality in a socio-cultural building

Cătălin-George Popovici[a], Valeriu Sebastian Hudișteanu[a,]*

[a]"Gheorghe Asachi" Technical University of Iasi, Faculty of Civil Engineering and Building Services, 1, D.Mangeron, Iasi-700050, Romania

Abstract

The study presents the functionality of the heating, ventilation and air conditioning (HVAC) system for an important and prestigious objective of Iasi, the "Vasile Alecsandri" National Theatre. A numerical model was created, for the indoor climate analysis, obtaining the main thermal comfort parameters, in different zones of the auditorium. The model carried out on the CFD tool ANSYS-Fluent, is based on the recently implemented HVAC system of the theatre. The results are presented comparatively in two distinct scenarios of the ventilation and conditioning system: when the theatre is occupied and during the breaks. Results from simulation showed that the system provides suitable conditions for occupants and decorative finishing.

© 2016 The Authors. Published by Elsevier Ltd. This is an open access article under the CC BY-NC-ND license (http://creativecommons.org/licenses/by-nc-nd/4.0/).

Peer-review under responsibility of the "Petru Maior" University of Tirgu Mures, Faculty of Engineering

Keywords: numerical modeling; HVAC system; indoor climate; thermal comfort; social and cultural building

1. Introduction

The functionality of the HVAC system and other building services is a very important target for all type of buildings and even more for locations with high density of people, such as theatres. An important and prestigious objective of Iasi is the "Vasile Alecsandri" National Theatre, Fig. 1, one of the most representative historical monuments of the city, rehabilitated and consolidated until 2012.

The main technical requirements of this project were heating, cooling and ventilation installations re-dimensioning. The existing installations have never been dimensioned for cooling. Another important requirement was the control of indoor air parameters, especially temperature and humidity.

* Corresponding author. Tel.: +4-074-632-8149.

E-mail address: seby_hudisteanu@yahoo.com

2212-0173 © 2016 The Authors. Published by Elsevier Ltd. This is an open access article under the CC BY-NC-ND license (http://creativecommons.org/licenses/by-nc-nd/4.0/).
Peer-review under responsibility of the "Petru Maior" University of Tirgu Mures, Faculty of Engineering
doi:10.1016/j.protcy.2016.01.113

The novelty element of the project was brought by the humidity control extremely important for the preservation of paintings and architectural elements.

Nomenclature

p	Pressure (Pa)
v	Overall velocity vector (m/s)
t	Time (s)
ρ	Density (kg/m^3)
τ	Shear stress (Pa)
g	Gravitational acceleration (m/s^2)
F	Force vector (N)
E	Total energy (J)
h	Enthalpy (J/kg)
J	Mass flux; diffusion flux (kg/m^2-s)

The main condition for HVAC installations re-dimensioning was highly limited by imposing the use of existing air channels, including dimensions and shape as well as grilles, all embedded in concrete walls, floors or ceilings.



Fig. 1. The "Vasile Alecsandri" National Theatre, Iasi

Initial project was designed in 1896 by Koerting brothers in Paris, Fig. 2. and solved only the problem of heating using natural circulation air combined with mechanical ventilation.



Fig. 2. Initial project from 1896 [1]

After careful examination and verifications of status of these elements the followings have been established: they had irregular shapes and some were even blocked. Moreover, intervention inside the channels for widening or rehabilitation of interior surfaces was not possible seeing that the resistance structure of the building could have been affected.

Under these circumstances and according to scientific literature specifications, the solution implemented for "Vasile Alecsandri" National Theatre Iasi consists in 4 HVAC integrated systems serving: Main Hall, stage, foyer and adjacent areas. It is a multi-zone solution which divides the building into 3 areas whose utilization is never simultaneous:

- Zone 1- stall, lodges and balcony;
- Zone 2 - stage and orchestra pit;
- Zone 3 - foyer and adjacent areas.

Most important decisions made were: the placement of 6 air handling units (AHU) respectively - 4 inside the technical room at semi-basement and 2 in the attic of the building, thermal insulation and usage of overpressure room from stall and balcony and keeping all inlet and outlet grilles with initial dimensions respectively all air channels impeded inside the walls. It was only allowed dimensioning of air channels in the basement and attic according with technical requirements.

The air circulation for the Main Hall, Fig. 3, is achieved through three systems for fresh air supply: stall, lodge and balcony, and one system for exhaust air: ceiling. For Zone 2-stage, inlet air is introduced trough grilles mounted at floor level and in Zone 3 -foyer trough inlet grilles mounted in the concrete floor.

All 229 inlet grilles in stall zone are mounted in the floor, under the seats. At lodges, the inlet grilles are placed in the vertical air channels, while the balcony is connected through channels with the overpressure room, and the inlet grilles are in the tiers. The exhaust air from Main Hall is realized through twelve circular outlet grilles, symmetrically placed in the circular ceiling. The total airflow of the auditorium zone is of 21000 m^3/h, while the amount of the fresh air equals the exhaust air.

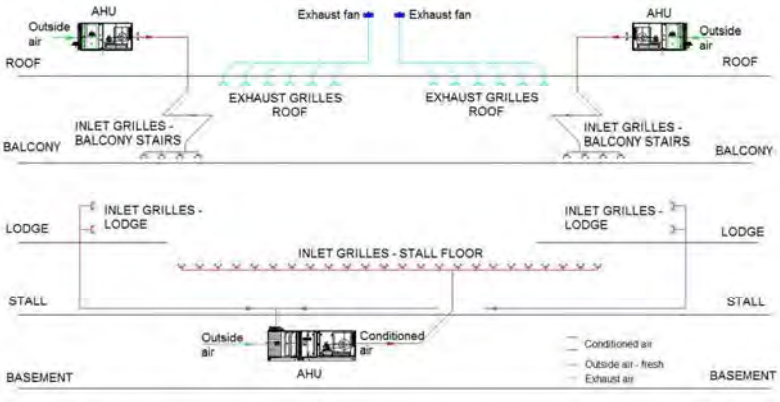


Fig. 3. Functional scheme of the HVAC system for Zone 1-Main Hall

The capacity of the theatre is about 800 places, which are often occupied during spectacles.

The purpose of this paper is to check if the recently implemented ventilation and air conditioning system is satisfying all technical requirements, taking into consideration all technical constraints on ventilation channel dimensioning as well as grilles number, shape and positioning due to architectural reasons. Thus resulted the need of simulation using specific software in the designing phase of the project and as well as understanding and interpretation of the results. This task was achieved by using the specialized software ANSYS-Fluent.

2. Problem description

The main problem in case of these types of buildings consists of high level of heat and vapor emission, when the entire auditorium is occupied. For modeling the phenomenon, a 2D model was created. The emissions were quantified properly for this type of approach by imposing heat and water mass fluxes, corresponding to maximum capacity of the objective. In literature there are many attempts to simulate air flow inside buildings and its effects over indoor climate [2] and also for the influence of the outside air circulation over interior climate [3]. This type of approach is also widely used in medical field, most of the time for obtaining preliminary information on the surgery or emergency ward climate [4, 5].

The thermal indoor climate, investigated in present study, is defined by the following parameters: air temperature, surface temperatures, air movements and relative humidity [6]. The HVAC system and the position of inlet and outlet grilles have an important role in order to provide these values.

3. Numerical approach

The numerical model was created for the indoor climate analysis, obtaining the main thermal comfort parameters, in different zones of the auditorium. In literature there are many attempts of using CFD software Fluent for simulating the airflow inside buildings [7, 8] or the impact of relative humidity [9]. The present model is carried out on the ANSYS-Fluent tool, which is appropriate for qualitative and quantitative evaluation of airflow and heat transfer inside closed domains [10]. The model is based on the real HVAC system. The 2D geometry, was created using ANSYS-Design Modeler with small control volumes, with refinements near the walls and near important areas, while the mesh was realized using ANSYS-Meshing. The geometrical dimensions used in model were those of the real building, Fig. 4. The resulting mesh consists of 5638 mixed cells, 12018 faces and 5884 nodes.

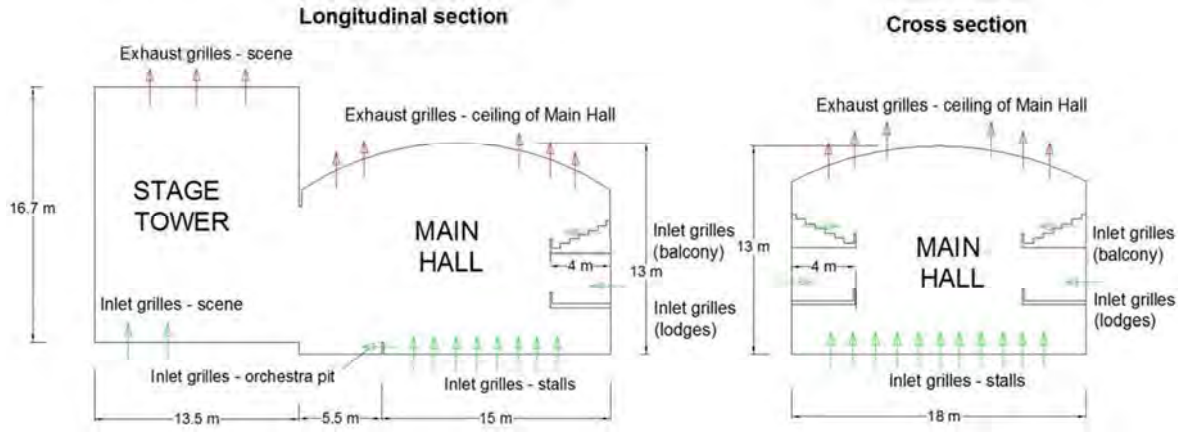


Fig. 4. Longitudinal section and cross section of the building

Applying the differential equations of heat transfer and fluid mechanics, the temperature, velocity and relative humidity data inside the main hall of the theatre were obtained. The CFD tool, ANSYS-Fluent, uses the finite-volume method to solve the following conservation equations [11]:

- Momentum equation:

$$\frac{\delta}{\delta t}(\rho\vec{v}) + \nabla\cdot(\rho\vec{v}\vec{v}) = -\nabla p + \nabla(\bar{\bar{\tau}}) + \rho\vec{g} + \vec{F} \tag{1}$$

- Energy conservation equation:

$$\frac{\delta}{\delta t}(\rho E)+\nabla\cdot(\vec{v}(\rho E+p))=-\nabla\cdot(\sum_j h_j J_j)+S_h \quad (2)$$

- Continuity equation (conservation of mass):

$$\frac{\delta p}{\delta t}+\nabla\cdot(\rho\vec{v})=S_m \quad (3)$$

As boundary conditions, at the inlet sections, the conditioned fresh air temperature of 20 °C was imposed and the mass flow inlet, as an equivalent velocity for each grille, taking into account the 2D simplified geometry. The outlet sections were set as outflow zones. The external conditions imposed to the walls and windows in simulations were the air temperature of -18 °C and the convective heat transfer coefficient of 24 W/m^{2}K, typical for Iasi.

The Reynolds number resulted for the imposed velocities lays between 4310 and 13100, therefore, the flow regime considered is the turbulent one. There is no universal appropriate turbulence model that can be used for all types of flows. Therefore, an important task consists of choosing the appropriate turbulence model. In this numerical approach, the k-ε RNG model was used, which is considered the most realistic for air flow inside large domains [11]. The semi-empirical model k-ε is based on the transport equations model for the turbulence kinetic energy (k) and the dissipation rate (ε) [4].

For modeling humidity inside building, the species model was activated. The two volumetric species used are air and water-vapors. The moisture sources were calculated taking into account that a group of people can be modeled as a mass flow inlet of water, with a mass flux proportional to the number of occupants and considering the 2D model similarity. According to [12], a sitting person produces around 70 g H_20/h. Applying heat generation rate under the circumstance of full occupancy, a constant source of energy of 100 W/m^3 was imposed.

4. Results

The results are presented comparatively in two distinct scenarios for the ventilation system: when the theatre is occupied - system is functioning at maximum capacity and during the breaks - emissions are lower and the ventilation system works at reduced load.

The extracted data are presented as contours, vectors and charts for different plans, at variable cross section heights. The numerical results show that the system provides suitable conditions for occupants and also for decorative finishing.

Fig. 5 and Fig. 6 show the important gradient of temperature in the investigated zone. Despite this, in the main areas where spectators are present, stall, lodge and balcony respectively, temperature measures between 20 °C and 23 °C. The temperatures are lower during breaks, when most of the people are outside the Main Hall. This is the favorable moment when the HVAC system can adjust the controlled values to the nominal ones.

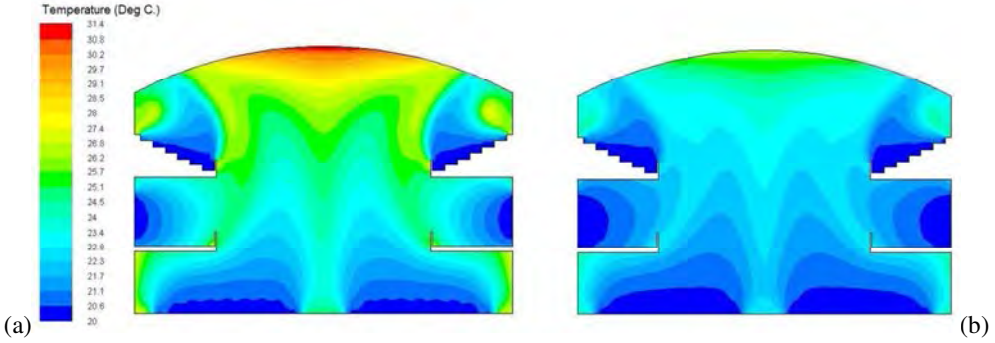
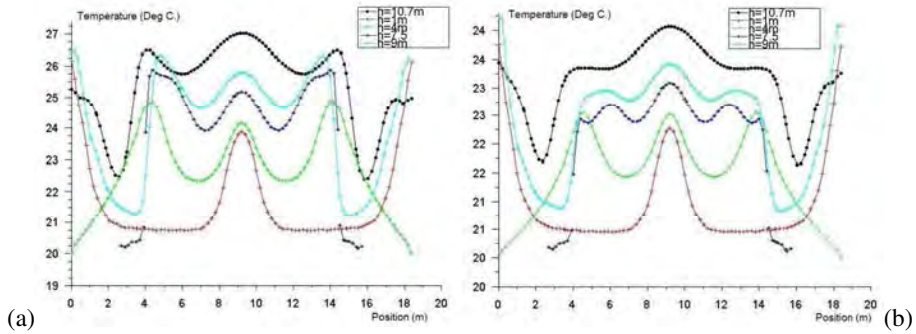


Fig. 5. Temperature contours in cross section (a) during spectacles; (b) during breaks

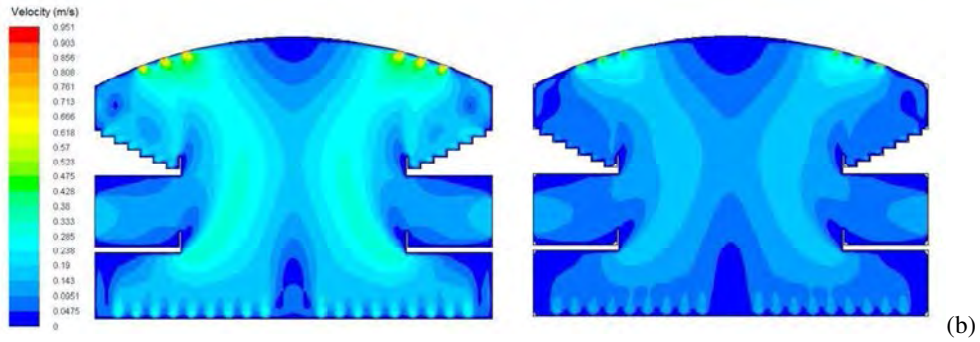
Fig. 6 presents more accurate quantitative values for vertical plans of 1m height – stall zone, 4m height – lodge zone and 7.5 m height – balcony zone, which are the most occupied areas. As expected, the temperatures have similar distributions in both moments, but with smaller amplitude during breaks, Fig. 6.



(a) (b)

Fig. 6. Temperature chart (a) during spectacles; (b) during breaks

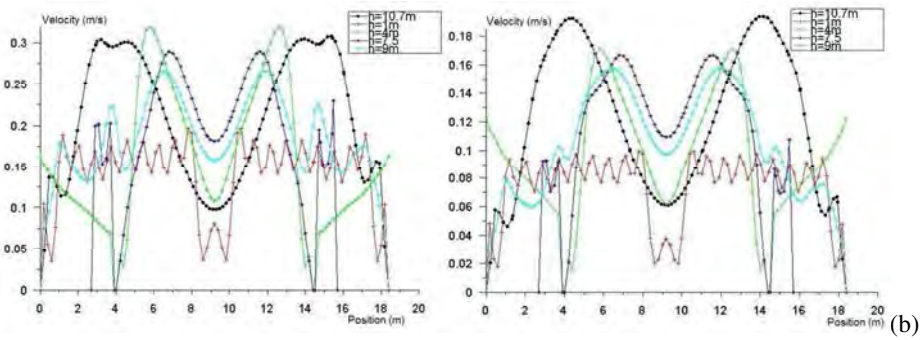
The contours of velocities, Fig. 7, show the main circulation zones of the fresh air. The inlet zones are supplying a proper ventilation of the occupied zones.



(a) (b)

Fig. 7. Velocity contours (a) during spectacles; (b) during breaks

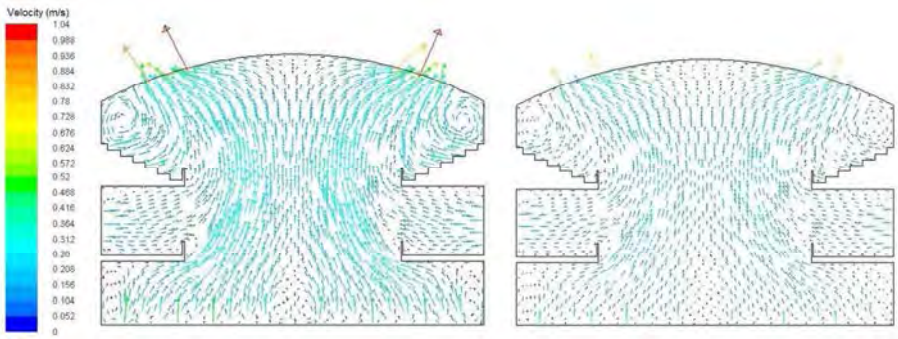
The average velocities are about 0.2 m/s and the peak values are recorded in the outlet and inlet zones, due to 2D simplified assumptions of the ventilation airflow. During breaks, when the HVAC system is at most half loaded, the air circulation is tempered. The same aspects are underlined by velocity profiles in the occupational zone, Fig. 8.



(a) (b)

Fig. 8. Velocity chart (a) during spectacles; (b) during breaks

Fig. 9 shows the vectors of velocity in the study field. There are some differences between the studied cases, in terms of velocity magnitude, while the direction is almost identical. When seeking air velocity and direction, while the auditorium is occupied, we distinguish a very smooth air flow in the comfort zones. Some recirculation zones are recorded in the upper side of the hall, in the balcony zones, determined by the vicinity of the outlet grilles, but the velocities are below 0.3 m/s.



(b)

Fig. 9. Vectors of velocity (a) during spectacle; (b) during breaks

In terms of relative humidity, Fig. 10, values are placed into a relatively narrow range, between 50% and 65%.

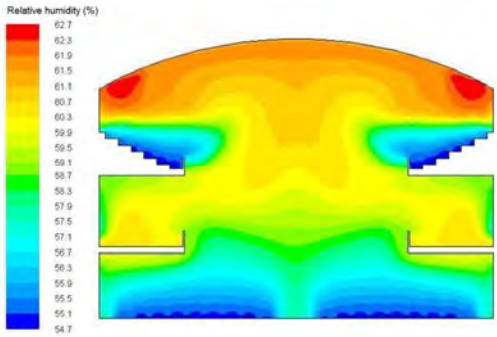


Fig. 10. Contours of relative humidity during spectacles

As expected, the highest values are recorded in the upper side of the room, but the amount of moisture of 65%, is not too high for determining condensation at ceiling and walls.

5. Conclusions

A 2D model was realized for the cross section of the building, taking into account the actual position of the inlet and outlet grilles of ventilation. The model was simulated using ANSYS-Fluent CFD package, considering the implemented HVAC system, and parameters like temperature, velocity and relative humidity were evaluated.

Considering the simultaneous effects of the results, the new installed HVAC system performed its contribution in maintaining the indoor parameters at optimum values in this historical, social and cultural edifice. Another effect consists of ensuring the comfort of people and integrity of paintings by humidity control.

This study shows that for this type of buildings, even during the winter season, when outside temperatures are very low, in particular moments, it could be necessary to cool the auditorium hall and evacuate the excess heat and moisture.

More general conclusions can also be drawn from the consolidation works analysis of the historical monument "Vasile Alecsandri" National Theatre. Interventions of such amplitude on objectives with cultural, religious or historical importance always have to take into account:

- Preservation of original architectural elements of the building;
- Adjustment of engineering design of specialized works with existent conditions;
- The limitation of air channels and grilles dimensions due to the initial architectural constraints; Close correlation between installations and construction works;
- Simulation with specific software, ANSYS-Fluent, in the designing phase and results interpretation;
- The importance of understanding and applying the simulations results by both engineering designers and architects.

This type of approach can be used for future projects in order to achieve functional systems that meet all the special requirements of buildings with national historical value.

References

[1] National Archives of Romania; 2007.
[2] Thiyagarajan GM, Raj KS. Velocity optimisation using computational fluid dynamics as a tool in leed rated building to reduce energy consumption. Journal of Chemical and Pharmaceutical Sciences; 2015. p.142-145
[3] Mahu R, Popescu F, Ion IV. CFD Modeling Approach for HVAC Systems Analysis. Chemical Bulletin of "Politehnica" University of Timisoara; 2012. p. 69-73
[4] Peri A, Fernandes PM, Vishwanadha C. Numerical simulation of air flow in a general ward of a hospital. IJRRAS 8 (3); 2011. p.400-444
[5] Balocco C, Petrone G, Cammarata G, Vitali P, Albertini R, Pasquarella C. Indoor Air Quality in a Real Operating Theatre under Effective Use Conditions, Biomedical Science and Engineering; 2014, 7. p.866-883
[6] Hudisteanu VS, Baran AI, Balan M, Chereches NC, Mateescu T, Ciocan V. Improvement of the indoor climate conditions inside orthodox churches. Proceedings of the International Scientific Conference CIBv; 2014. p. 61-66
[7] Masine MT, Haslinda MK, Abdul KM, Nazri K, Khairul AMS. Simulation of thermal comfort of a residential house. IJCSI Vol. 8 (5); 2011. p.200-208
[8] Leo NYC, Junji C, Shuncheng L, Yunwei Z, Xuexi T. Numerical Simulation of the Micro Environment in the Han Yang Mausoleum Museum. Aerosol and Air Quality Research; 2012. p.544-552
[9] Ahmed R, Reaz H, Jenna T. Simulation of flow and heat transfer of humid air in spent fuel cooling ponds. Proceedings of the World Congress on Engineering; 2014. p.1508-1512
[10] Schwarz W, Marchal T. Innovation in Building Design through Engineering Simulation. ANSYS, Inc.; 2009.
[11] ANSYS-Fluent 13.0. Theory Guide.
[12] Uyttenhove W, De Paepe M, Janssens A. CFD-modelling of Temperature and Humidity Distribution in the St. Pieter's Church. IAE-Annex 41, Subtask 1; 2004.